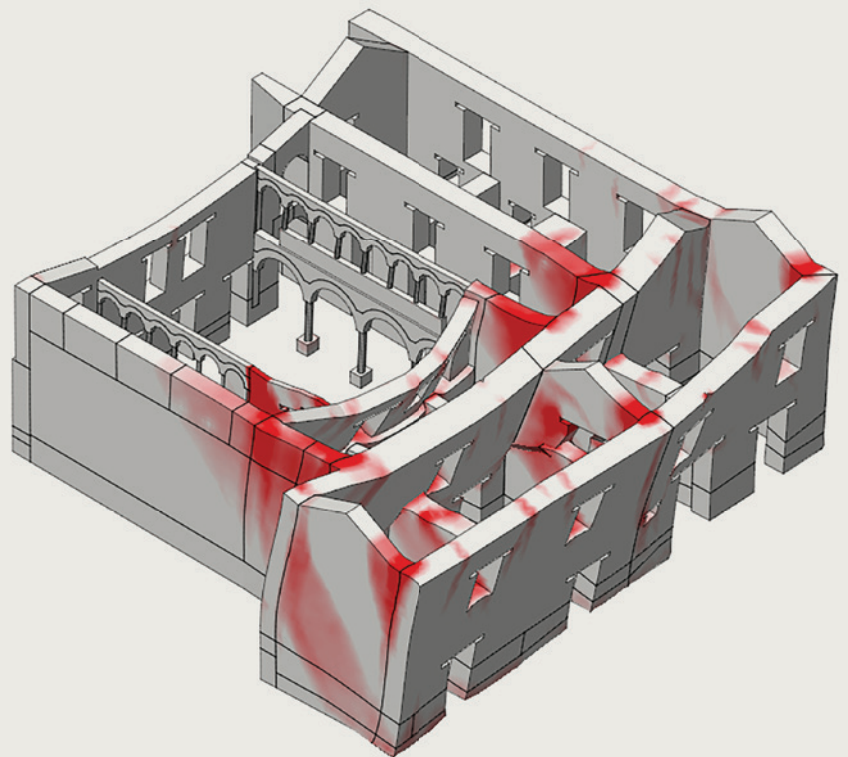


# Seismic Retrofitting Project Modeling of Prototype Buildings

## Research Report

Paulo B. Lourenço, Federica Greco,  
Alberto Barontini, Maria Pia Ciocci,  
and Giorgos Karanikoloudis

In collaboration with Daniel Torrealva  
and Claudia Cancino



# Seismic Retrofitting Project

## Modeling of Prototype Buildings

Paulo B. Lourenço, Federica Greco, Alberto Barontini,  
Maria Pia Ciocci, and Giorgos Karanikoloudis

In collaboration with Daniel Torrealva and Claudia Cancino

THE GETTY CONSERVATION INSTITUTE  
LOS ANGELES  
TECMINHO – UNIVERSITY OF MINHO  
GUIMARÃES, PORTUGAL

© 2019 J. Paul Getty Trust and TecMinho – University of Minho

The Getty Conservation Institute  
1200 Getty Center Drive, Suite 700  
Los Angeles, CA 90049-1684  
United States  
Telephone (+1) 310 440-7325  
Fax (+1) 310 440-7702  
E-mail: [gciweb@getty.edu](mailto:gciweb@getty.edu)  
[www.getty.edu/conservation](http://www.getty.edu/conservation)

TecMinho – University of Minho  
Campus de Azurém  
Alameda da Universidade  
P-4800-058 Guimarães  
Portugal  
Telephone (+351) 253 510-590  
Fax (+351) 253 510-591  
E-mail: [tecm@tecminho.uminho.pt](mailto:tecm@tecminho.uminho.pt)  
[www.tecminho.uminho.pt](http://www.tecminho.uminho.pt)

The Getty Conservation Institute (GCI) works internationally to advance conservation practice in the visual arts—broadly interpreted to include objects, collections, architecture, and sites. The Institute serves the conservation community through scientific research, education and training, field projects, and the dissemination of information. In all its endeavors, the GCI creates and delivers knowledge that contributes to the conservation of the world's cultural heritage.

Founded in 1990, TecMinho is a private non-profit association supported by the University of Minho and the Association of Municipalities of Vale do Ave, Portugal. Its mission is to connect the University of Minho to society, especially in the areas of science and technology, and to contribute to regional development by improving the competitiveness of organizations and increasing the skills of individuals.

ISBN: 978-1-937433-63-5 (online resource)

ISBN: 978-1-937433-64-2 (print on demand)

Cover: © J. Paul Getty Trust, 2019. Model: Federica Greco



**The Getty Conservation Institute**



Universidade do Minho



# Contents

|  |     |
|--|-----|
| Project Participants   | v   |
| SRP Peer Review Group  | vii |
| <b>CHAPTER 1</b>   |     |
| <b>Introduction</b>  |     |
| The Seismic Retrofitting Project   | 1   |
| Objectives   | 2   |
| <b>CHAPTER 2</b>   |     |
| <b>Brief Description of the Case Studies</b>   |     |
| The Church of Santiago Apóstol de Kuñotambo (the Church of Kuñotambo)  | 5   |
| The Ica Cathedral  | 8   |
| Casa Arones  | 12  |
| Hotel El Comercio  | 16  |
| <b>CHAPTER 3</b>   |     |
| <b>Modeling Approach</b>   |     |
| Material Model   | 19  |
| <i>Total Strain Rotating Crack Model</i>   | 20  |
| <i>Von Mises Model</i>   | 20  |
| Material Properties  | 21  |
| <i>Masonry</i>   | 22  |
| <i>Timber</i>  | 23  |
| <i>Quincha Walls</i>   | 23  |
| Safety Assessment  | 24  |
| Sensitivity Analysis   | 26  |
| <b>CHAPTER 4</b>   |     |
| <b>Unstrengthened and Strengthened Case Studies:<br/>The Church of Santiago Apóstol de Kuñotambo<br/>and the Ica Cathedral</b> |     |
| Unstrengthened Structure of the Church of Santiago Apóstol de Kuñotambo  | 27  |
| Numerical Analysis   | 28  |

---

|   |    |
|---|----|
| Conclusions   | 31 |
| Strengthened Structure of the Church of Kuñotambo                         | 32 |
| <i>Description of the Strengthening</i>                                   | 32 |
| <i>Characteristics of the Numerical Model</i>                             | 35 |
| <i>Numerical Analysis</i>   | 36 |
| <i>Sensitivity Analysis</i>   | 38 |
| <i>Conclusions</i>  | 40 |
| Unstrengthened Structure of the Ica Cathedral                             | 41 |
| <i>Numerical Analysis</i>   | 41 |
| <i>Conclusions</i>  | 44 |
| Strengthened Structure of the Ica Cathedral                               | 44 |
| <i>Description of the Strengthening</i>                                   | 44 |
| <i>Characteristics of the Numerical Model</i>                             | 47 |
| <i>Numerical Analysis</i>   | 47 |
| <i>Conclusions</i>  | 51 |
| <br><b>CHAPTER 5</b>  |    |
| <b>Unstrengthened Case Studies:<br/>Casa Arones and Hotel El Comercio</b> |    |
| Characteristics of the Numerical Model of Casa Arones                     | 53 |
| <i>Contribution of the Horizontal Diaphragms</i>                          | 54 |
| <i>Numerical Analysis</i>   | 58 |
| <i>Sensitivity Analysis</i>   | 60 |
| <i>Conclusions</i>  | 64 |
| Characteristics of the Numerical Model of Hotel El Comercio               | 66 |
| <i>Numerical Analysis</i>   | 67 |
| <i>Sensitivity Analysis</i>   | 69 |
| <i>Conclusions</i>  | 72 |
| <br><b>CHAPTER 6</b>  |    |
| <b>Conclusions</b>  | 75 |
| <b>References</b>   | 77 |

# Project Participants

## **Seismic Retrofitting Project—Modeling Phase**

### **PROJECT DIRECTORS**

Paulo B. Lourenço  
Professor, University of Minho, Portugal

Claudia Cancino  
Senior Project Specialist, Getty Conservation Institute, Los Angeles

### **PARTICIPANTS**

Alberto Barontini  
Research Assistant, University of Minho, Portugal

Cindy Calbimonte  
Graduate Intern (2018–19), Getty Conservation Institute, Los Angeles

Maria Pia Ciocci  
Research Assistant, University of Minho, Portugal

Nicole Declat  
Graduate Intern (2017–18), Getty Conservation Institute, Los Angeles

Federica Greco  
Research Assistant (2015–2016), University of Minho, Portugal  
Graduate Intern (2016–17), Getty Conservation Institute, Los Angeles

Giorgos Karanikoloudis  
Research Assistant, University of Minho, Portugal

Elena Macchioni  
Associate Project Specialist, Getty Conservation Institute, Los Angeles

Susan Macdonald  
Head, Buildings and Sites, Getty Conservation Institute, Los Angeles

João M. Pereira  
Postdoctoral Research Associate, University of Minho, Portugal

Kelly Wong  
Project Specialist (2015–2017), Getty Conservation Institute, Los Angeles



# SRP Peer Review Group

Organized by the Getty Conservation Institute (GCI) as part of the Seismic Retrofitting Project (SRP), the following professionals participated in peer review meetings in Lima on July 18–21, 2011 and in Cusco on January 23–27, 2017. The SRP peer review group consists of experienced professionals in seismic retrofitting, analytical modeling of historic masonry structures, and conservation of earthen architecture. The meetings, which included formal talks and site visits, were designed to provide maximum opportunity for informal discussion among a select group of experts.

The objective of the first meeting was to review the SRP Construction Assessment of selected building prototypes. The meeting also included a review of the SRP Proposal for the Testing and Modeling Phase, which was developed in collaboration with the GCI by the Escuela de Ciencias e Ingeniería of the Pontificia Universidad Católica del Perú (PUCP, SRP partner) and the Department of Architecture and Civil Engineering at the University of Bath (SRP partner from 2011 to 2014), respectively. The objective of the second meeting was to review the results of the completed testing developed by PUCP and the modeling results of the un-retrofitted and retrofitted SRP building prototypes, designed and developed by TecMinho, University of Minho (GCI consultant from 2015 to 2018).

In advance of both meetings, peer reviewers received extensive documentation of the work carried out by the SRP team. Peer reviewers' comments were highly valuable for the SRP team and enriched the methodology and results of the project. This publication serves as a testament to their voice and influence.

Eng. Rafael Aguilar \*\*

Associate Professor, Pontificia Universidad Católica del Perú

Arch. André Aninat Jolly \*\*

Head, Sustainable Conservation Project Workshop, Fundación Altiplano Msv, Chile

Eng. Carlos Casabonne \*\*

Senior Principal, Gallegos, Casabonne, Arango, Ingenieros Civiles SAC

Arch. Mariana Correia \*\*

President, ESG/Escola Superior Gallaecia, Portugal, and former President PROTERRA Iberian-American Network

Eng. Matthew DeJong \*\*\*

Senior Lecturer, University of Cambridge

Eng. Carmen Kuroiwa \*

Gerente de Investigación y Normalización, Servicio Nacional de Capacitación para la Industria de la Construcción (SENCICO)

Arch. Philippe Garnier \*\*\*

Director, Human Settlements, CRAterre-ENSAG

Arch. Eng. Stephen Kelly \*\*\*  
Secretary-General, International Scientific Committee on the Analysis and Restoration of Structures of Architectural Heritage (ISCARSAH)

Eng. Terrence Paret \*\*  
Senior Principal, Wiss, Janney, Elstner Associates, Inc.

Eng. Pere Roca \*\*  
Professor, Technical University of Catalonia

Eng. Nicola Tarque \*\*  
Associate Professor, Pontificia Universidad Católica del Perú

Eng. Julio Vargas Neumann \*\*\*  
Member, International Scientific Committee on the Conservation of Earthen Architectural Heritage (ISCEAH) and World Heritage Earthen Architecture Programme (WHEAP)

Eng. Humberto Varum \*  
Professor, University of Porto, Member of ISCEAH

Eng. Fred Webster \*  
Former Member, Getty Seismic Adobe Project (GSAP)

\* = Attended first meeting (July 2011)

\*\* = Attended second meeting (January 2017)

\*\*\* = Attended both meetings

# Introduction

Mud brick, commonly known as adobe, is one of the oldest and most widely used natural materials and accounts for a significant part of the built heritage. It is associated with early building techniques, widely dispersed material availability, and low-cost construction. Adobe buildings have low mechanical properties, insufficient connections between structural parts, brittle behavior, and critical out-of-plane resistance. Thus, when subjected to seismic actions, they are usually susceptible to early structural damage, including cracking, separation of structural elements, and, often, collapse of large structural parts. Aspects such as lack of maintenance and absence of adequate retrofitting techniques further contribute to the loss of historic fabric (Cancino and Lardinois 2012).

## The Seismic Retrofitting Project

During the 1990s, the Getty Conservation Institute (GCI) carried out a major research and laboratory testing program, the Getty Seismic Adobe Project (GSAP), which investigated the performance of historic adobe structures during earthquakes and developed cost-effective retrofit methods that substantially preserve the authenticity of these buildings. Results of this research have been disseminated in a series of publications in both English and Spanish (Tolles, Kimbro, and Ginell 2002).

In 2006, the GCI's Earthen Architecture Initiative convened two meetings: the Getty Seismic Adobe Project Colloquium and New Concepts in Seismic Strengthening of Historic Adobe Structures. Held at the Getty Center, the meetings focused on implementation of the GSAP. Papers presented at the colloquium, as well as the main conclusions of the colloquium's roundtable discussions, were published as part of the colloquium proceedings (Hardy, Cancino, and Ostergren 2009). The participants in the colloquium concluded that the GSAP methodology was excellent and effective. However, the methodology's reliance on high-tech materials and professional expertise was a deterrent to it being more widely implemented.

After the colloquium, an earthquake of 8.0 Moment Magnitude (Mw) and a maximum local Modified Mercalli Intensity (MMI) of VII–VIII occurred on August 15, 2007, with an epicenter off the coast of the city of Pisco, Peru, resulting in 519 deaths and 1,366 injured. A total of 650,000 people were affected and 80,000 dwellings damaged. From October 28 to November 2, 2007, a rapid assessment to better understand the failure of fifteen historic earthen sites was performed by a multidisciplinary team of national and international experts convened by the GCI. The assessment, which was organized in response to a request from the former Instituto Nacional de Cultura del Perú (INC; Peruvian National Institute of Culture; now the Ministerio de Cultura del Perú, or Ministry of Culture), was also published (Cancino 2011).

Following the GSAP conclusions and the findings after the Pisco earthquake, the GCI initiated in 2009 the Seismic Retrofitting Project (SRP), with the objective of adapting GSAP techniques to better match the equipment, materials, and technical skills available in many countries with earthen sites. Using four Peruvian historic earthen buildings representing typologies across Latin America, the GCI—in collaboration with the Ministerio de Cultura del Perú, the Escuela de Ciencias e Ingeniería of the Pontificia Universidad Católica del Perú (PUCP), and the University of Minho—is designing, testing, and implementing seismic retrofitting techniques and maintenance programs with locally available materials that will improve the structural performance and safety of earthen buildings while minimizing loss of historic fabric. The Department of Architecture and Civil Engineering at the University of Bath and the Department of Civil, Environmental and Geomatic Engineering at University College London have also been SRP partners from 2010 to 2012 and from 2013 to 2014, respectively.

From 2015 until 2017, the University of Minho used modeling as a method to understand structural behavior of the SRP building prototypes and validate the retrofitting techniques later designed for them. The way modeling has been used is quite innovative, has advanced the field of structural analysis of structures made of earth, and is worth publishing.

The SRP was subdivided into four phases:

- Phase I: Feasibility and Research;
- Phase II: Methodology;
- Phase III: Testing and Modeling; and
- Phase IV: Dissemination and Implementation.

As a result of Phase I of the project, four Peruvian historic earthen buildings representing typologies, designated as prototype buildings, were selected: the church of Santiago Apóstol de Kuñotambo (the church of Kuñotambo) (KT), near Cusco; the Ica Cathedral (IC); Casa Arones (CA), Cusco; and Hotel El Comercio (HC), Lima. Visual inspection and damage identification were the final goals of the first phase and resulted in a publication in two volumes: *Seismic Retrofitting Project: Assessment of Prototype Buildings* (Cancino and Lardinois 2012). Phase II of the project consisted of the assessment of the current conditions of the prototype buildings through numerical modeling and testing on the main structural materials and components (Torrealva, Vicente, and Michiels 2018). Phase III involved the design of the seismic retrofitting solutions, the testing of the techniques, and the modeling of the prototype buildings, together with the designed retrofitting solutions. Finally, Phase IV, in progress, consists of the dissemination and implementation of the retrofitting projects for the sites.

## Objectives

This publication presents the main results of the numerical modeling performed on the four prototype buildings. The buildings have been studied in their current condition (Phase II) and in their retrofitted configuration (Phase III). This report is intended to be used for dissemination to the engineering community of advanced numerical modeling approaches used on historic adobe structures. A brief description of the case studies is provided in chapter 2 and a detailed description of the approach followed for the advanced numerical modeling strategies is given in chapter 3. Specific attention is paid to the characterization

of structural materials and to the definition of safety levels for historic buildings. Following evaluation of the seismic capacity of the structures studied, retrofitting solutions are presented for those buildings for which necessary strengthening is significant and being implemented. Chapter 4 addresses performance of the church of Kuñotambo and the Ica Cathedral for the unstrengthened and strengthened numerical models. Finally, the studies performed on Casa Arones and Hotel El Comercio in their current conditions are presented in chapter 5. Guidelines are available on usage of advanced computations for structural engineers, as well as on usage of simplified approaches for safety assessment and strengthening design for practitioners (structural engineers and technical architects) (Lourenço and Pereira 2018).

The 3D numerical models of the structures, characterization of the material properties, and damage comparison are based on visual inspection of the four prototype buildings and the testing program performed in the previous phases of the SRP (Cancino and Lardinois 2012; Torrealva, Vicente, and Michiels 2018; Lourenço, Karanikoloudis, and Greco 2016).



## Brief Description of the Case Studies

### The Church of Santiago Apóstol de Kuñotambo

Dating to 1681, the Church of Santiago Apóstol de Kuñotambo (the church of Kuñotambo) is a religious structure of the seventeenth century and is representative of churches built in the Andes during the period of the Spanish viceroyalty. It stands as a typical example of churches or chapels in the Peruvian highlands that consist of a single nave leading to an elevated presbytery and altar, with an adjacent sacristy and baptistery (figs. 2.1a, 2.1b). The walls and buttresses are made of adobe masonry, with a single-gable timber roof. The structure is built on a base course plinth of rubble stone masonry with earth mortar over a sloping natural rock, with varying layers of compacted clay. The historic significance of the church lies in the fact that it has retained much of its authenticity, with a limited number of past interventions, and that mural paintings are present in the interior (fig. 2.2).

FIGURES 2.1A, 2.1B.

Church of Kuñotambo: (a) aerial view (adapted from Cancino and Lardinois 2012); (b) view of the main facade (facing east) (photo: Scott S. Warren for the GCI, 2011).



(a)



(b)

FIGURE 2.2.

Mural paintings on the interior of the north lateral wall of the church of Kuñotambo (Percy et al. 2013).



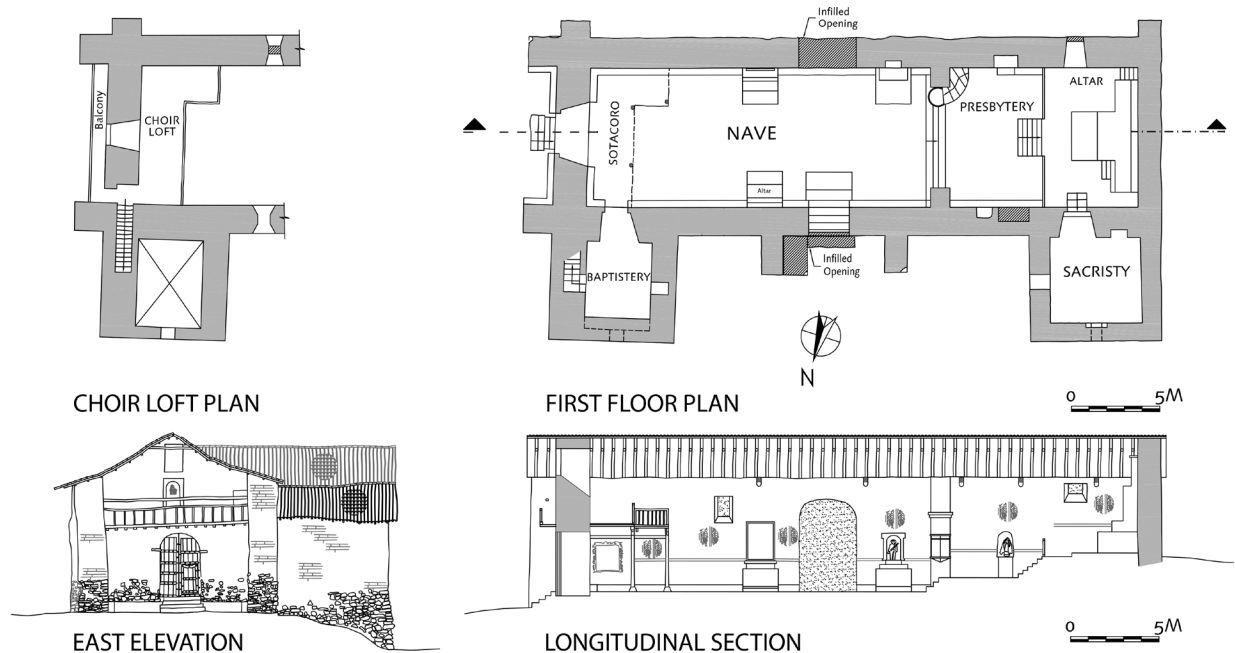


**FIGURE 2.3.** Architectural plans and elevations of the church of Kuñotambo (north is indicated in the first-floor plan) (Cancino and Lardinois 2012).

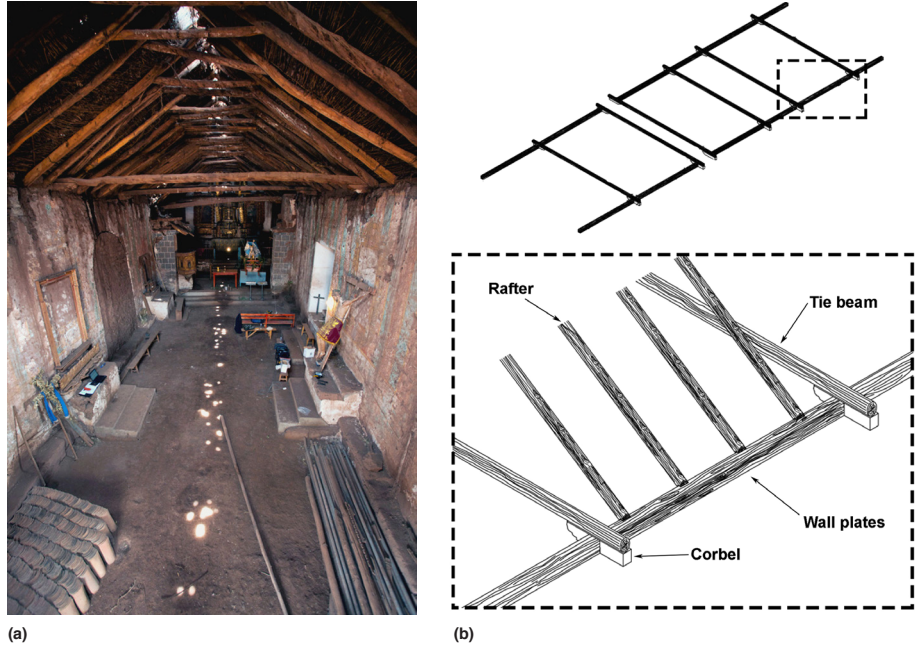
The church is characterized by a relatively simple geometry of two longitudinal walls and two gable walls (facades), with a maximum height of 6.6 m from ground level (fig. 2.3). Due to the sloping ground, the base course rubble stone masonry varies in height, typically between 1.2 m and 1.5 m, with extremes of 3.5 m at the northeast corner of the baptistery. The lateral walls have been strengthened with buttresses of adobe masonry placed on either side of the currently infilled openings; however, at the south facade, the buttresses seem to have collapsed and only parts of their base courses remain. Extensions of walls beyond the corner intersections also serve as buttresses.

The roof system is single gable, with trusses composed of two rafters (wood trunks) joined with timber collar ties by means of nails and leather straps. The trusses are very weakly connected to a ridge beam on top (small cross section and noncontinuous), with leather straps, ropes, and wrought-iron nails. The roof cover is composed of canes, a layer of earth and straw, and clay roof tiles. Embedded timber wall plates run along the lateral walls and serve partly to support the rafter ends. These wall plates are not continuous and are partly nonexistent. In total, six timber ties run along the span of the nave at the eave level of the lateral walls. They are placed on top of embedded corbels and between the timber wall plates. The whole system is discontinuous and does not act as a ring beam. Two additional timber ties, at the far east ends of the lateral walls and in the timber beam of the choir loft, appear to help brace the roof of the nave (figs. 2.4a, 2.4b). In the roofs of the baptistery and sacristy, there are no wall plates; the rafters sit directly on top of the adobe walls. Adjacent to the interior face of the east facade is the choir loft. There is also an exterior balcony, with wood joists cantilevered from the wall of the east facade (Cancino and Lardinois 2012).

Structural damage was observed to have been influenced by the poor connection between parts and by erosion from improper drainage and maintenance (Cancino and Lardinois 2012). The main facade has vertical cracks at both ends, visible from the exterior and interior, as shown in figures 2.5a–c. The size and extent of these cracks are indicative of low connectivity between walls, but no horizontal cracks are present. Also, the baptistery presents cracks in the corners and in the middle span of the walls (Cancino and Lardinois 2012). The lateral walls exhibit signs of erosion on the exterior surfaces and many altera-

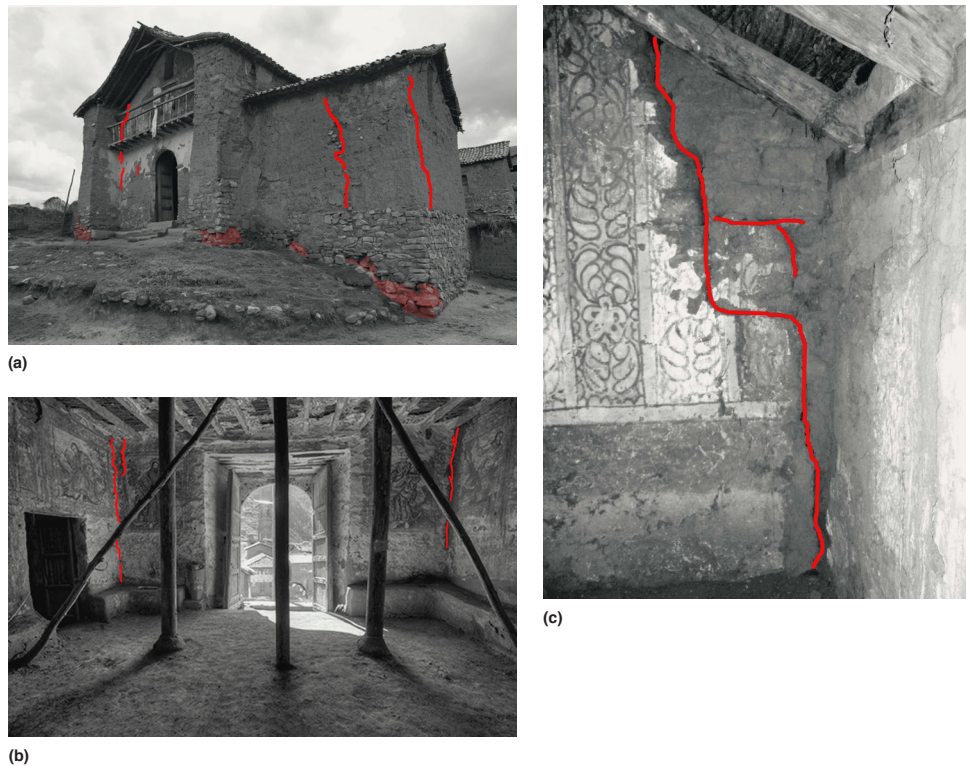
FIGURES 2.4A, 2.4B.

Timber roof system of the church of Kuñotambo: (a) interior view of the main nave, looking west (photo: Scott S. Warren for the GCI, 2011); (b) structural scheme of the wall plates, corbels, and tie beams, with diagram (inset) showing the connection between the rafters and wall plates (adapted from Cancino and Lardinois 2012).



FIGURES 2.5A–C.

Photos of damage inspection on the church structure, showing crack patterns or propagation (in red): (a) crack patterns and areas of material loss in the main facade and baptistery; (b) crack patterns in the interior of the main facade (adapted from De Corso 2013); (c) crack propagation in the south corner of the choir loft (photo: Scott S. Warren for the GCI, 2011).



tions, such as the opening or filling of doors and niches. The south lateral wall exhibits outward displacements. On the north lateral wall there are several vertical cracks close to the east side. The damage found can be related to settlements of the base course, magnified by rising damp, loss of mortar or erosion below the base course, and possible past earthquakes (Cancino and Lardinois 2012). In many areas, the base course has evident signs of erosion and deterioration, with loose stones and missing mortar from joints. Mapping of damage to the facades is shown in figure 2.6.

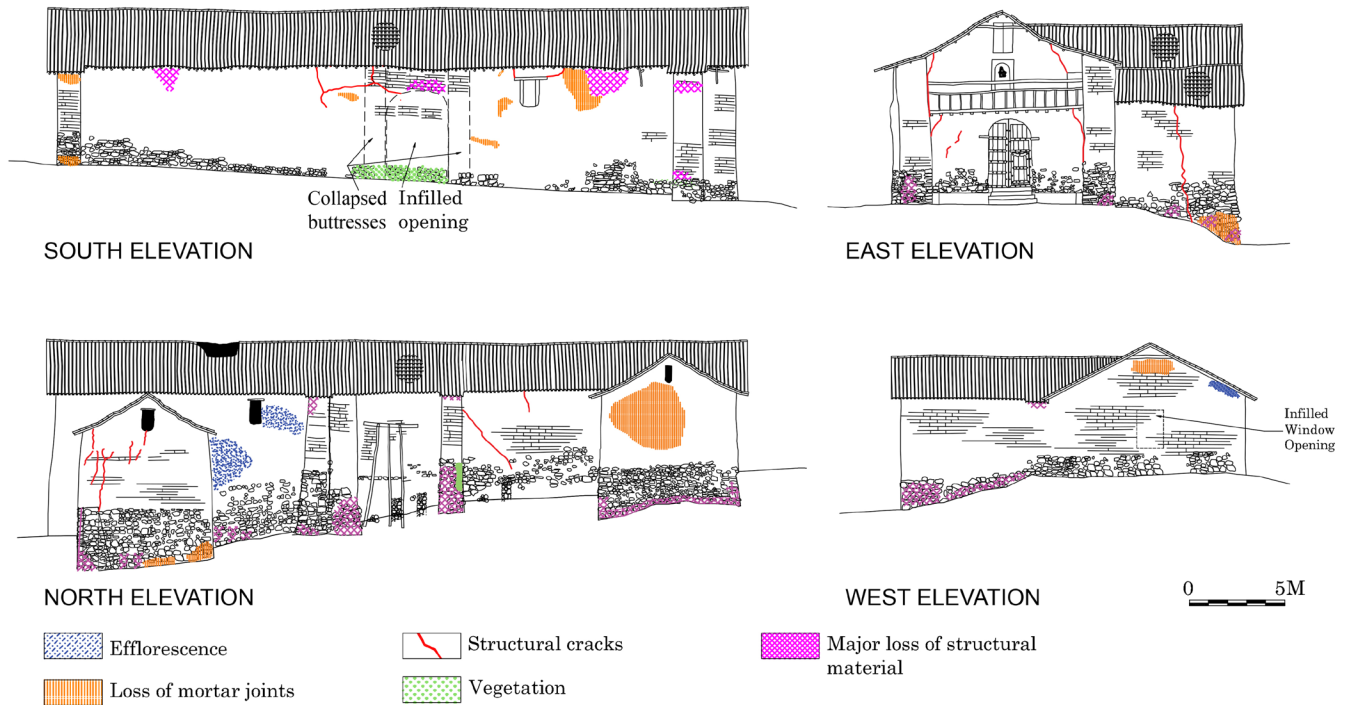


**FIGURE 2.6.**  
Elevations of the church of Kuñotambo, indicating the various types of damage observed (Zanotti 2015).

## The Ica Cathedral

Considered a national monument since 1982, the Ica Cathedral is representative of churches built during the viceroyalty of Peru (figs. 2.7a, 2.7b). Located in the historic center of Ica, at the corner of Jirón Libertad (Libertad Street) and Jirón Bolivar (Bolivar Street), the cathedral is adjacent to a cloister and a single-story adobe construction to the south, while a three-story concrete and fired-brick structure is located toward its western side (Cancino and Lardinois 2012).

Accessible by two entrances, one at the front facade and one at the northern wall, the rectangular plan of the cathedral consists of the main entrance, above which rests the choir loft—the so-called *sotacoro*—flanked by two lateral extensions; the main nave, with four rectangular bays; two side aisles composed of four square bays each; the transept; and the altar, flanked by two chapels on its lateral sides (fig. 2.8). Other spaces are present at the back of the building, including the sacristy, a reception area, a deposit, offices, and an internal courtyard.

**FIGURES 2.7A, 2.7B.**  
Photos of the Ica Cathedral in its current condition: (a) front facade; (b) nave, looking toward the altar.

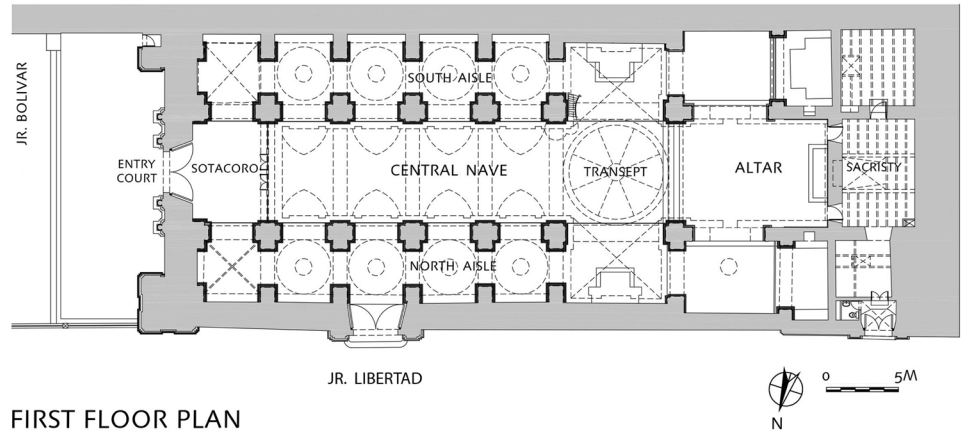


(a)

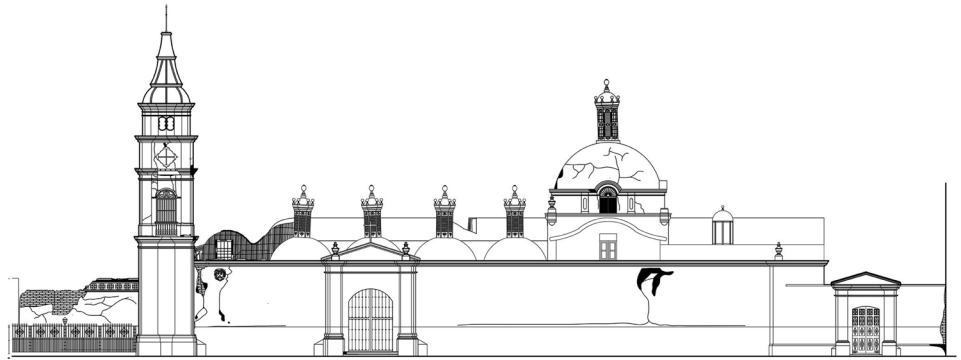


(b)

**FIGURE 2.8.**  
Architectural drawings of the Ica Cathedral (Cancino and Lardinois 2012).



FIRST FLOOR PLAN



NORTH ELEVATION (JR. LIBERTAD)

The structural system of the cathedral can be divided into two main parts: an external masonry envelope and an internal timber frame. The massive load-bearing masonry envelope consists of the front facade with two bell towers, two lateral walls, and the back facade, which is not visible externally (figs. 2.9a–c). Measuring 21 m in length, the neoclassical front facade is made of fired-brick masonry with a thickness that varies with height, ranging from 2.25 m at its base to approximately 0.60 m at the top. The bell towers are composed of timber frames made of posts resting on wooden plates embedded in the brickwork of the bases.

**FIGURES 2.9A–C.**  
Photos of the masonry envelope of the cathedral, showing (a) southern bell tower; (b) northern lateral wall; (c) detail of the northern lateral wall, showing the different masonries.



(a)



(b)



(c)

Both lateral walls are constructed of adobe masonry, with a slenderness ratio of approximately 3.35 (see fig. 2.9b). The northern lateral wall, which faces the street, rests over a 0.90-m-high fired-brick masonry base course on top of a 0.40 m rubble stone masonry wall (see fig. 2.9c). The height of the base course in the southern lateral wall is 0.60 m, while the rubble stone wall is 0.48 m deep. A series of adobe piers, connected to the lateral walls by fired-brick connections, supports the beams of the internal timber structure (Cancino and Lardinois 2012).

The internal space of the Ica Cathedral is divided by a series of pillars, pilasters, and piers that support the complex roof framing system (figs. 2.10a–c). The timber elements, which are made of different wooden species and connected using several types of timber joints, are constructed by applying the technique of *quincha*. *Quincha* was originally used to construct primitive huts with frames made from branches and trunks of small trees that were tied together using vegetal fibers and covered with mud. Currently, the term is used for a variety of traditional systems involving timber and earth in Latin America (Ciocci, Sharma, and Lourenço 2018).

FIGURES 2.10A–C.

Photos of the timber structure of the cathedral, showing (a) pilaster; (b) barrel vault; (c) dome.



(a)



(b)



(c)

The pillars and pilasters are composed of numerous posts with a wood sill plate embedded in the fired-brick base. Horizontal and diagonal timber elements are used to brace these posts. These hollow structures are wrapped with flattened cane reeds (*caña chancada*), which are attached to the battens using nailed leather strips and finished with earth plaster and gypsum. The complex roof system consists of several structural systems, including domes, barrel vaults, and flat ceilings. *Caña chancada* and cane reeds finished with layers of mud plaster (*caña brava*) cover the intrados and extrados of the vaulted roofing frame, respectively, whereas layers of fired-brick masonry and sand, lime, and cement mortar cover the flat wooden ceiling. A detailed description of the complex timber system is given in Cancino and Lardinois (2012). The geometry of a representative bay of the cathedral is illustrated in figure 2.11.

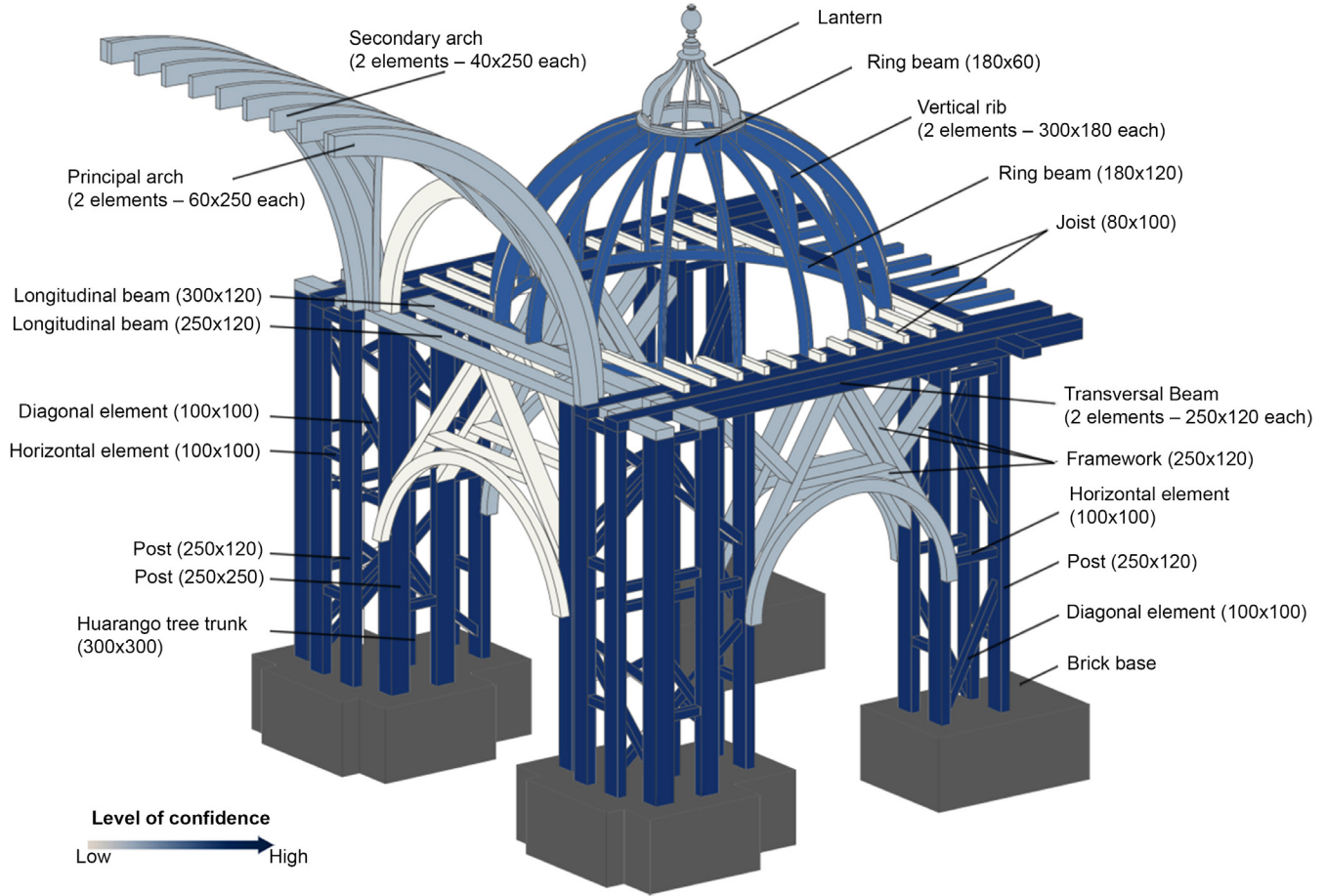


**FIGURE 2.11.** Geometrical drawing showing the main elements of a representative bay of the cathedral. Dimensions are in mm.

**FIGURE 2.12.** Damage maps of the cathedral, showing structural cracking (in red) after the 2007 Pisco earthquake. Adapted from Cancino and Lardinois (2012).

Historically, the Ica Cathedral has suffered heavy damage, mainly due to the large number of earthquakes that have affected this area. Partial collapses from the 2007 Pisco earthquake (fig. 2.12), which were later aggravated by another seismic event in 2009, have led to the cathedral not being currently in use. Collapses of the interior timber frame of the cathedral are mostly in the roof structure, namely the central dome, the barrel vaults covering the main nave, and the roof over one of the bays near the southern aisle (figs. 2.13a–d). In addition, extensive cracking, displacements, loss of connection between structural members, and other damages are observed throughout the interior and the roof structure. A rocking mechanism of the pillars was observed during the 2007 Pisco earthquake with loss



**FIGURES 2.13A–D.**

Photos of the current damage to the cathedral, showing (a) collapse of the central dome; (b) partial collapses of the roofing system; (c) cracks separating the pediment from the lower part (photo: Scott S. Warren for the GCI, 2011); (d) horizontal and vertical cracks in the northern wall.



(a)



(b)



(c)



(d)

of connection between the pillars and their base, and between the pillars and the timber structure above. However, failure of the beams at the top of the lunettes is thought to be the main reason for the collapse of the roofing system (Cancino and Lardinois 2012).

Cracking, loss of connection, and out-of-plane deformations can be observed also in the masonry envelope, particularly in the main facade and the northern wall. The main facade is characterized by horizontal cracks between the pediment and the lower part (see fig. 2.13c). Extensive damage is present also at the connection of the bell towers with the front facade and lateral walls. The northern lateral wall presents horizontal cracks at the interface of the different types of masonry, as well as vertical cracks at the connection with the internal timber structure (see fig. 2.13d) (Cancino and Lardinois 2012).

## Casa Arones

Casa Arones is a representative example of a two-story *casona* (large house) located in the heart of Cusco, at the corner of Calle Arones and Calle Nueva Alta (fig. 2.14). It is thought to have been built by the end of the sixteenth century (Cancino and Lardinois 2012). Originally a residential building with ground-floor commercial spaces, it has been significantly altered, becoming a multifamily residential building. As shown in figures 2.15a and 2.15b, the building sits on a slope.

The main volume of the building is situated in an L shape, with two arcades parallel to Calle Nueva Alta, an interior patio, and a longitudinal wall along Calle Arones, which is the only extant remains of the rear-collapsed area (fig. 2.16). Access is provided from a portal on Calle Arones (east side) leading to the interior patio through a masonry arch. The external slope of the street defines the floor level of the rooms on the main floor. The second story is accessible by a staircase and a timber-cantilevered balcony.

**FIGURE 2.14.**  
View of Casa Arones (© 2018  
Google).



**FIGURES 2.15A, 2.15B.**  
Elevations of Casa Arones: (a) view  
from Calle Nueva Alta; (b) view  
from Calle Arones (Cancino and  
Lardinois 2012).

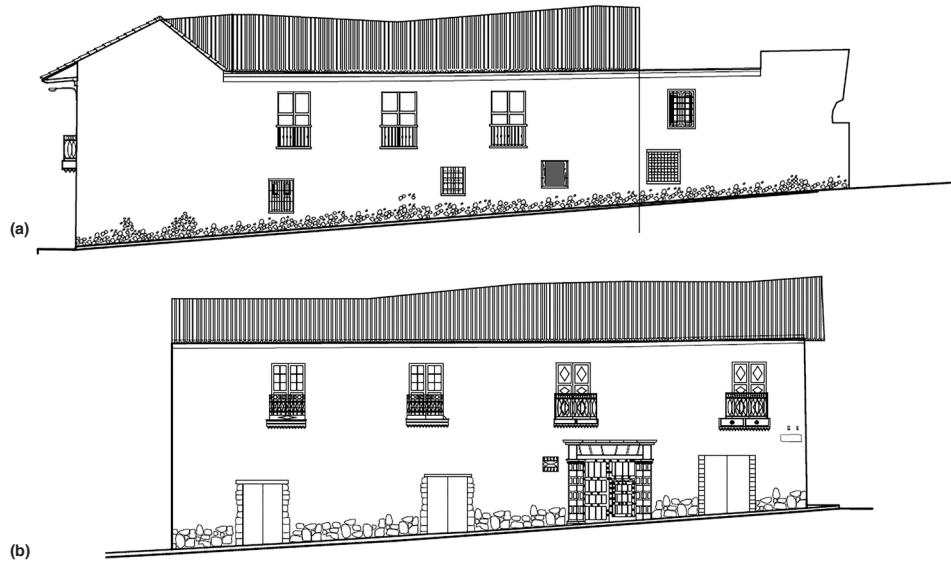
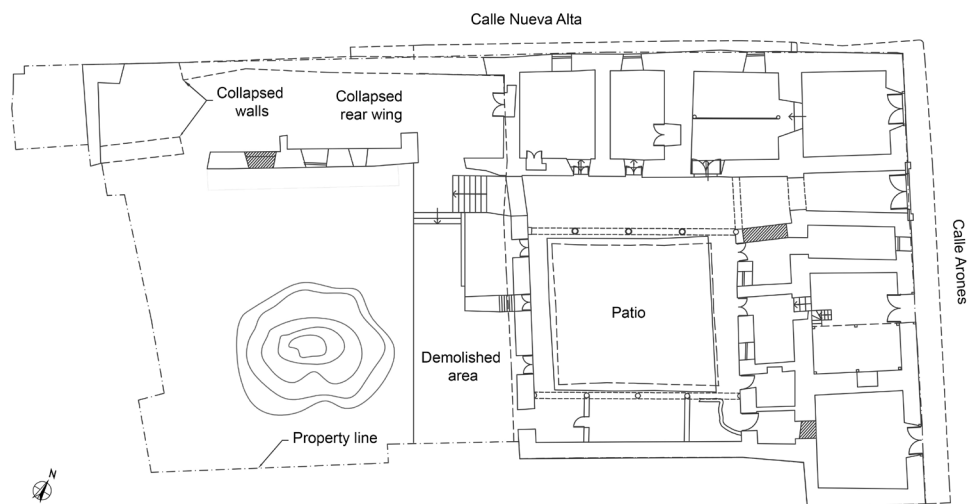


**FIGURE 2.16.**  
Main floor plan of Casa Arones  
(Cancino and Lardinois 2012).

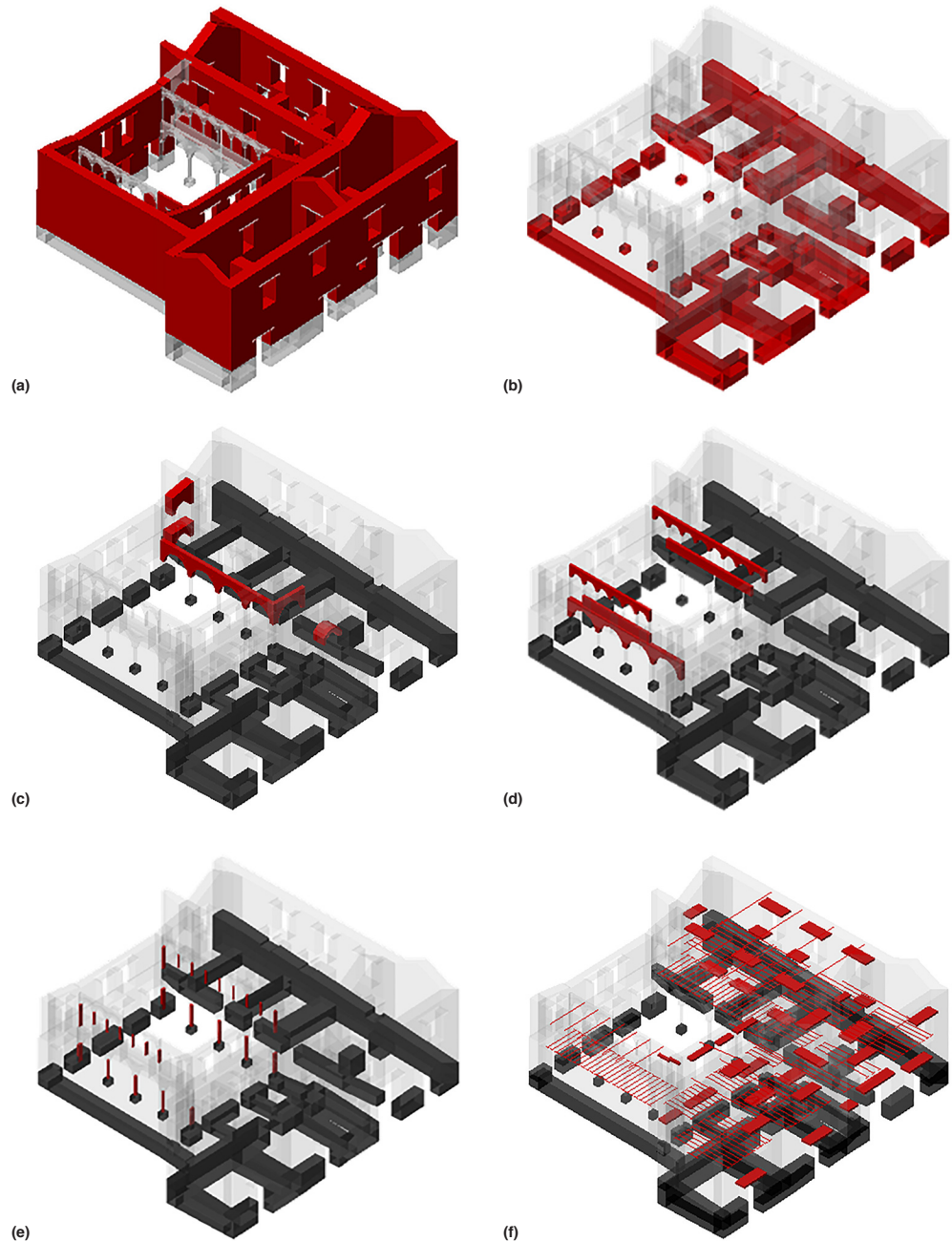


The house's extensive damaged condition seems to be the result of abandonment, lack of maintenance, and, possibly, past earthquakes. The rear part of the building collapsed and is under partial reconstruction (currently stopped). There is a massive presence of temporary shoring to support the sagging floors and roofs and to prevent out-of-plane movement of the arcades.

The presence of plastering and wallpaper makes it difficult to identify wall materials, and the building's precarious condition makes it less accessible for in situ testing. Still, the structure is mainly composed of load-bearing adobe masonry walls (figs. 2.17a–f), together with some internal partitions and stone and brick masonry arcades. The internal partitions, perpendicular to the main walls, are made of quincha and are not structurally connected

FIGURES 2.17A–F.

Diagrams identifying areas (in red) of structural materials in Casa Arones: (a) adobe masonry, in the walls of the structure; (b) rubble stone masonry, in the base course foundation of the walls; (c) fired-brick masonry, in the first level of the arcade facing Calle Nueva Alta and in the internal arches; (d) stone masonry, in the arcades of the patio; (e) stone, in the columns of the patio; (f) timber, in the lintels above the openings and in the floor and roof structures.



**FIGURES 2.18A–E.**

Photos showing main cracks (in red) on the second floor: (a) south wall; (b) longitudinal wall on Calle Arones; (c) central transversal wall on Calle Arones; (d) south transversal wall on Calle Arones; (e) west transversal wall on Calle Nueva Alta.



to the walls (Cancino and Lardinois 2012). The slenderness of the adobe masonry walls is around 6 to 8, with a thickness of about 1 m (Cancino and Lardinois 2012). On the second floor, rooms have large spans due to the lack of transversal walls. The walls present several openings, usually not aligned between the first and second levels, with a timber lintel above each opening. The adobe walls rest on a base course and foundation made of rubble stone masonry (see fig. 2.17b), even if their morphology is not fully known (Cancino and Lardinois 2012).

The two arcades present a similar structure, with wider arches on the main floor and smaller span arches on the first floor. The first floor is representative of a typical timber structure of the *casernas*, with parallel timber joists embedded in the adobe masonry covered by several thick layers of mud and straw (Cancino and Lardinois 2012). The roof structure of the main L-shape volume of the building is constructed using the traditional *pares y nudillos* system (rafters and collar tie system) that is very popular in Latin America.

Several important cracks are present, as shown in figures 2.18a–e. Diagonal cracks are found in the connection between the external wall on Calle Arones and the transversal walls. The south wall has several vertical cracks, and shear cracks were found on the west transversal wall on Calle Nueva Alta. The longitudinal wall along Calle Arones also has several cracks. Finally, the stone blocks are in good condition, but the joints have suffered a significant loss of mortar combined with cracking and deformation in the arcades (figs. 2.19a, 2.19b). A temporary shoring system is present, but the west end of the arcades remains unstable.

Finally, other extensive damage is present, such as that caused by humidity and rising damp at foundation level and erosion of the external layer of the adobe walls. The structure

FIGURES 2.19A, 2.19B.

Photos identifying damage (in red) in the arcade between the first and second floors: (a) crack on the parapet approaching the north side; (b) cracks on the arch of the second floor on the north side.



of the roof shows large deformation, loss of material, and rotten timber elements. This condition allows rain to further damage the building. As stated earlier, most floors are significantly deformed, compromising the safety and use of the rooms.

## Hotel El Comercio

Hotel El Comercio is a typical three-story *casona* situated in Lima at the corner of Jirón Carabaya and Jirón Ancash, near the Government Palace and Plaza Mayor (figs. 2.20a, 2.20b). The site dates to the mid-nineteenth century as a reconstruction following the earthquake of October 28, 1746. The building is now owned by the Ministerio de Cultura del Perú and is mostly uninhabited and in a state of decay, excluding a few commercial activities carried out on the first floor (Cancino and Lardinois 2012).

Presenting an L-shape construction, Hotel El Comercio is built around two interior patios, with the longest wing surrounded by a four-story concrete building on Jirón Carabaya and a two-story adobe-and-quincha *casona* on Jirón Ancash. The shortest wing, facing Jirón Carabaya (called left wing), is the only part still in use. The farther end hosts El Cordano, a historically and socially significant bar. Out of the six portal openings at Jirón Carabaya, a wooden double door at the west end opens into the entry hall and, through this, into the first patio. Both patios are surrounded by open galleries on the second and third floors.

Upon inspection, uniform materials and techniques were recognized, confirming a single phase of construction for the whole building except for a few localized interventions that were easily recognizable and relevant to the structural behavior (Cancino and Lardinois 2012). The area of El Cordano bar was subject to the main alterations, as some of the

FIGURES 2.20A, 2.20B.

Views of Hotel El Comercio: (a) northeast view (Cancino and Lardinois 2012); (b) satellite image of the structure in the historic center of Lima (© 2018 Google).

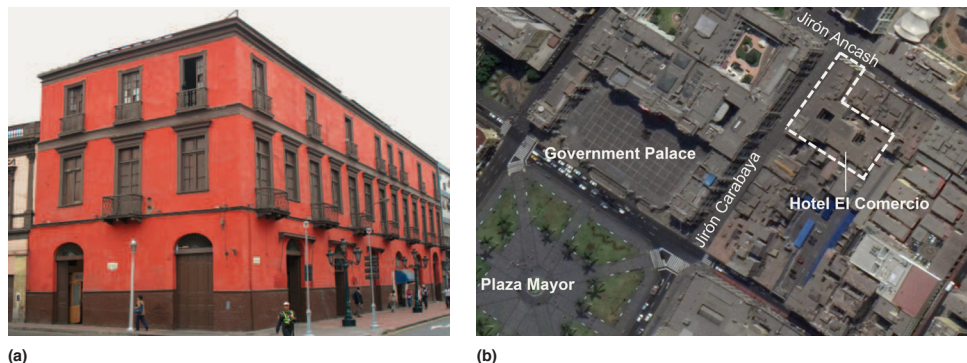
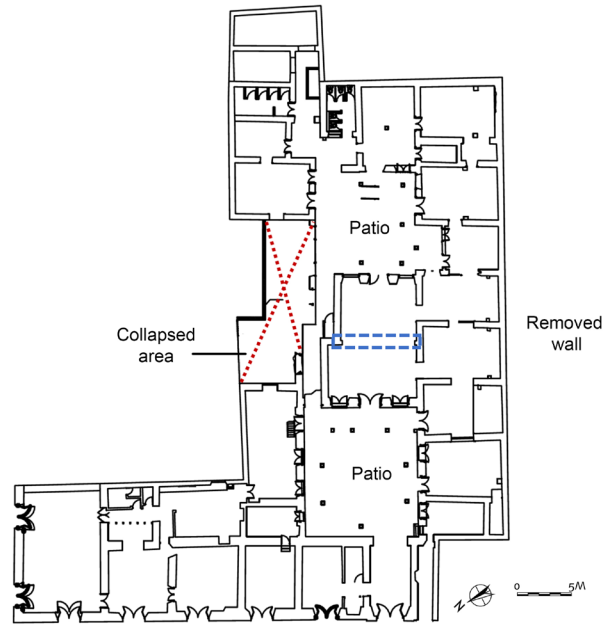


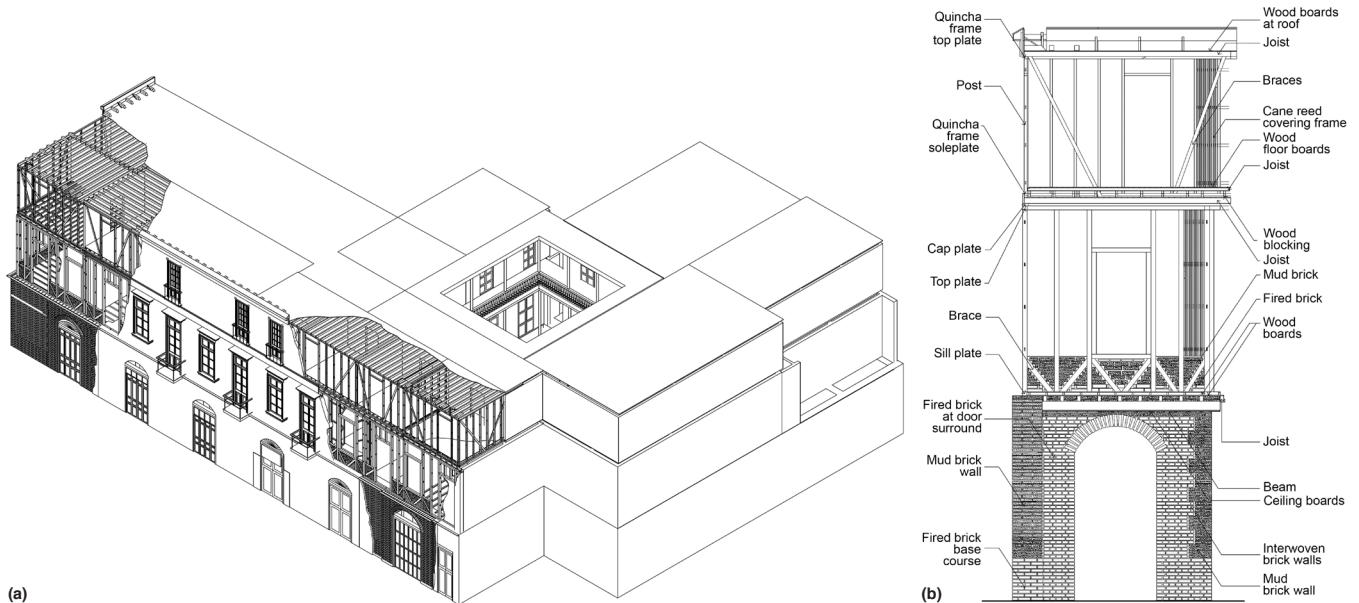
**FIGURE 2.21.**  
First-floor plan of Hotel El Comercio. The dashed line indicates the collapsed area. Adapted from Cancino and Lardinois (2012).



adobe walls were cut or replaced by metal or wooden columns and by reinforced lintels. Shoring elements were found to have replaced a wall removed between the patios, indicated in figure 2.21.

Hotel El Comercio rests on damp soil containing a large quantity of cobblestones. The foundation is composed of rubble stone masonry set in a lime-and-sand mortar, with a depth of 0.5 m, under the patio pavement level. A base course in fired-brick masonry rests above it, rising to a height of 0.7 to 1.0 m above the finished floor level. Fired brick also surrounds the arched door opening on the patio and on the streets, with a width ranging from 0.4 to 1.0 m, through the full depth of the wall. The first story is made with adobe walls, whereas the second and third stories have quincha walls that are taller and thicker in the second story than in the third (Cancino and Lardinois 2012). Structural elements are shown in figures 2.22a and 2.22b.

**FIGURES 2.22A, 2.22B.**  
(a) Architectural drawing showing overall structure, and (b) elevation showing structural elements of Hotel El Comercio (Cancino and Lardinois 2012).



**FIGURES 2.23A, 2.23B.**  
 Photos showing collapsed area in Hotel El Comercio: (a) northwest view; (b) southeast view.



(a)



(b)

The second and third floors are constructed with several layers composed of wooden boards over wooden joists. Wooden sleepers rest above these elements, to increase the floor level, and at the second story, to accommodate a mud and lime-based mixture. The joists of the second story are covered by wooden boards that provide a finished ceiling for the room below, whereas the joists of the third story are exposed. The roof is constructed in the same way, with the joists exposed (except for several layers of mud and straw), over the wood decking up to 0.11 m (Cancino and Lardinois 2012).

The lack of maintenance led to localized damage in the quincha panels, including cracks, plaster detachment, and exposure of the internal wood structure to deterioration. The section between the two patios, adjacent to the two-story *casona*, has collapsed (figs. 2.23a, 2.23b; see fig. 2.21). Humidity due to improperly installed plumbing or improper site drainage was likely the cause of localized damage in the adobe.

## Modeling Approach

In most engineering applications, masonry is assumed as a continuous and homogeneous material for modeling purposes, usually isotropic (Lourenço and Pereira 2018). Masonry behavior is affected by the characteristics of its components (units, mortar, and interface), even if they are not represented in a discrete way. This strategy is the most appropriate for large-scale models and allows optimization of time and storage requirements to develop the model (implementation of the geometry and generation of the mesh) while providing adequate results for the analyses (Lourenço 1996). The commercial software DIANA, with Midas FX+ Version 3.3.0 Customized Pre/Post-processor, is used for finite element discretization and for nonlinear analysis, based on a developed 3D CAD model (DIANA 2014).

The four prototype buildings selected for the SRP—the church of Santiago Apóstol de Kuñotambo (church of Kuñotambo), the Ica Cathedral, Casa Arones, and Hotel El Comercio—are represented in their current configuration. Their geometry includes some of the alterations carried out over the years as well as the collapsed parts, where relevant to the global seismic behavior of the building. It is noted that these are prototype buildings of different typologies in Peru; that is, their study aims to provide a representation of the structural behavior of similar structures under horizontal loading, assuming that they are in use and reasonably well maintained. Therefore, the buildings are modeled in their original, undamaged conditions. This reflects the fact that, as a minimum intervention technique, the buildings need to be repaired to a condition similar to that of the original. The approach adopted also allows comparison of the damage obtained with the unstrengthened numerical models after the load application with the current damage observed during the surveys. Comparison between the analytical results and the reality allows model validation.

The numerical models of the church of Kuñotambo, the Ica Cathedral, and Casa Arones are characterized by a similar finite element model discretization. The base course, foundations, walls, and lintels have been represented by 3D solid elements, whereas the timber elements have been represented using linear-type elements (trusses or beams). As needed, spring elements have been introduced to replicate boundary conditions with adjacent buildings. A different approach was followed for Hotel El Comercio, given its large size and structural configuration. In this case, the adobe walls, the quincha panels, and the floors are modeled using shell elements. The internal timber and steel columns, together with the post of the quincha panels, are modeled again with linear-type elements (beams).

A detailed description of the finite element mesh of each prototype building is given in this chapter. The chosen material behavior for the different structural materials is described in the next section, followed by the section on material properties.

### Material Model

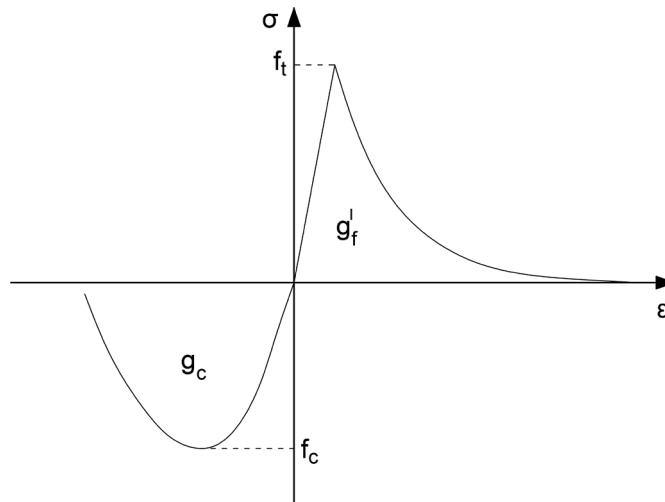
Nonlinear material models have been specified for the prototype buildings (Lourenço and Pereira 2018). The total strain rotating crack model (DIANA 2014) is used for masonry

(either stone, fired brick, or adobe) and is explained below. The von Mises model was also used as a simple stress limiter in timber and quincha walls.

### Total Strain Rotating Crack Model

The physical, nonlinear compressive and tensile behavior of masonry is described through a total strain rotating crack model, replicating the elastic phase through material degradation until total loss of strength (fig. 3.1). This constitutive law assumes a smeared approach for the fracture energy and describes the stress  $\sigma$  as a function of the strain  $\epsilon$ , evaluating a relationship in the principal directions of the strain vector. The total strain rotating crack model requires, as input, two sets of properties: a first set collects the basic elastic mechanical properties (Young's modulus and Poisson's ratio); a second set defines tensile and compressive inelastic behavior, with a tensile strength of  $f_t$  and a compressive strength of  $f_c$ . Cracking is quantified by the integral of the stress-strain diagram, denoted as fracture energy  $g_f$  for tension and  $g_c$  for compression. Tensile stresses are assumed to diminish exponentially (softening), while compression combines a hardening parabolic phase and a softening parabolic phase.

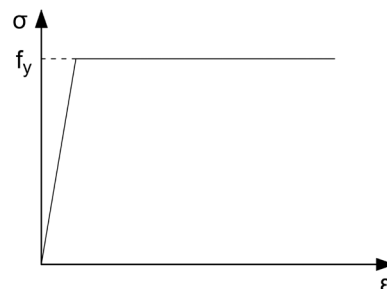
FIGURE 3.1.  
Stress-strain relationship for the total strain rotating crack model (DIANA 2014).



### Von Mises Model

The von Mises stress model is used to predict yielding of materials under any loading condition from the results of simple uniaxial tensile tests. Figure 3.2 shows the stress-strain relationship adopted for the von Mises model (ideal plasticity). This model was used as a stress limit, mostly in timber elements, with a maximum stress in tension or a compression of  $f_y$ , known as yield strength.

FIGURE 3.2.  
Stress-strain relationship for the von Mises model (ideal plasticity) (DIANA 2014).



## Material Properties

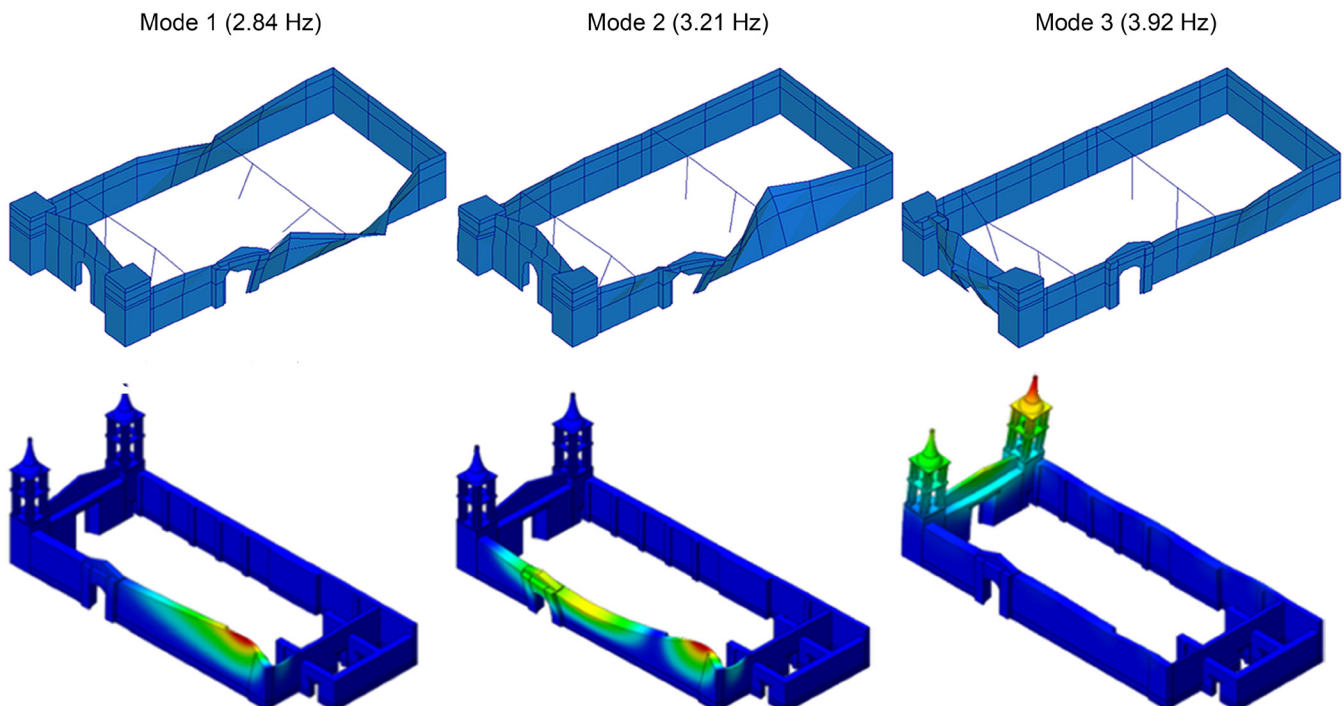
The material properties for the prototype buildings were determined from literature, standards, the experimental campaign conducted by the Pontificia Universidad Católica del Perú (PUCP) in 2011 and 2012, and the on-site testing campaign conducted by the University of Minho in May 2015 (NTC 2008; EC6 2005; FEMA 306 1998; IS 13827 1993; Torrealva, Vicente, and Michiels 2018; Lourenço, Karanikoloudis, and Greco 2016; Angelillo, Lourenço, and Milani 2014). The sections that follow present the approach adopted for the definition of elastic and nonlinear material properties.

Design resistance values for structural members are usually derived from characteristic values of strength properties, which correspond to a fractile of 5%. In historic structures, lower partial safety values are often used (NTC 2008). For low mechanical properties of adobe masonry and the usage of properties such as (a vanishing) tensile strength, usually considered as zero for design, nominal values for the properties may be used. In the case of nonlinear structural analysis, the overall response should, in any case, be based on average, unreduced values of strength (Tomažević and Lutman 2007).

In addition to the visual inspection in Cancino and Lardinois (2012), sonic testing and dynamic identification testing were carried out in the prototype buildings. Sonic tests allow Young's modulus to be obtained based on local readings. Dynamic tests can help determine the actual structural behavior and damage condition. Once the dynamic properties of a structure are known experimentally (frequencies and mode shapes), the mechanical properties of the numerical model (mass and stiffness) can be adjusted to resemble the properties observed. This process is known as model updating and provides a measure of the global Young's modulus of the structure (Lourenço et al. 2012).

A calibration of the numerical model of the Ica Cathedral and the church of Kuñotambo was conducted. As an example, figure 3.3 shows the comparison of mode shapes obtained

**FIGURE 3.3.**  
Comparison of mode shapes obtained experimentally and numerically for the Ica Cathedral (Ciocci, Sharma, and Lourenço 2018).



experimentally and numerically for the Ica Cathedral. Note that the safety assessment of the Ica Cathedral was performed using the updated model; more details are provided in Ciocci, Sharma, and Lourenço (2018). The model updating for the church of Kuñotambo was extremely complex given the interfaces from numerous vertical cracks, and was used only for understanding the current level of damage and connectivity between parts. Dynamic tests, available from previous testing campaigns at Hotel El Comercio, were also used (Aguilar et al. 2012).

### **Masonry**

Adobe masonry is the main structural material in the prototype buildings. The mechanical properties of adobe masonry have a wide range of variation depending on soil characteristics and workmanship. Compressive strength is mostly dependent on the properties of the adobe blocks and the thickness of mortar joints (Paulay and Priestley 1992). Yet, the heterogeneity and large scatter of adobe masonry mechanical properties are evident even on a given site (Lourenço and Pereira 2018). An average compressive strength of 0.45 MPa was obtained from compression tests on adobe wallets, taken from the Ica Cathedral and from two sites in the center of Lima (Torrealva, Vicente, and Michiels 2018). The value for Young's modulus  $E$  ranged from 70 to 100 MPa. Considering the low results from the dynamic identification performed on the church of Kuñotambo and the Ica Cathedral, as well as the results of the sonic testing, values in the range of 250–275 MPa were adopted. A value of tensile capacity equal to 0.05 MPa was considered for the adobe masonry (Lourenço and Pereira 2018).

Rubble stone masonry characterizes the foundation of the buildings, and in some of the buildings it is present until a certain height, defining the base course level. The mechanical properties were specified from minimum reference values for rubble stone masonry (OPCM 3431 2005) as 0.6 MPa for the compressive strength. Young's modulus  $E$  is usually associated with the compressive strength  $f_c$  by  $E = 550f_c$  (Lumantarna, Biggs, and Ingham 2014), which corresponds to a value of 300 MPa. Still, a value of 690 MPa specified for Hotel El Comercio was used as the minimum value recommended from the Italian code for irregular stone masonry (NTC 2008). After calibration of the models of the church of Kuñotambo and the Ica Cathedral, values of 1570 MPa and 720 MPa were found, respectively. This confirms how difficult it is to estimate Young's modulus, even if this value has very low influence on the maximum lateral base shear capacity of these structures, mostly defined by their geometry. Conversely, the influence of this parameter in displacements is obviously very high. For the tensile bond strength of rubble stone masonry, the assigned tensile strength is slightly higher, 0.06 MPa, than adobe masonry.

Fired-brick masonry characterizes the base course of Hotel El Comercio, the Ica Cathedral, and parts of the arcades of Casa Arones. The tests performed on the masonry wallets extracted from Hotel El Comercio were considered in defining the mechanical capacity of the fired-brick masonry (Torrealva, Vicente, and Michiels 2018). Thus, a value of compressive strength of 1.7 MPa was adopted. The results of Young's modulus obtained from the experimental campaign show a very high scatter, and hence they are not considered. A value close to the lower limit of the range of the suggested values by Tomažević (1999) is 340 MPa. Again, after the model updating, a value of 850 MPa was used for the fired-brick masonry of the Ica Cathedral. The bond strength of weak mortar fired-brick masonry is typically very low, ranging from 0.1 to 0.2 MPa (Pluijm 1999; Rots 1997), and a tensile strength of 0.1 MPa is assumed in the numerical model.

Finally, ashlar stone masonry is present in the arcades of Casa Arones. The value of the compressive strength and Young's modulus of stone masonry were taken from the

range prescribed by OPCM 3431 (2005). The assumed values correspond to a compressive strength of 3 MPa and Young's modulus of 2340 MPa. A value of 0.2 MPa was considered as tensile capacity of the stone masonry.

### Timber

The mechanical properties of timber depend on parameters such as density, shape and size, moisture content, and presence of defects. Different timber species are identified in the prototype buildings (Cancino and Lardinois 2012). Three main timber species compose the internal frame of the Ica Cathedral, the lintels, and the structure of the towers: huarango (*Prosopis* sp.), cedar (*Cedrela odorata* L.), and sapele (*Entandrophragma* sp.). In Hotel El Comercio, sapele, cypress (*Cupressus* sp.), and Oregon pine (*Pseudotsuga menziesii*) characterize the structures of the floors, quincha walls, and roof, respectively.

The density and Young's modulus of the existing timber adopted in the numerical model are based on the results obtained from the experimental campaign carried out by the Centro de Producción Forestal of the Universidad Nacional Agraria La Molina (UNALM) (Custodio, Mallque, and Delgado 2012). A summary of the material properties of the different types of timber adopted is given in table 3.1. It should be mentioned that, where applicable, the density values assigned to timber elements in the numerical models were increased to account for the weight of the quincha covering layers (Ciocchi, Sharma, and Lourenço 2018). The load-carrying capacities are assumed considering the structural wood classes recommended by the Peruvian code (E.010 2006). In particular, huarango corresponds to Class A, while sapele and cedar correspond to Class B. For the strengthening elements in the Ica Cathedral, the wood structural class was assumed as Class B. For the church of Kuñotambo, eucalyptus (*Eucalyptus globulus*) was used for the strengthening elements, corresponding to timber Class B.

TABLE 3.1.  
Material properties of the various wood species adopted in the numerical models, according to UNALM and the Peruvian code.

| Properties                   | Huarango<br>(Class A) | Oregon Pine<br>(Class B) | Eucalyptus<br>(Class B) | Cedar<br>(Class C) | Sapele<br>(Class C) | Cypress<br>(Class C) |
|------------------------------|-----------------------|--------------------------|-------------------------|--------------------|---------------------|----------------------|
| Density [kg/m <sup>3</sup> ] | 1040                  | 600                      | 560                     | 380                | 490                 | 470                  |
| Young's modulus [MPa]        | 16900                 | 10680                    | 9806                    | 9380               | 8610                | 5470                 |
| Poisson's ratio              | 0.3 (for all)         |                          |                         |                    |                     |                      |

The von Mises model yield criterion was applied to the following timber strengthening elements: the connecting elements between the internal timber structure and the strengthening embedded in the masonry envelope in the Ica Cathedral, and the embedded timber frame system and tie beams in the church of Kuñotambo. To apply the von Mises criterion and perform the verifications for the strengthening timber members, the expected mean values of the load-carrying capacities of the wood species were derived by applying the Peruvian code (E.010 2006) and the JCSS Probabilistic Model Code (JCSS 2006).

### Quincha Walls

Two different sets of material properties were considered for Hotel El Comercio for the quincha walls: the Test Data model involves the material properties from the PUCP testing campaign and the testing campaigns from the University of Bath and later the University College London, while the modal material model involves the material properties from the model updating of part of the structure using the dynamic identification test results (Aguilar

et al. 2012). To a large extent, this affects the quincha walls with dramatic consequences in terms of Young's modulus. In the Test Data model, not only the quincha panels but also the posts, which are considered to be made of cypress, are implemented. The constitutive laws adopted for the panels and the posts are based on the von Mises criterion, and the values of the material properties are assumed from the structural element tests (Torrealva, Vicente, and Michiels 2018). On the contrary, in the modal data model, the quincha panels of both stories assume a linear elastic model in compression and perfect plasticity with the limit in the capacity given by the total strain rotating crack model in tension (table 3.2).

TABLE 3.2.  
Material properties of the quincha panels for Hotel El Comercio.

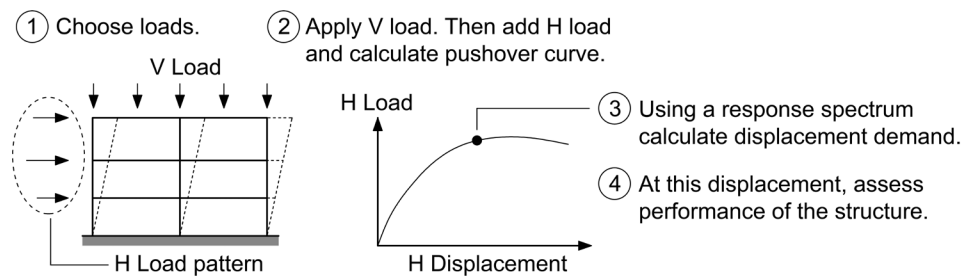
| Material             | Second Story                |                      | Third Story                 |                      |
|----------------------|-----------------------------|----------------------|-----------------------------|----------------------|
|                      | Modal Data                  | Test Data            | Modal Data                  | Test Data            |
| Young's modulus      | 2.7 GPa                     | 0.05 GPa             | 4.2 GPa                     | 0.05 GPa             |
| Poisson's ratio      | 0.2                         |                      | 0.2                         |                      |
| Density              | 1160 kg/m <sup>3</sup>      |                      | 1160 kg/m <sup>3</sup>      |                      |
| Constitutive model   | Total strain rotating crack | von Mises plasticity | Total strain rotating crack | von Mises plasticity |
| Tensile behavior     | Ideal plastic               |                      | Ideal plastic               |                      |
| Tensile strength     | 200 kPa                     | 125 kPa              | 200 kPa                     | 125 kPa              |
| Compressive behavior | Linear elastic              | Perfect plasticity   | Linear elastic              | Perfect plasticity   |
| Compressive strength | na                          | 125 kPa              | na                          | 125 kPa              |

### Safety Assessment

The best representation of the seismic performance of a historic earthen building is obtained by nonlinear dynamic analysis. However, this process is complex and not practical in general (Lourenço and Pereira 2018). Pushover analysis is a well-established tool for seismic assessment (fig. 3.4). This static nonlinear method accounts for inelastic behavior and dynamic effects in a simplified manner and is described in many national and international standards such as Eurocode 8, Part 3 (EC8-3 2005) and ASCE-SEI 41-06 (2007). The performance level of the building is defined by comparing the demand required by the code to the capacity of the structure. This is related to the type of earthquake considered during the analysis, as well as displacement, inter-story drift, and cross-section rotation.

The base shear (or load factor applied) versus top displacement curve of the structure, usually called capacity curve, is obtained using pushover analysis. There are different ways to define the load pattern: (a) mass proportional, (b) first mode proportional, and (c) inverted triangle; mass proportional is recommended for historic masonry structures (Lourenço and

FIGURE 3.4.  
Summary of the process involved in pushover analysis for seismic assessment.



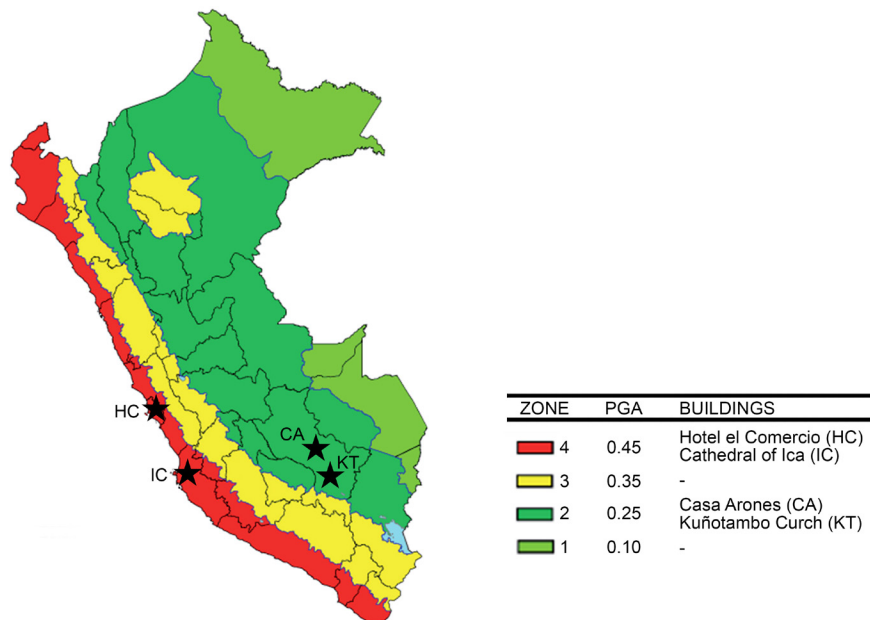
Pereira 2018). Once the capacity curve is obtained, it is possible to define performance in terms of displacements (EC8-3 2005, ASCE-SEI 4106 2007), but this approach is less reliable for structures where Young’s modulus (and thus the displacements and periods) seems to exhibit a large scatter.

On the contrary, the maximum capacity in terms of force is usually based mostly on geometry and is weakly sensitive to Young’s modulus. For this reason, a force-based seismic assessment criterion is adopted. If it is difficult to define the maximum acceleration that the structure can withstand and consensus has not emerged, the use of peak ground acceleration (PGA) seems the most adequate value and was used in this case. A lower safety level is allowed for existing buildings (see JCSS 2006, for example), meaning that a reduction of the code PGA value for new buildings might be applicable. For this reason, no soil amplification factor has been used in this case. Finally, it is stressed that unrealistically high values of displacement can be found in some of the analyses shown in presence of very low values of Young’s modulus of the adobe masonry. This is questionable not only because of the usual finite element formulation but also because the structure cannot withstand such large displacements without disintegration. This is intrinsic to the approach and data adopted and poses no problem in terms of safety assessment based in equilibrium mostly controlled by geometry.

The definition of a value of PGA depends on the return period of a maximum likely earthquake and a given performance level. For this study, the PGA values specified by the Peruvian code were directly considered (E.030 2016). The Peruvian code identifies four seismic zones of the territory, as shown in figure 3.5. For each zone, the code establishes maximum ground acceleration, with a probability of 10% to be exceeded in fifty years.

The prototype buildings will be required to have a higher capacity than that requested by the Peruvian code (E.030 2016). Analyses were performed in the two main directions of the buildings, defined as X and Y. In each direction, the earthquake was applied in both the positive and negative directions. The different analyses help to evaluate not only the capacity of the structure under lateral loads in terms of load-displacement curves (capacity curves) but also the progression of the damage and corresponding failure modes. Thus, the most relevant results will be presented in terms of capacity curves, displacements, and

**FIGURE 3.5.** Map showing seismic zones identified by the Peruvian code, as well as the locations of the four prototype buildings.



crack-width distribution plots (DIANA 2014). When possible, the model was evaluated in terms of crack correlation between in situ observations and the damage obtained with pushover analysis on the numerical models.

### Sensitivity Analysis

In contrast to the study of new buildings, the approach to structural evaluation of historic buildings involves a number of assumptions on parameters linked to the level of knowledge of the building in terms of alterations, structural interactions, materials, and constructive technology. The study of how the output of a mathematical system responds to different input parameters is called sensitivity analysis. Such an approach is highly recommended to check reliability of results and the importance of the parameters to the structural response. Sensitivity analysis was used on several parameters of the four prototype buildings, as shown in table 3.3.

**TABLE 3.3.**  
Results of sensitivity analysis for the four prototype buildings.

| Casa Arones   | Hotel El Comercio  | Ica Cathedral   | Church of Kuñotambo  |
|---|--|---|--|
| <ul style="list-style-type: none"> <li>• Tie-beam presence and anchoring</li> <li>• Floor presence</li> <li>• Adobe Young's modulus</li> <li>• Horizontal thrust from roof</li> <li>• Presence of roof tie beams</li> </ul> | <ul style="list-style-type: none"> <li>• Young's modulus</li> <li>• Connection between adobe and quincha walls</li> <li>• Vertical load</li> <li>• Floor stiffness and isotropy</li> </ul> | <ul style="list-style-type: none"> <li>• Connection between masonry envelope and internal timber structure</li> </ul> | <ul style="list-style-type: none"> <li>• Young's modulus</li> <li>• Damaged model vs. undamaged model</li> <li>• Presence of ties</li> </ul> |

# Unstrengthened and Strengthened Case Studies: The Church of Santiago Apóstol de Kuñotambo and the Ica Cathedral

## Unstrengthened Structure of the Church of Santiago Apóstol de Kuñotambo

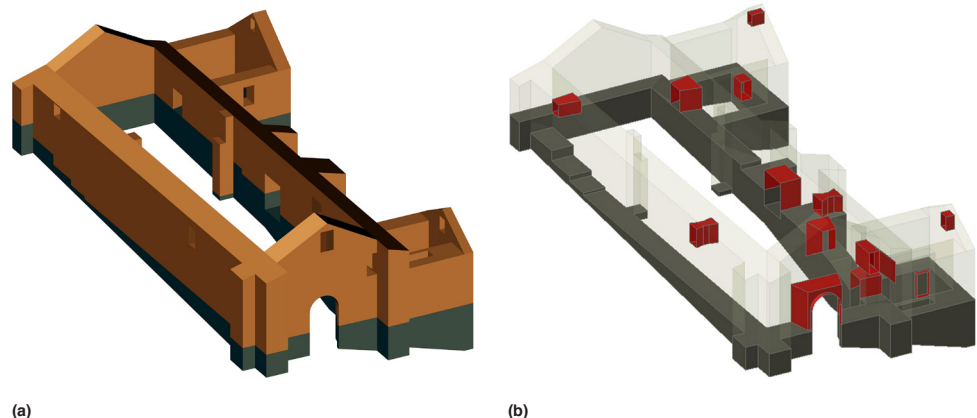
The numerical model of the church of Santiago Apóstol de Kuñotambo (the church of Kuñotambo) is characterized by a simplified 3D geometry of the building. As shown in figures 4.1a and 4.1b, the adobe masonry walls, represented in light brown, rest over a base course plinth and foundation of rubble stone masonry, represented in gray. The openings in the adobe walls were replicated according to the architectural drawings (Cancino and Lardinois 2012) and the in situ inspections. Three-dimensional timber lintels were placed over the openings. Given the limited information regarding their geometry and mechanical properties, visual inspection indicates that no damage is present near the openings.

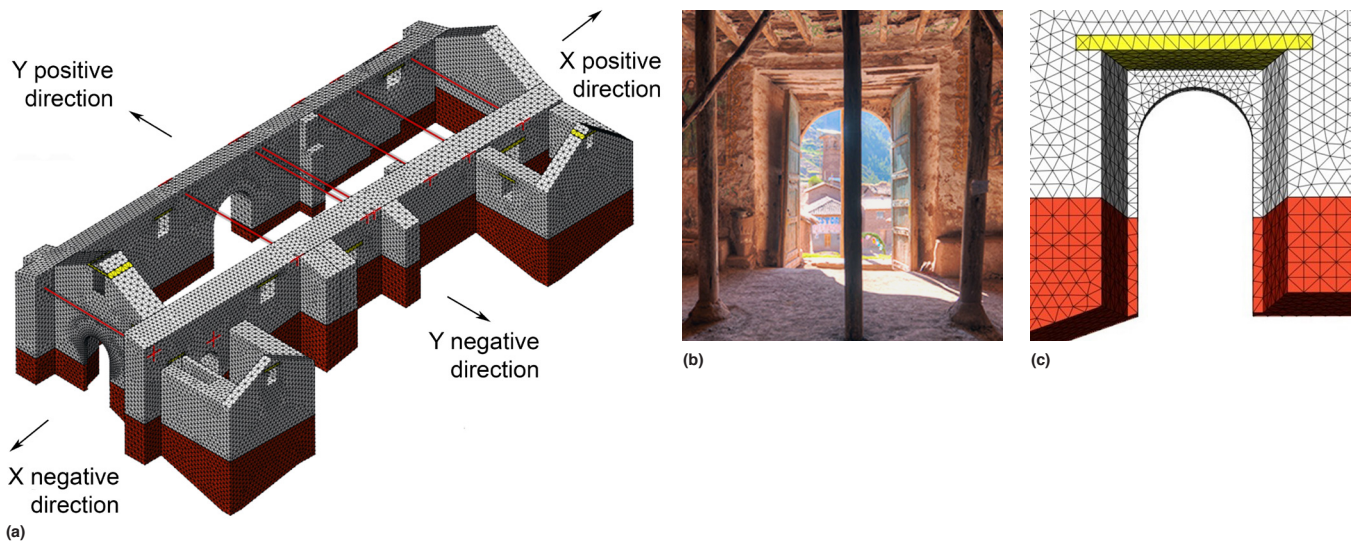
Considering the damage to the timber elements, poor masonry at the connection, and loss of the majority of the exterior timber keys, the tie beams at the roof level have been designated inactive in the unstrengthened structure. Results of the dynamic identification tests performed in the church show lack of box behavior with independent movements of the external walls, confirming the lack of connection between the two longitudinal walls. However, the contribution of the tie beams will be considered in the strengthened model, as the connection will be re-established.

The roof is not part of the global finite element (FE) model, but the resulting lateral thrust and vertical load are taken by the lateral walls. Therefore, a uniform distributed load was assigned to the longitudinal walls to represent the vertical weight of the roof and the resulting lateral thrust. A significant amount of soil, used to level the floor of the church, is present in the baptistery and sacristy with varying heights up to 4.0 m. Thus, the influence of the backfill was modeled as a distributed surface load, according to Coulomb's theory of earth pressure.

FIGURES 4.1A, 4.1B.

Model of the church of Kuñotambo, showing (a) a global perspective, with adobe masonry walls (in light brown) and rubble stone masonry plinth and foundation (in gray); (b) adobe wall openings (in red).





FIGURES 4.2A–C.

(a) View of the FE model of the church of Kuñotambo, showing base course and foundation (in brown) and ties (in red); (b) photo showing interior view of the main entrance (De Corso 2013); (c) modeling of the main entrance.

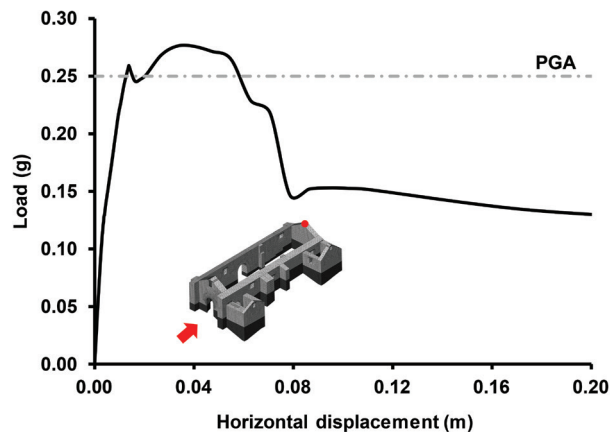
### Numerical Analysis

The numerical model of the church of Kuñotambo is presented in figures 4.2a–c. It includes the nave, with the adjoining buttresses; the sacristy and baptistry; the corresponding base course foundation, with its differences in elevation; and the system of timber ties and anchors (not considered in the unstrengthened model). The created FE mesh is composed of 321,827 isoparametric tetrahedral linear elements and 374,828 nodes in total.

In all, four pushover analyses were conducted, with the lateral loads applied in the X and Y main axes, in both positive and negative directions (see fig. 4.2a). Regarding the pushover analysis in the X positive direction, the maximum lateral load applied is 0.28 g (fig. 4.3). After peak, the structure enters a softening behavior, with large values of displacement recorded in the west gable wall and the adjoining wall of the sacristy. Severe load drops are found in the load-displacement diagram as a result of localized failure and internal force rearrangement, with extensive tensile damage and loss of stiffness in some parts. The failure mechanism consists of vertical separation cracks in the corners in the west part of the church. As the tensile damage propagates along the thickness and elevation of the walls, with horizontal hinge lines at the bottom of the base course and foundation, the west part becomes structurally independent. The failure mechanism consists of the out-of-plane overturning of the west gable and sidewalls. Plots of crack widths at ultimate stage are presented in figures 4.4a and 4.4b. Such a damage pattern could not be identified in the current state, as no specific crack pattern exists on the corners of the west part of the structure.

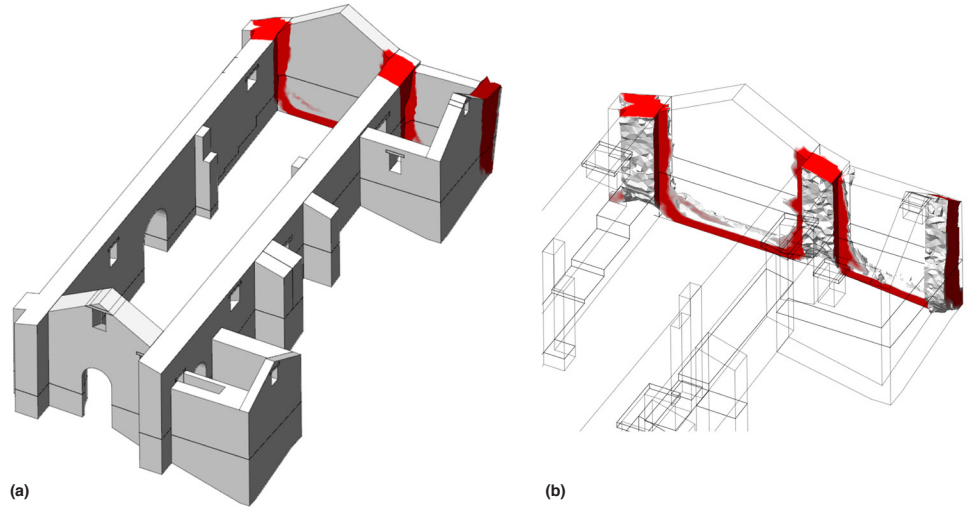
FIGURE 4.3.

Load-displacement diagram in X positive direction for the church of Kuñotambo.



FIGURES 4.4A, 4.4B.

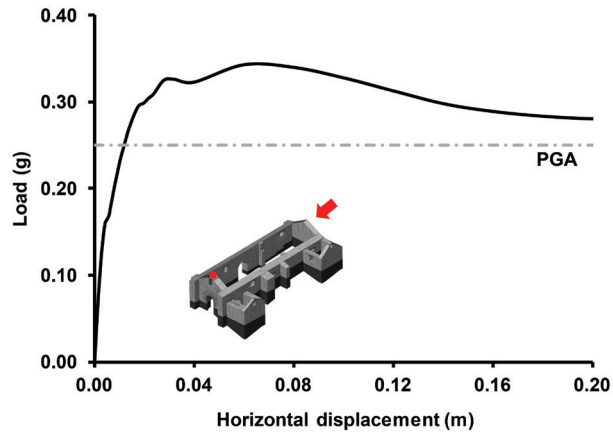
Plots of crack patterns (in red) at ultimate stage for loading in X positive direction for the church of Kuñotambo, showing (a) a global perspective; (b) detail of the cracking between the back wall and the longitudinal walls.



When the lateral load is applied in the X negative direction, the failure mode consists mainly of the out-of-plane overturning of the east facade, together with adjacent fragmented parts of the lateral walls. From the obtained capacity curves, the lateral capacity in the X negative direction of the model is 0.34 g (fig. 4.5). Maximum outward displacement is recorded at the top of the east gable end wall. From the plot of the crack width at peak, it is evident that the structure has undergone extensive structural damage, with tensile failure zones in both corners of the east facade in the entire elevation and thickness. In-plane shear cracks appear also in the front end of the lateral walls and in the northeast corner of the gable end of the baptistery (figs. 4.6a–c). Similar cracks are present in the structure (figs. 4.7a, 4.7b).

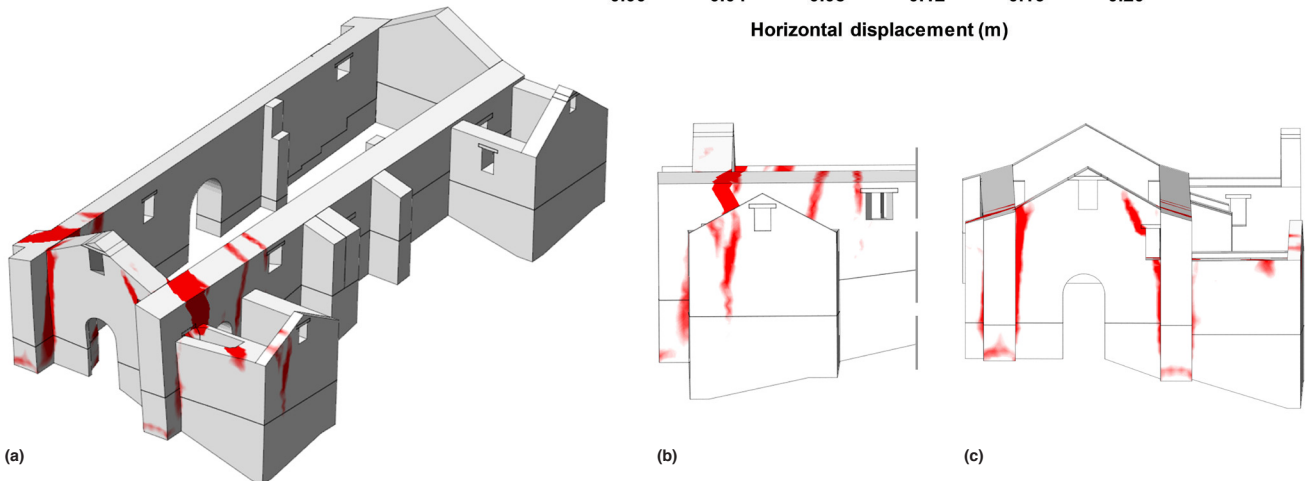
FIGURE 4.5.

Load-displacement diagram in X negative direction for the church.



FIGURES 4.6A–C.

Plots of crack patterns (in red) at ultimate stage for loading in X negative direction for the church at (a) northeast view; (b) north gable wall of baptistery; (c) main facade.



FIGURES 4.7A, 4.7B.

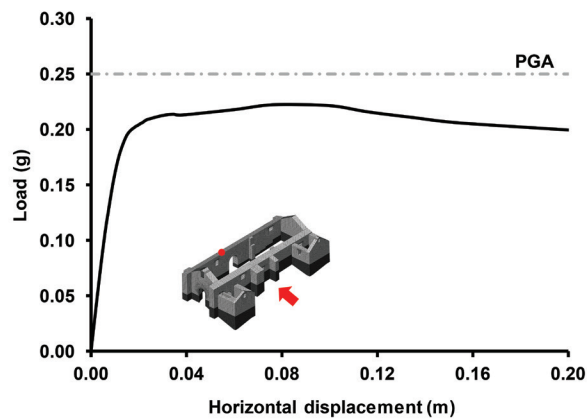
Photos of crack-pattern correlation (in red), showing (a) crack pattern in east facade; (b) crack pattern in north gable wall of baptistery.



For the pushover nonlinear analysis along the Y positive direction, the failure mechanism consists of the separation and out-of-plane overturning of the south lateral wall, with large deformations in the top eaves of the mid-span and significant tensile failure zones at the intersections with the west and east facades. The structure's lateral capacity reaches 0.22 g with maximum outward displacements recorded at the middle top of the south lateral wall (fig. 4.8). Cracking starts forming at the southeast and propagates diagonally along the connection, followed by cracking at the southwest corner. In later stages, a continuous flexural crack is formed at the interface with the base course and foundation and where the wall enters a rigid out-of-plane body motion, with large incremental displacements (figs. 4.9a, 4.9b). Similar cracks are present in the structure.

FIGURE 4.8.

Load-displacement diagram in Y positive direction for the church.



FIGURES 4.9A, 4.9B.

Plots showing crack patterns (in red) at ultimate stage for loading in Y positive direction, showing (a) the south lateral wall; (b) detail of the cracking in the south lateral wall.

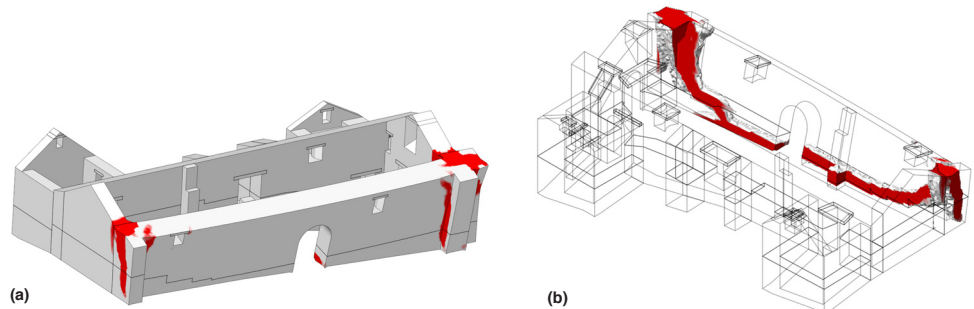
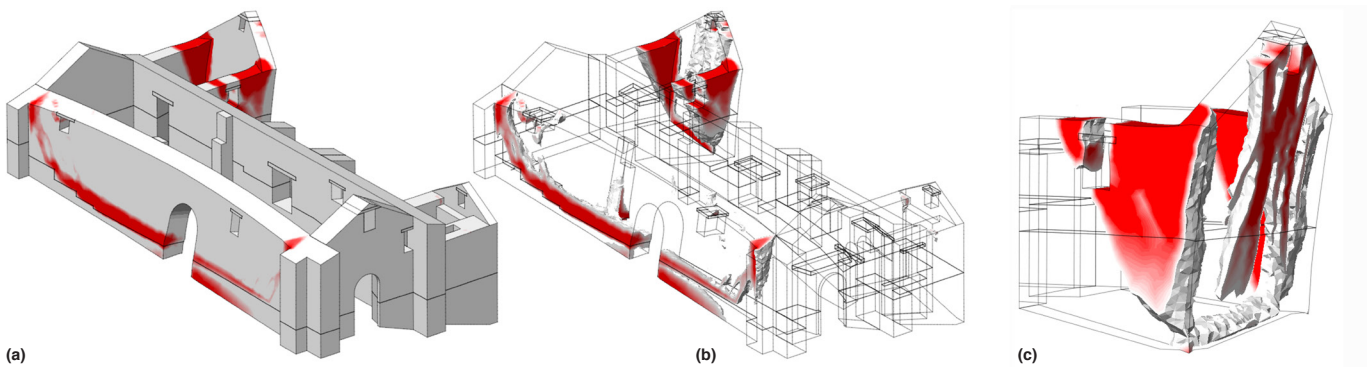
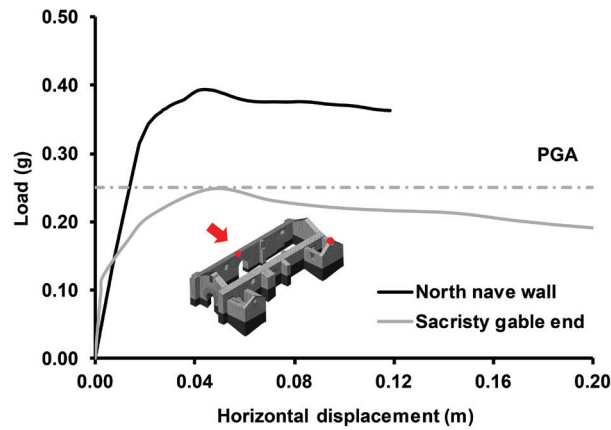


FIGURE 4.10.  
Load-displacement diagram in Y  
negative direction for the church.



FIGURES 4.11A–C.  
Plots of crack patterns (in red)  
at ultimate stage for loading in Y  
negative direction, showing (a, b)  
southeast views; (c) sacristy.

Finally, figure 4.10 displays the results from the pushover analysis in the Y negative direction. Lateral capacity is controlled by early failure of the sacristy gable wall and, in this case, is 0.25 g. The capacity of the south lateral wall is much larger than in the Y positive direction (0.39 g) due to the external lateral parts and buttresses contributing to overall stiffness of the nave. Tensile damage is mostly concentrated in the sacristy, with vertical tensile failure zones in the corners of the side and gable walls, as seen from the ultimate principal crack-width distribution (figs. 4.11a–c).

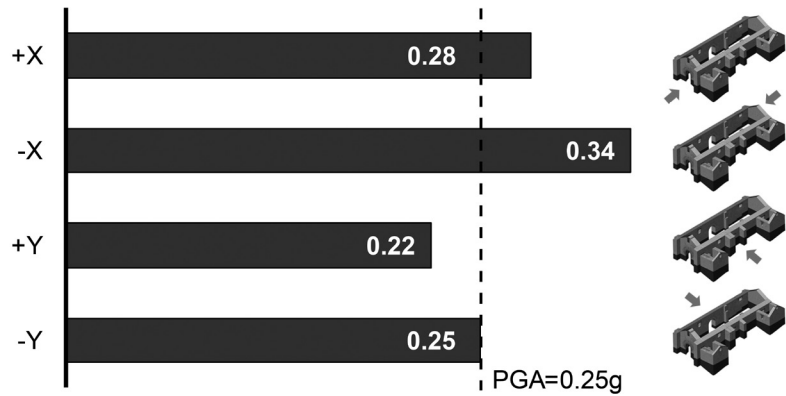
### Conclusions

Using pushover analyses, crack patterns were obtained and correlated with the observed patterns, indicating that the current damage might have been induced partly by past seismic actions. For the current condition, given the visual inspection and the results of the dynamic identification tests, the system of ties is considered inactive. The numerical model was capable of reproducing reasonably well the damaged condition of the structure.

One of the structural deficiencies of the church of Kuñotambo is the large asymmetric distribution of stiffness in the transverse direction of the nave. The aligned walls and buttresses along the north wall, when activated through diagonal compression strength, have a stiffer response and a larger lateral capacity. The failure mode with the lowest capacity is the out-of-plane overturning of the south lateral wall, which is the controlling failure mode at a minimum value of 0.22 g. According to the pushover analyses, strengthening is needed in multiple directions, since the overall capacity does not reach peak ground acceleration (PGA) for the Cusco region (0.25 g) (E.030 2016), as depicted in figure 4.12. The weakest directions, with very low lateral capacity for the structure, are north-south (+Y) and

FIGURE 4.12.

Maximum lateral capacity (g) from pushover analyses in each direction for the church of Kuñotambo.



east-west (+X). With an adequate tying and buttressing system, the capacity of the structure in the north-south direction (+Y) can increase significantly. Also, connectivity in the intersections of transversal walls and means of efficient anchoring in timber-strengthening elements are issues that must be addressed. Further information on the assessment of the unstrengthened state of the church of Kuñotambo can be found in Karanikoloudis and Lourenço (2018).

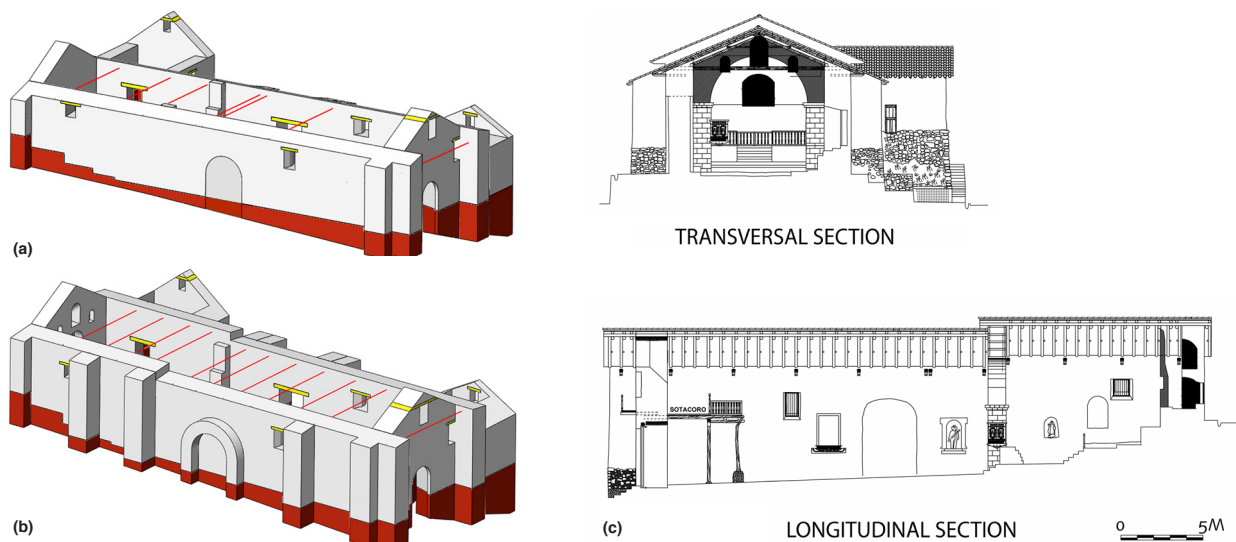
## Strengthened Structure of the Church of Kuñotambo

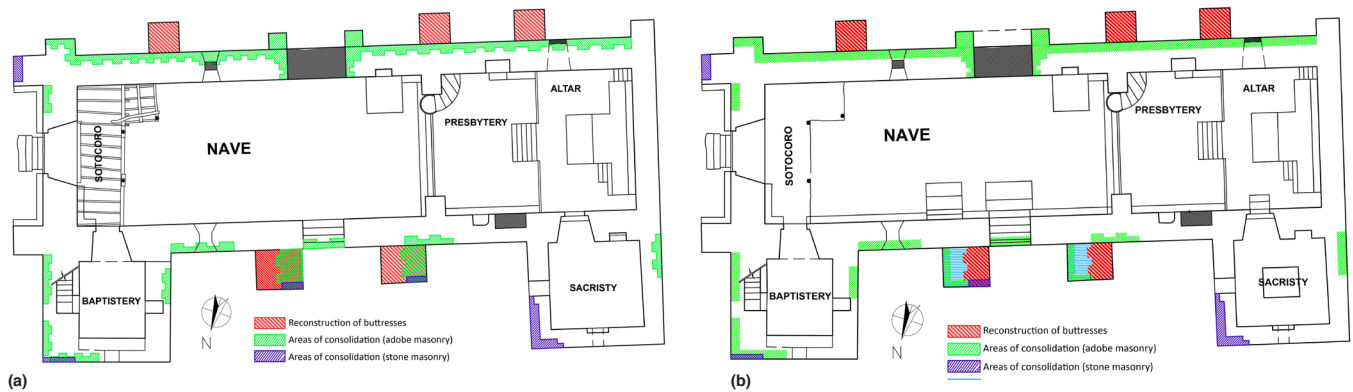
### Description of the Strengthening

The overall objective for the seismic strengthening of the church of Kuñotambo is to improve the structure's lateral resistance and, ideally, its energy dissipation capacity. To this end, the global structural performance needs to simulate a global box (or integral) behavior so that the building can dissipate energy by redistributing the seismic loads that prevent out-of-plane local collapse mechanisms (Lourenço et al. 2011). The strengthening measures can be identified as two specific groups: (1) with the addition of buttresses adequately connected to the adjoining walls by horizontal timber keys, and (2) by tying the walls and ensuring their connectivity through timber elements (ring beams - wall plates, anchored ties, and corner keys). Full details of the design are given in Getty Conservation Institute and Dirección Desconcentrada de Cultura–Cusco (2017).

FIGURES 4.13A–C.

Maps of the church of Kuñotambo (a) under current conditions; (b) after strengthening; (c) transversal and longitudinal architectural sections of the strengthened structure. Adapted from Moscoso et al. (2015).





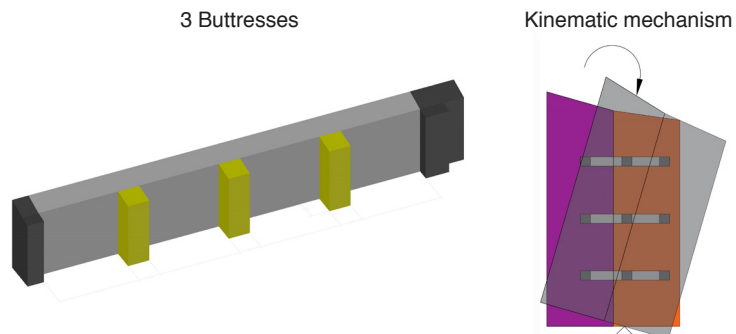
**FIGURES 4.14A, 4.14B.** Plans showing areas of reconstruction and consolidation at the church (a) at the level of adobe masonry; (b) at the level of the base course and foundation. Adapted from Torrealva and Vicente (2016).

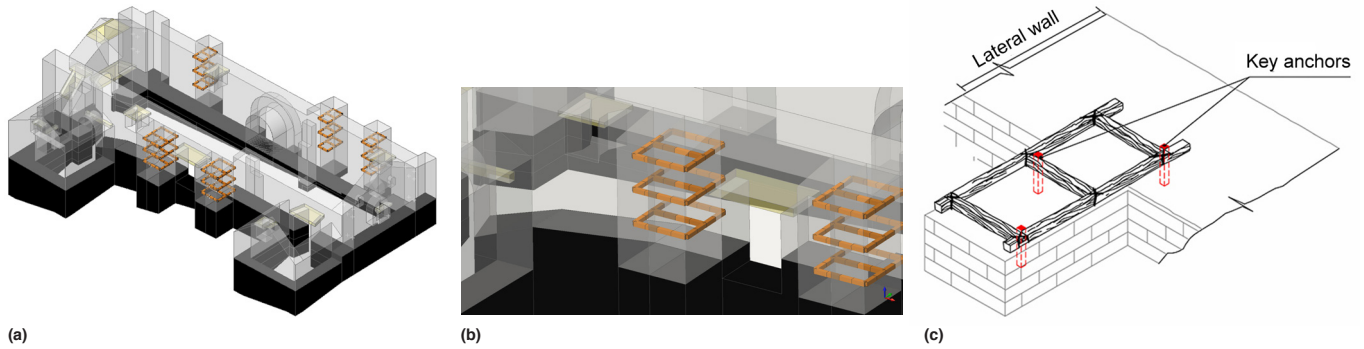
Timber elements, introduced or reestablished in the existing structural system of adobe masonry, can substantially enhance the capacity under lateral forces (Tomažević 1999; Vintzileou 2008). In order for the new system to perform, timber elements need to mobilize enough friction in the masonry substrate. The proposed strengthening must respect conservation principles for cultural heritage buildings, namely authenticity, minimal intervention, minimal invasiveness, and reversibility (AIC 1994; ICOMOS 2003).

To address the poor out-of-plane capacity of the south lateral wall of the nave, three additional buttresses were proposed and distributed along the length of the wall. The adobe-arched pilaster, in place of the infilled side gate, is only an architectural element (figs. 4.13a–c). Interlocking adobe blocks will ensure a bond with the existing walls. The deteriorated areas of the existing adobe and the stone masonry base course will be consolidated, and severely damaged areas will be replaced by new adobe units and stone blocks up to half of the existing thickness (figs. 4.14a, 4.14b). The collapsed semicircular quincha arch, dividing the nave from the presbytery and altar, will be reconstructed according to existing documentation from churches of similar typology. Following this same documentation, the triumphal arch will not have a structural role and was not included in the model. The rear part of the lateral walls will be raised in elevation 0.65 m by adding more courses of adobe (see figs. 4.13b, 4.13c). Finally, a new roof will be designed, composed of double rafter timber trusses, and will rest on wall plates, connected by a collar tie beam and a ridge beam on top. Again, the roof has a weakly relevant global structural role and was not included in the model.

Minimum lateral capacity for the out-of-plane failure of the south lateral wall of the nave is controlling the structural response. Thus, a preliminary design of buttresses was developed based on recommendations for earthen buildings provided by the Bureau of Indian Standards (IS 13827 1993). Three square buttresses of minimum dimensions equal to the thickness of the adjoining wall are distributed along the span of the wall (fig. 4.15). From

**FIGURE 4.15.** Design of buttresses for the span of the south lateral wall.





FIGURES 4.16A–C.

Schematic representations showing locations of horizontal timber keys in buttresses: (a) 3D view; (b) existing buttresses in north lateral wall; (c) detail of timber key, showing location of anchors. The timber elements are shown larger than their actual size for better visual understanding of their location.

the applicable kinematic mechanisms under horizontal equivalent seismic forces, the maximum capacity  $\alpha_o^*$  for the ultimate limit state (ULS) is 0.33 g, higher than the PGA design demand for the Cusco region (0.25 g).

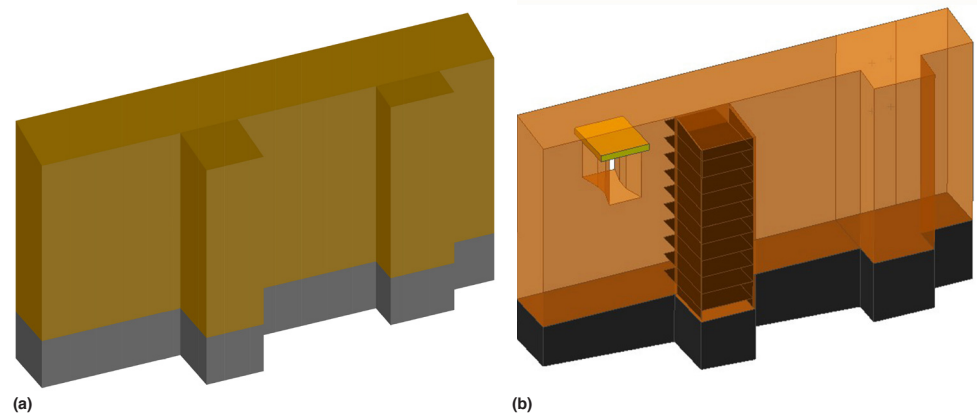
For the buttresses to be designed efficiently, connectivity with the adjoining wall has to be ensured. Horizontal timber keys are placed in each buttress (existing and new) at three levels; the middle tie is placed at mid-height in the adobe masonry wall, with distances of 1.20 m and up to 1.50 m between the keys. The length of embedment of these keys extends until half of the thickness of the adjoining wall. Configurations of the horizontal keys are presented in figures 4.16a–c.

Part of the strengthening proposal for the church of Kuñotambo is the placement of geogrid sheets in the buttresses of the lateral walls of the nave. The goal is to improve confinement under high compressive stresses, enhancing the ductility of adobe masonry and preventing disintegration under seismic loads. The exterior surfaces of the buttresses will be wrapped with geogrid along their elevation. In horizontal planes, geogrid will be placed between every four adobe blocks. In vertical and horizontal planes, sheets will be connected with nylon straps, forming a 3D embedded reinforcement frame (figs. 4.17a, 4.17b).

To enhance connectivity in corners and junctions, orthogonal timber keys, composed of two sets of timber beams connected transversally with timber blockers, will be inserted in horizontal planes of various elevations. Accounting for the crack formation from the nonlinear pushover analyses and documented damage on site, the keys were extended in order to intersect with cracks close to the corners. Given the presence of the composite system of ring and tie beams at the top part of the walls, the corner keys were located at two lower levels, around 1.0 m and 2.5 m from the top wall elevation down (exterior edge), as shown in figures 4.18a and 4.18b. A continuous configuration of the corner keys was chosen, which covers parts of the gable and sidewalls of the sacristy and baptistery, as well as the southeast corner of the nave (see fig. 4.18b).

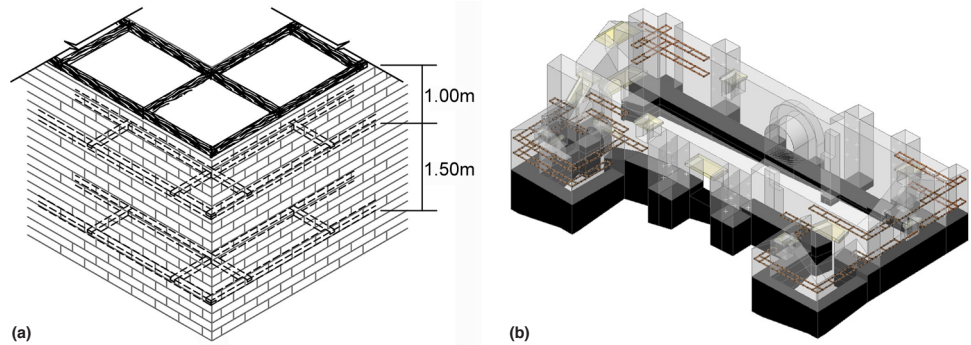
FIGURES 4.17A, 4.17B.

Schematic representation of the south wall (a) without geogrid sheets; (b) with vertical and horizontal geogrid sheets.



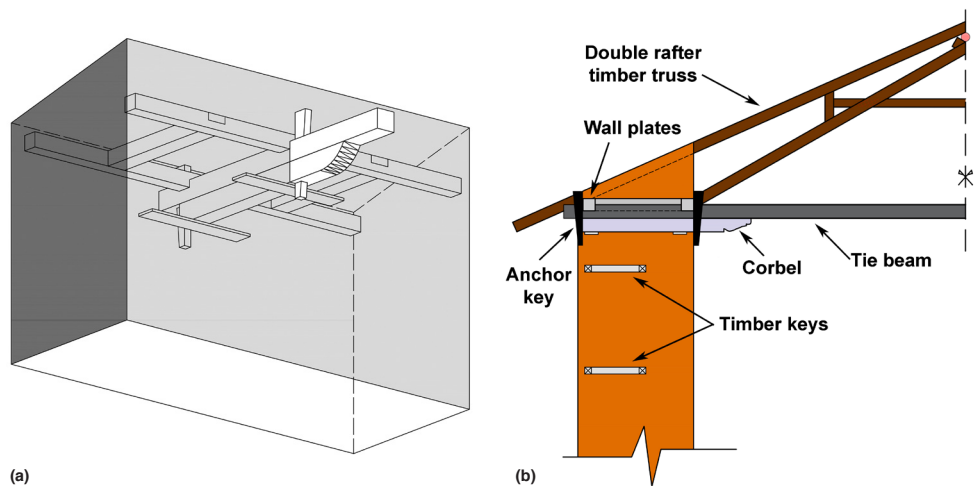
FIGURES 4.18A, 4.18B.

Schematic representation of corner keys: (a) general scheme; (b) front and rear ends from the FE model. The timber elements are shown larger than their actual size for better visual understanding of their location.



FIGURES 4.19A, 4.19B.

3D (a) and 2D (b) schematic representations of the anchoring system. Note the double system of vertical timber anchors attached to the interior and exterior surfaces of the adobe wall.



On top of the lateral walls, a combined internal and external bracing system of timber-strengthening elements will be implemented. A system of tie beams is designed to offer lateral restraint mostly to the weaker south lateral wall of the nave. For the ties to work in the event of an earthquake, in both tension and compression, an adequate anchoring system was adopted (figs. 4.19a, 4.19b). The timber trusses of the roof rest on the ring beam system, with each rafter connected to the interior and exterior beam elements.

### Characteristics of the Numerical Model

The new numerical model accommodates the addition of new buttresses on the south lateral wall, the rise in height of the lateral walls in the presbytery and altar, and the new timber-strengthening elements (figs. 4.20a, 4.20b). The created FE mesh is now composed

FIGURES 4.20A, 4.20B.

FE model for the church of Kuñotambo: (a) global view, showing configuration of timber-strengthening elements; (b) close view of bond beam, tie beam, and timber box in the rise of elevation of the lateral walls. The timber elements are shown larger than their actual size for better visual understanding of their location.

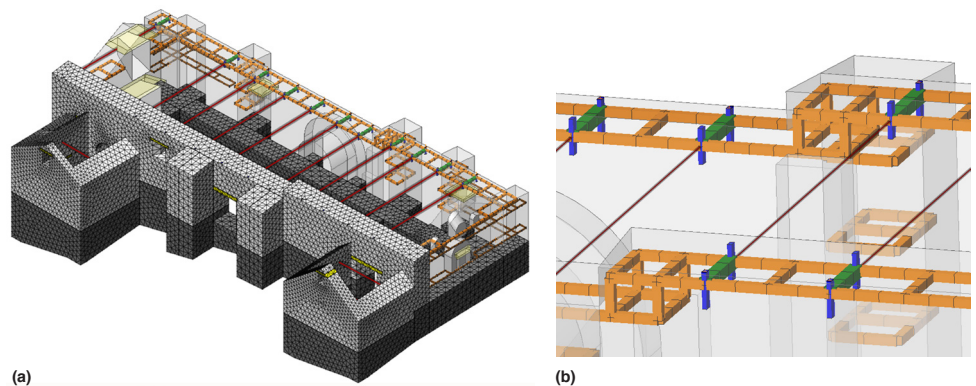
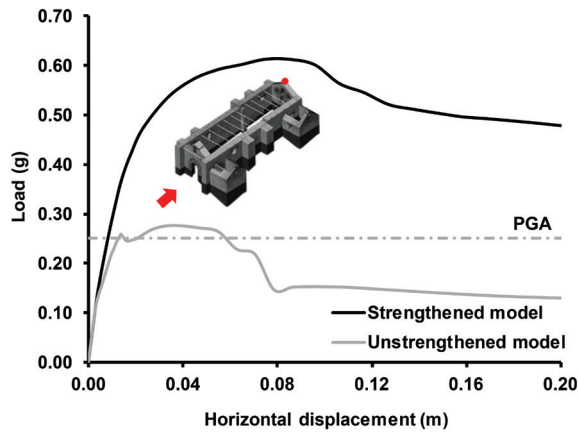


FIGURE 4.21.

Load-displacement diagram for the strengthened (SM) and unstrengthened (UM) models in X negative direction.



of 239,298 10-node tetrahedron elements (due to their compatibility with quadratic beam elements) of accounted shear and bending stiffness. In total, the FE model contains 354,134 nodes.

### Numerical Analysis

Regarding the pushover analysis in the X positive direction, the maximum lateral load obtained is 0.61 g (fig. 4.21), and the failure mechanism is determined by the out-of-plane collapse of the west gable wall of the altar. The obtained capacity is twice that of the current condition, thus providing an adequate safety level. The structure enters a softening behavior with significant cracks and high values of displacement at collapse. Some load drop is found after the maximum capacity, the result of crack propagation and internal force rearrangement with moderate loss of strength.

Failure is indicated by vertical separation cracks along the corners and at the middle of the gable wall, covering the entire elevation and thickness, with a horizontal hinge line at the adobe–base course interface. Also, diagonal shear cracks are present in the gable wall of the baptistery and north lateral wall of the nave, close to the sacristy sidewall (figs. 4.22a, 4.22b). The out-of-plane bending of the west gable wall occurs in the strengthened model, versus the direct separation and out-of-plane collapse of the entire west part, observed in the unstrengthened model (see figs. 4.4A, 4.4B).

FIGURES 4.22A, 4.22B.

Plots of crack patterns (in red) at ultimate stage for loading in X positive direction for the church of Kuñotambo (strengthened), showing (a) the gable wall of the altar; (b) detail of the cracking of the back wall.

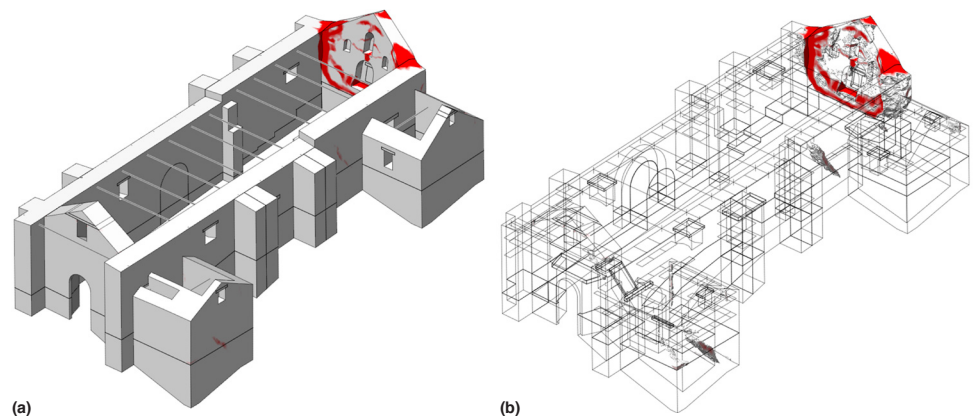


FIGURE 4.23. (LEFT)  
Load-displacement diagram  
in the X negative direction  
for the church of Kuñotambo  
(strengthened).

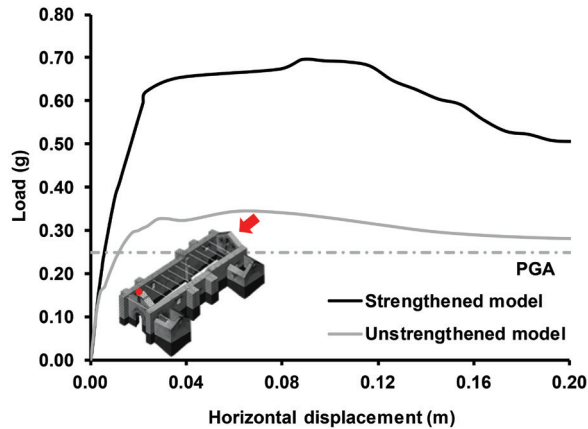
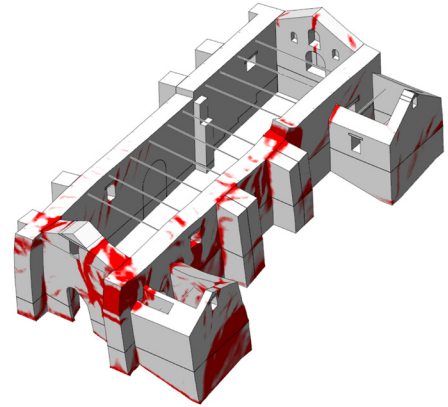


FIGURE 4.24. (RIGHT)  
Plot of crack patterns (in  
red) at ultimate stage  
for loading in X negative  
direction for the church of  
Kuñotambo (strengthened).



Due to the parallel configuration of the tie beams, the actual contribution of the strengthening elements is found on the bond beam and corner keys at the rear end. Regarding the level of stress in the timber-embedded elements, the part of the bond beam at the rear end is mostly activated in tension, bending, and shear. At maximum capacity, no local failure in timber elements is obtained.

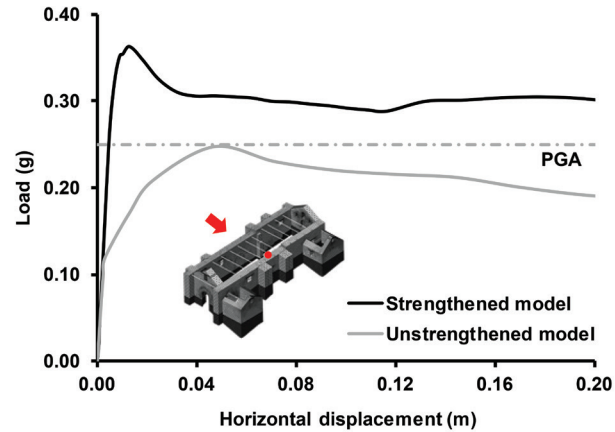
The lateral capacity of the church in the X negative direction, after the elastic range, is 0.69 g, twice than for the FE model of the current state (fig. 4.23). Maximum outward displacements are recorded at the top of the gable end wall of the sacristy, and tensile damage is concentrated in the northeast part of the church. The presence of more openings and voids in the northeast part, along with lack of continuity in the configuration of corner keys, results in lower strength and larger deformations. Due to the tying effect at intersections created by the timber-embedded elements, the failure mode consists mainly of shear cracks (in walls aligned in the direction of the seismic force) and flexural out-of-plane cracks (in the transversal walls), which differs from the model in the current condition (fig. 4.24). Both lateral nave walls experience diagonal shear cracks. Portions of the front facade, sacristy, and baptistery, as well as the buttresses of the north part, also experience failure, mainly in out-of-plane bending modes. Such structural damage can be associated with nonuniformity in plan, mainly due to an uneven distribution of structural elements, which shifts the center of mass and stiffness, inflicts eccentricities, and partly redirects inertia forces.

Near collapse, maximum axial forces are located in the bond beams at the middle of the nave, close to maximum tensile capacity, with bending failure and close to shear failure.

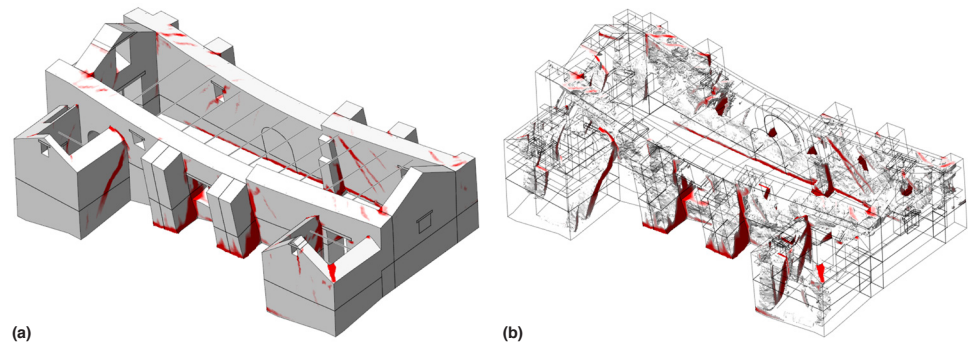
Regarding the pushover analysis in the Y negative direction, the maximum lateral load applied is 44% higher and equal to 0.36 g (fig. 4.25), and the failure mechanism is mainly due to the out-of-plane bending of the lateral walls of the nave, toward the direction of the seismic force. The structural behavior under strengthening is highly improved given the fact that under the current condition, the main failure mechanism is the out-of-plane failure of the thin gable wall of the sacristy (figs. 4.26a, 4.26b). The timber ring beams in each of the lateral walls deform as a unified beam, clamped at both ends.

The bending cracks in the lateral walls of the nave are widespread and formed a diagonal pattern; the highest curvature was found at the top height and middle span of the walls. Flexural hinge lines formed at the base, and the lateral walls fragmented in a sort of a circular pattern. Walls in the transversal direction are cracked in shear, with more severe damage in the sidewalls of the baptistery and sacristy. Also, the buttresses in the north front are cracked diagonally at the base, while those in the south front follow the out-of-plane

**FIGURE 4.25.**  
Load-displacement diagram in Y negative direction for the church of Kuñotambo (strengthened).



**FIGURES 4.26A, 4.26B.**  
Plots of crack patterns (in red) at ultimate stage for loading in the Y negative direction for the church of Kuñotambo (strengthened), showing (a) both lateral walls, baptistry, and sacristy; (b) detail of the cracked areas.



bending of the south lateral wall, with large tensile cracks in the interface with the adobe–base course foundation. The east facade experiences cracks exhibiting a cone failure around the corner keys at the north junction (see figs. 4.26a, 4.26b).

The tie beams appear to make a marginal contribution to the overall response with moderate axial forces, mainly because both lateral walls deform in a similar way. The forces in the timber-embedded elements are moderate with large safety margins at maximum capacity.

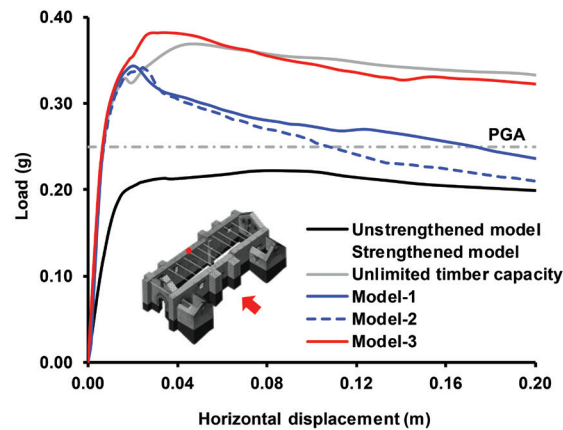
### Sensitivity Analysis

For the nonlinear pushover analysis, along the positive direction of the Y-axis, a parametric analysis was conducted in order to assess the effectiveness of the strengthening proposal on the direction of the weakest capacity.

First, the research team investigated the possibility that the infilled gate on the south lateral wall was not part of the structural system. It was noted that for the assessment of the current condition, the infilled gate was considered as a separate structural system, due to the absence of interlocking with the rest of the south lateral wall. Consolidation and replacement of damaged parts of adobe masonry on the exterior surfaces involve parts of the infilled south gate; thus, some interlocking is expected (Model 1). Still, a conservative hypothesis of no interaction and interlocking between the two parts was also considered (Model 2). Capacity curves of the FE model with strengthening, with (Model 1) and without (Model 2) the infilled south gate, are presented in figure 4.27. The maximum lateral load applied is 0.34 g for both cases, and the failure mechanism consists of the out-of-plane bending of the north and south lateral walls of the nave, with maximum outward displacements recorded at the middle top of the south lateral wall.

FIGURE 4.27.

Load-displacement diagram in the Y positive direction for the church of Kuñotambo (sensitivity analysis). Figures 4.28a–c. Plots of crack patterns (in red) at ultimate stage for loading in Y positive direction at failure: (a) strengthened model (with infilled gate); (b) strengthened model (with higher-resistant buttresses and improved ductility in compression); (c) unstrengthened model.



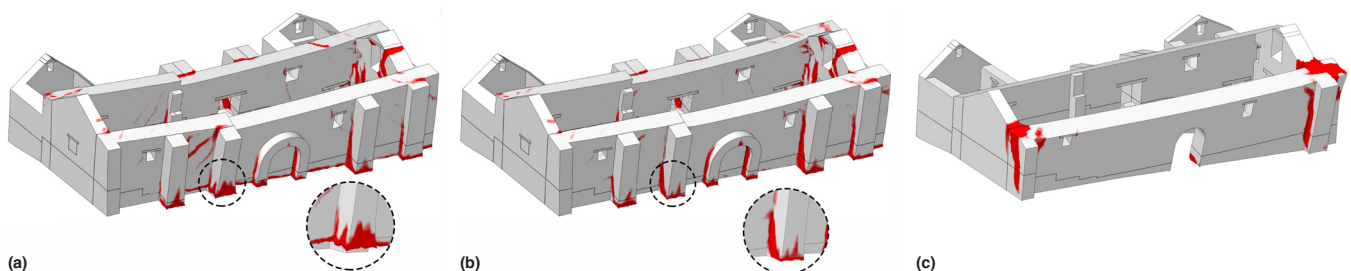
Second, the research team addressed the failure of the timber elements. Limiting the capacity of the timber-strengthening elements results in a decreasing slope in post-peak behavior. The area under the force-displacement diagram, compared to the response of the model with unlimited capacity to the timber elements, decreases by 22% and 28% for Model 1 and Model 2, respectively. For Model 2, the residual capacity approaches the response of the current state (see fig. 4.27). Yet, for both models, the strengthening scheme presents a substantially higher capacity with compliance to the seismic demand of 0.25 g. The participation of the infilled gate, in terms of mass and stiffness, mostly affects the capacity during post-peak.

The ring beam and corner keys increase the stiffness of the connections between the structural elements and allow the lateral walls to deform in out-of-plane bending while activating the transversal walls. Similar to the behavior on the Y negative direction, the ring beam in each of the lateral walls deforms as a unified beam connected transversally, with blockers and almost clamped at both ends. The ring beam has maximum compressive and tensile axial forces located at mid-span, again with moderate levels.

Compared to the unstrengthened structure, the tensile damage in the strengthened structure, at a load step near collapse, presents smaller crack widths that configure the rotation plane of the north lateral wall. The failure mechanism at full evolution consists of bending cracks in the lateral walls of the nave, which are widespread and form a diagonal pattern toward the corners (figs. 4.28a–c). A large portion of the east facade is fragmented, exhibiting cone failure of the embedded bond beam and corner keys. Parts of the sidewalls of the baptistery and sacristy are also under vertical separation cracks; while a tensile zone along a diagonal plane, vertical separation cracks are formed at the base of the north lateral wall.

FIGURES 4.28A–C.

Plots of crack patterns (in red) at ultimate stage for loading in Y positive direction at failure: (a) strengthened model (with infilled gate); (b) strengthened model (with higher-resistant buttresses and improved ductility in compression); (c) unstrengthened model.



Addressing the local performance of the strengthened structure, the center south buttress is failing under compression at the interface between the adobe and base course (see circled insets in figs. 4.28a and 4.28b). Such early failure has a direct influence on the stability and overall post-peak behavior of the structure, evidenced by the decreasing slope on the capacity curve at post-peak. Thus, the research team investigated the possibility of improving the material characteristics of adobe masonry. It was noted that the structure's lateral capacity at a point of large deformation is below the target limit of 0.25 g. Subsequently, a more robust structure needs to be obtained with a more ductile behavior. Also, the degradation process, either chemical, physical, or mechanical, can escalate under the presence of structural cracks and mechanical failure, leading to a reduction of performance and durability. Regarding the adobe masonry, the aim was to improve the compressive strength of new adobe blocks at the lower part of the new buttresses, so as to improve the behavior of out-of-plane rotation and avoid early crushing.

The proposed solution includes the introduction of a higher base course of stone masonry for the buttresses, which would increase compressive strength and compressive fracture energy (by using horizontal geogrids). The model with the new material (Model 3) shows significantly improved post-peak behavior (see fig. 4.28b), similar to the response of the model with unlimited timber capacity (see fig. 4.27).

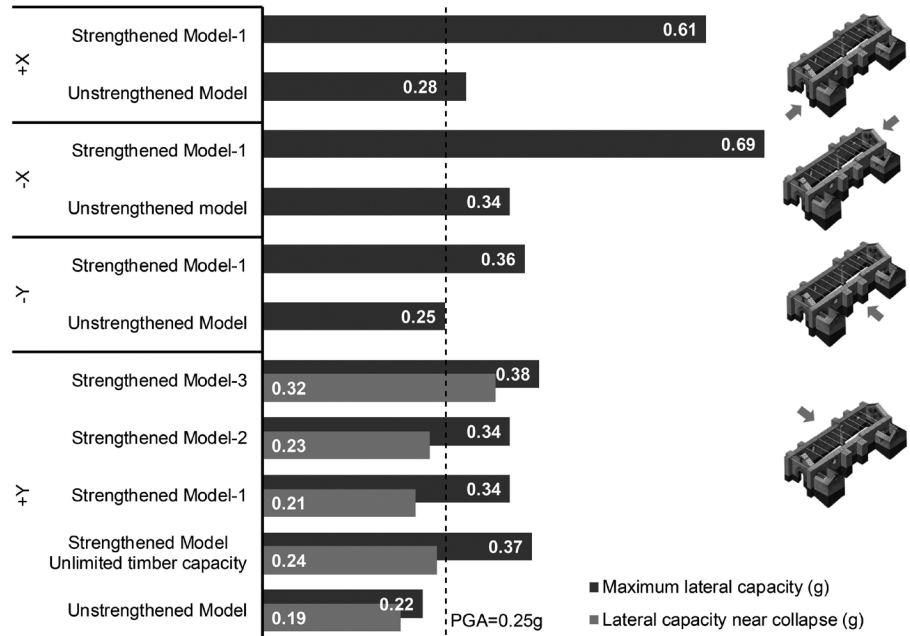
### Conclusions

Inspection, survey, in situ testing, and structural analyses in the current condition determined that the main structural deficiency in the church of Kuñotambo is lack of continuity between structural elements. This is due to low capacity of the adobe masonry and fragmentation at the corners. The correlation between documented crack patterns and those obtained from the numerical modeling shows that the current level of damage might have been partly induced by past earthquake events, together with soil movements and material deterioration. Given the mechanical properties of adobe masonry, lack of maintenance, and structural alterations over time, the structure will certainly perform inadequately in a future earthquake event in the absence of corrective measures.

The strengthening scheme was designed to provide integrity to the structure with external and internal bracing to reach a favorable integral structural behavior. The implementation of new buttresses, in combination with an embedded system of timber-strengthening elements such as bond beams, anchors and corner keys—all connected with tie beams—has improved performance under lateral loading and allowed redistribution of seismic loads between transversal and longitudinal walls. The capacity of the corners increased substantially, activating transversal walls and thus altering the structural behavior from out-of-plane rigid body motion of individual parts to a combination of out-of-plane bending (longitudinal walls) and in-plane bending and shear (transversal walls). The resulting damage, compared to the current condition in terms of cracks during a strong earthquake, is then distributed with smaller cracks. Issues of durability and long-term structural performance in areas governing early local failure are addressed by improving performance criteria under compressive loading.

From the results of the nonlinear pushover analyses, capacity curves were obtained, together with damage propagation characteristics and post-peak structural behavior, summarized in (fig. 4.29). In all principal directions, the capacity reached is higher than the design requirement in the Peruvian code (E.030 2016).

**FIGURE 4.29.** Maximum lateral capacity (g) in each direction, for models with and without strengthening, for the church of Kuñotambo.



## Unstrengthened Structure of the Ica Cathedral

### Numerical Analysis

Due to the complexity of the Ica Cathedral, several models were created to study different parts of the structure independently, namely a representative bay, the internal timber structure, and the external masonry envelope. This allowed a gradual and controlled increase in the sophistication of numerical modeling that culminated in a final, complete model incorporating the whole cathedral. It is interesting to note that the results obtained from these preliminary analyses demonstrated that the building is significantly influenced by the interaction of the timber and masonry structures. More information can be found in Ciocci, Sharma, and Lourenço (2018).

The model of the cathedral was constructed using 3D isoparametric solid elements for the masonry walls and bell towers, and beam elements were used for timber members (fig. 4.30a). Although the sacristy, reception, and offices were not included in the model, as they were observed to be independent from the structure, the effect of the cloister was simulated using calibrated springs located along the southern lateral wall at the level of the roof of the cloister (figs. 4.30b, 4.30c). The stiffness of these springs was calculated to account for the buttressing effect of the columns as well as the roof of the cloister.

**FIGURES 4.30A–C.** Views of the Ica Cathedral, showing (a) FE model; (b) photo of the cloister adjacent to the southern lateral wall; (c) springs simulating the cloister in the FE model.



A crucial aspect in modeling was the definition of the connection between the two structural systems, for which almost no information is available (Cancino and Lardinois 2012). In order to perform this study, connections are assumed to exist between the wooden beams in the upper part of the *sotacoro* and the fired-brick facade and the lateral masonry walls; between the transversal wooden beams of the bays and the lateral masonry walls; and between the wooden beams supporting the barrel vaults of the chapels and altar as well as the masonry walls (fig. 4.31). These connections were modeled by using beam elements and merging their nodes with the solid elements. Finally, timber lintels were assigned to all the openings, since no damage could be observed in the real structure during the in situ surveys (Cancino and Lardinois 2012).

Pushover analyses were carried out by applying the lateral loads in the X negative and Y negative directions of the numerical model, as the failure mechanisms identified in these two directions for the masonry envelope proved to be the most relevant. It should be noted that failure mechanisms are studied only in the masonry envelope, as timber is assumed to be a linear elastic material. The timber model was studied using specific models detailed in Ciocci, Sharma, and Lourenço (2018).

As shown in figure 4.32, the maximum lateral load that can be applied to the numerical model in the X negative direction is 0.45 g. The plot in figure 4.33a demonstrates that high values of displacements are observed in the facade, the adjoining bell towers, and the main dome. Also, the transversal walls between the altar and chapels experienced large deformation. The crack pattern in figure 4.33b shows the failure mechanism, which was identified as the out-of-plane failure of both the front facade and the bell towers. This out-of-plane failure also shows high concentration of tensile damage in the connection between the choir loft and the facade, as well as between the bell towers and the lateral walls. Moreover, flexural cracks are present at the base of the bell towers and in the front facade. Interestingly, separation cracks are observed between the pediment and the lower part of the facade, confirming the damage observed following the Pisco earthquake on August 15, 2007 (see chapter 2, figs. 2.12, 2.13a–d).

**FIGURE 4.31.** Diagram showing details of the connections in the numerical model between the masonry envelope and internal timber frame of the Ica Cathedral.

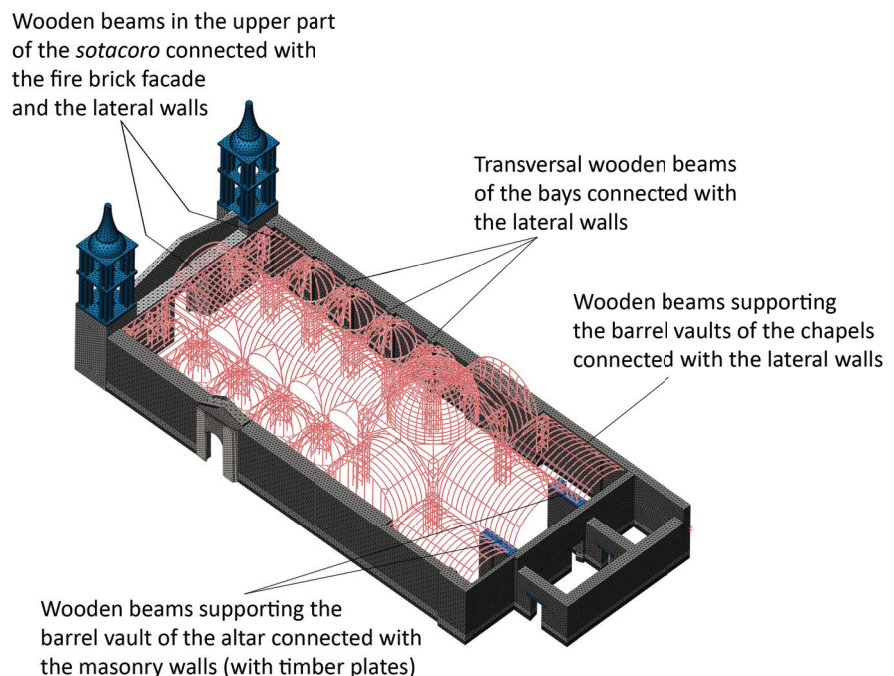
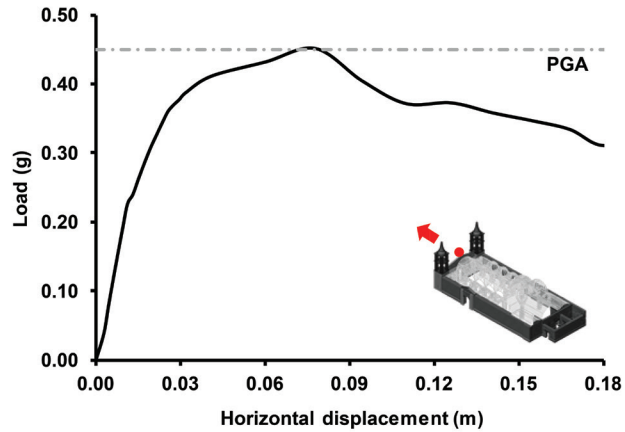
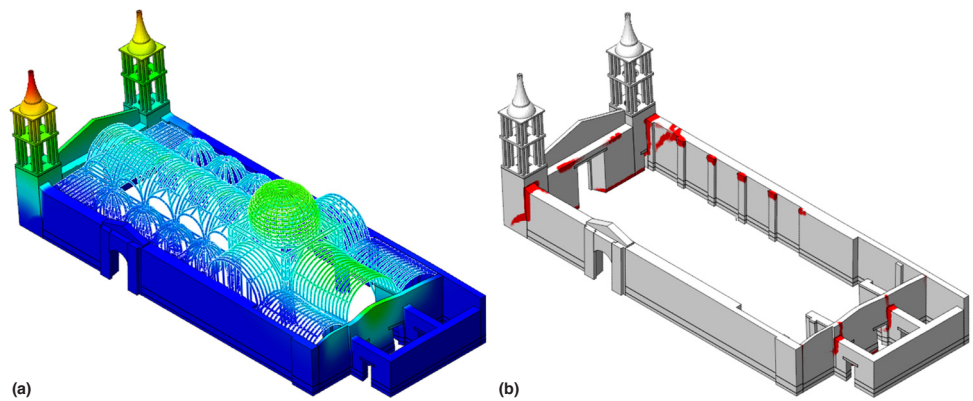


**FIGURE 4.32.**  
Load-displacement diagram for  
X negative direction for the Ica  
Cathedral.

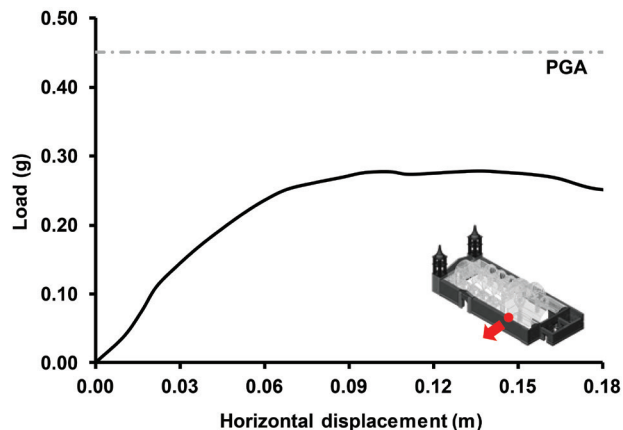


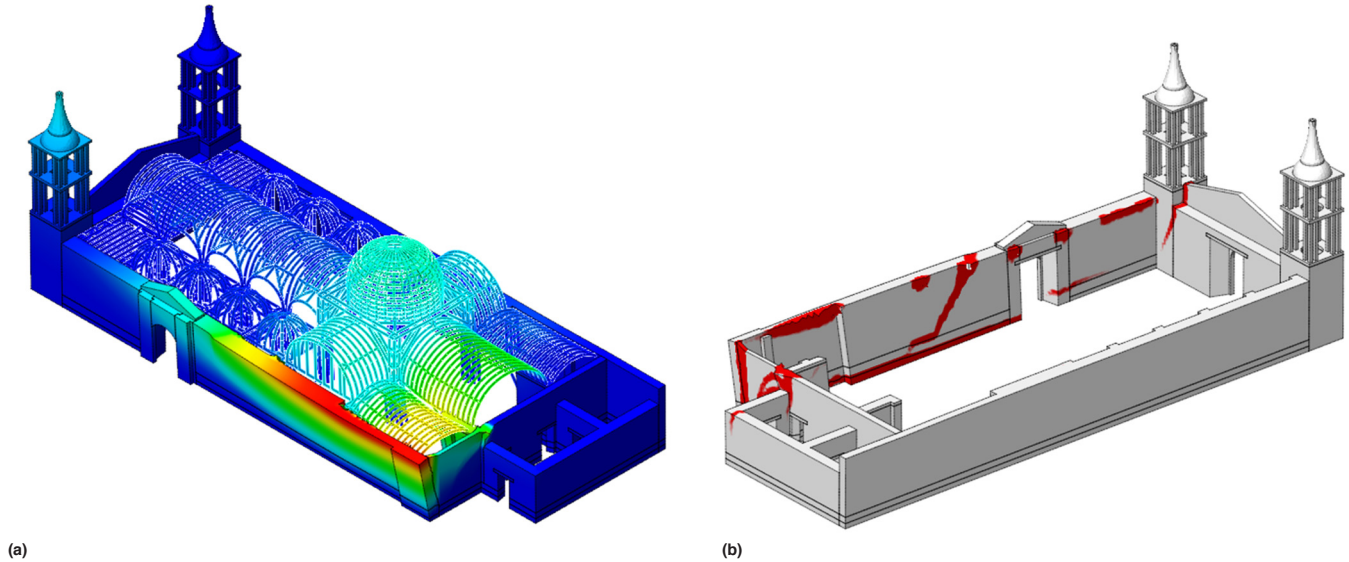
**FIGURES 4.33A, 4.33B.**  
Pushover analysis in X negative  
direction at ultimate stage for the  
Ica Cathedral: (a) deformed mesh  
of the numerical model, indicating  
maximum displacement (in red)  
and minimum displacement (in  
blue); (b) crack patterns (in red)  
in the masonry envelope.



Maximum lateral load for the Y negative direction is 0.28 g (fig. 4.34). As shown in figure 4.35a, high values of displacements are recorded in the northern wall, transept, and barrel vaults covering the altar and chapel on the street side. The failure mechanism in the masonry under this loading is identified as the out-of-plane failure of the entire northern lateral wall (fig. 4.35b). This failure mode also includes out-of-plane failure and separation of the northern bell tower from the brick facade and a portion of the transversal wall of the altar. Moreover, flexural cracks occur at the base of the northern wall and at the interface between the adobe masonry and the fired-brick base course, in agreement with the damage

**FIGURE 4.34.**  
Load-displacement diagram for  
Y negative direction for the Ica  
Cathedral.





**FIGURES 4.35A, 4.35B.**  
Pushover analysis in Y negative direction at ultimate stage for the Ica Cathedral: (a) deformed mesh of the numerical model, indicating maximum displacement (in red) and minimum displacement (in blue); (b) crack patterns (in red) in the masonry envelope.

observed in situ (see chapter 2, figs. 2.12, 2.13a–d). In addition, separation cracks are seen between the lateral wall and the chapel at the northwestern corner of the building.

### Conclusions

The analyses performed on the model of the Ica Cathedral demonstrate that the building is influenced by the interaction of the timber frame with the masonry envelope. Furthermore, the analyses allowed the research team to estimate the capacity of the structure in the two most critical directions, with a good correlation to the existing damage from recent seismic events. The capacity obtained with pushover analysis in the X negative direction is equal to 0.45 g, which corresponds to the limit required by the Peruvian code (E.030 2016). In the Y negative direction, the maximum capacity of the structure is significantly lower than demanded by the Peruvian code, corresponding to a value of 0.28 g. Therefore, the results obtained from the pushover analyses pointed out the need to reduce the out-of-plane vulnerabilities of the structure, especially at the northwestern corner of the cathedral.

## Strengthened Structure of the Ica Cathedral

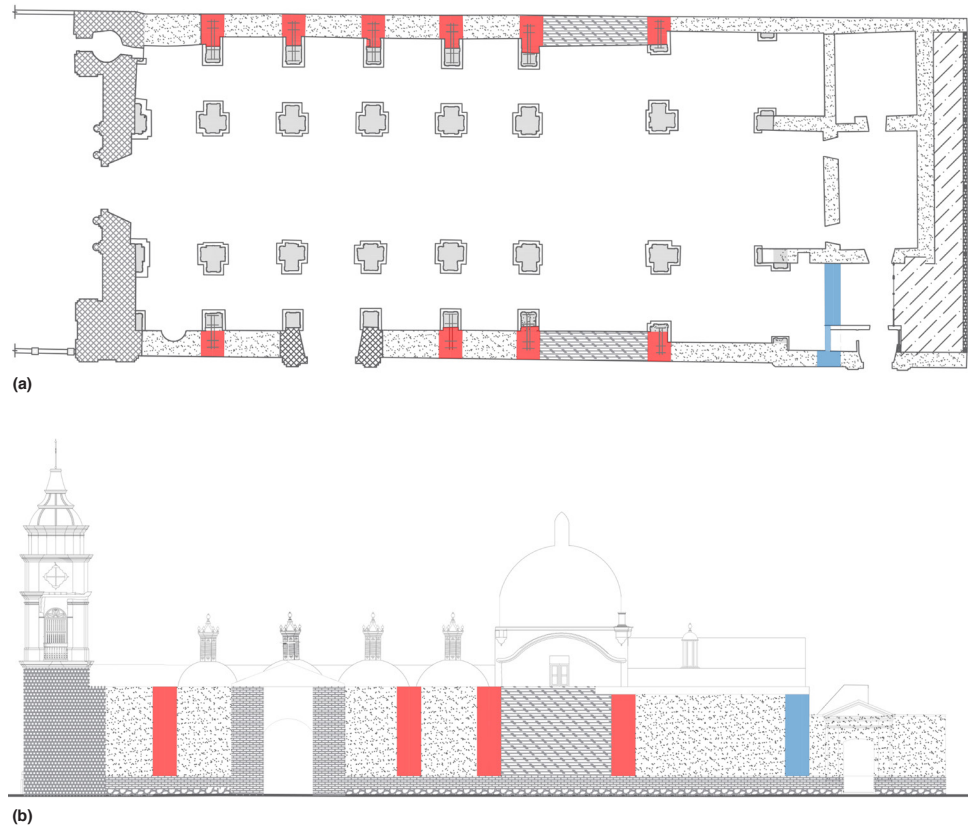
### Description of the Strengthening

The strengthening proposed for the external masonry envelope of the cathedral includes (a) new brick masonry to substitute for the existing masonry in selected parts; (b) timber anchoring systems; (c) a timber collar beam at the northwestern corner of the cathedral; and (d) steel anchoring systems connecting the internal timber structure with the front facade. More details can be found in Ciocci, Sharma, and Lourenço (2017) and in Lourenço et al. (2018).

The research team has proposed replacement of some sections of the existing masonry structure to strengthen the connection between the existing timber structure and the masonry envelope, to enhance the integrity of the envelope, and to ensure a limited long-term deterioration. Figures 4.36a and 4.36b show the location of the new brick masonry

FIGURES 4.36A, 4.36B.

(a) Floor plan and (b) elevation of the Ica Cathedral, showing the proposed new brick masonry columns (in red) and new brick masonry wall (in blue).



columns in the lateral longitudinal walls and the new brick masonry wall at the northwestern corner of the cathedral. It is important to mention that the inclusion of brick masonry in adobe walls—particularly around openings, as seen in Hotel El Comercio—was a traditional technique employed during the Spanish viceroyalty period. Connections between the strengthening and the existing structure must be ensured by interlocking the new brick masonry with existing masonry. Installing a relieving arch in the thickness of the wall has been proposed to allow space for maintaining the original location of the restroom adjacent to the new brick masonry wall.

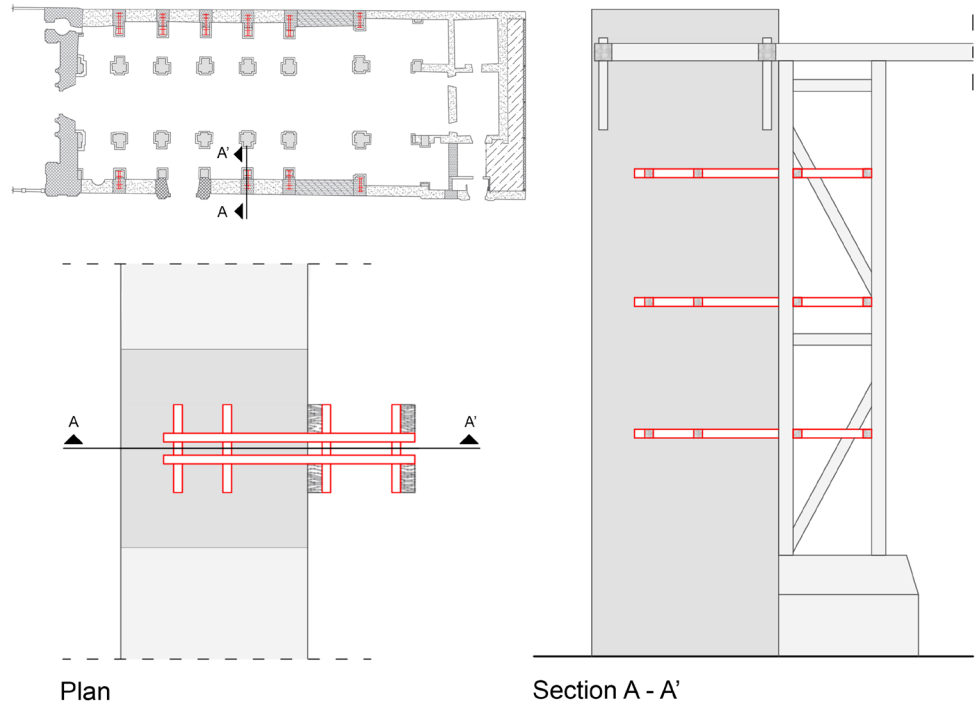
Timber anchoring systems are embedded in these new brick columns along the lateral longitudinal walls to improve the connection between the internal timber frame and the external masonry envelope. In general, each timber anchoring system is composed of keys and ties connected by nailed half-lap joints, and each has four levels along the height of the lateral walls (figs. 4.37a, 4.37b). It should be noted that the anchoring systems at the uppermost level have vertical keys to improve the resisting mechanism.

The research team has proposed incorporating a U-shaped timber collar beam at the back of the cathedral surrounding the altar and the chapels, with a frame composed of timber elements joined with nailed half-lap connections (fig. 4.38). This is intended to prevent the out-of-plane mechanism of the wall at the northwestern corner of the cathedral and enhance structural integrity. The collar beam is connected to the internal timber frame in proximity of the transept and the transversal walls flanking the altar.

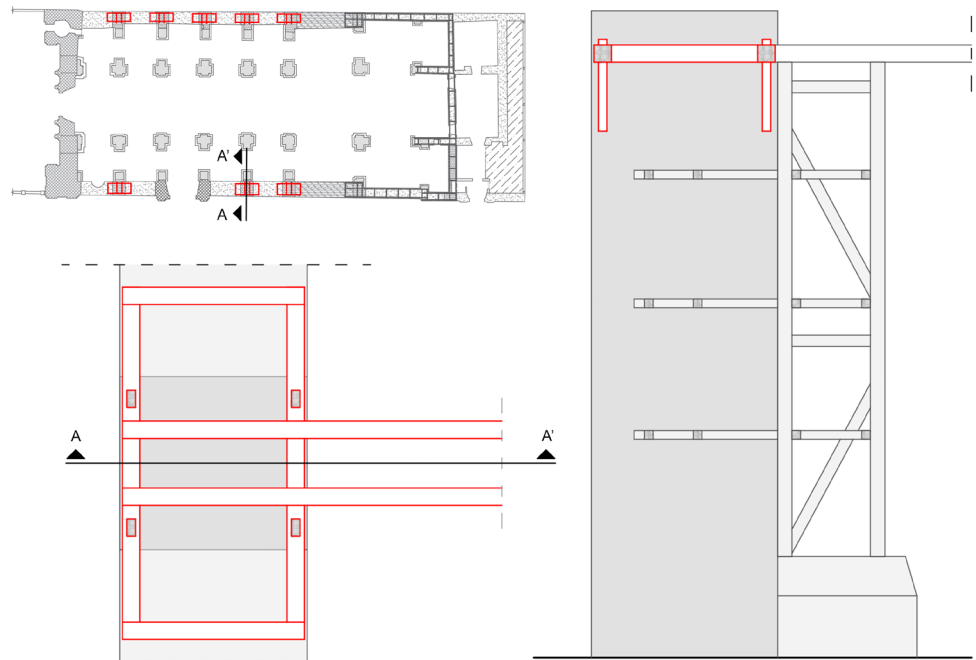
Finally, four steel anchoring systems have been proposed to address the out-of-plane mechanism of the front facade in order to improve its connection with the internal timber

FIGURES 4.37A, 4.37B.

Details of the proposed timber anchoring system at the Ica Cathedral, showing (a) the lowest levels; (b) the uppermost level.



(a)

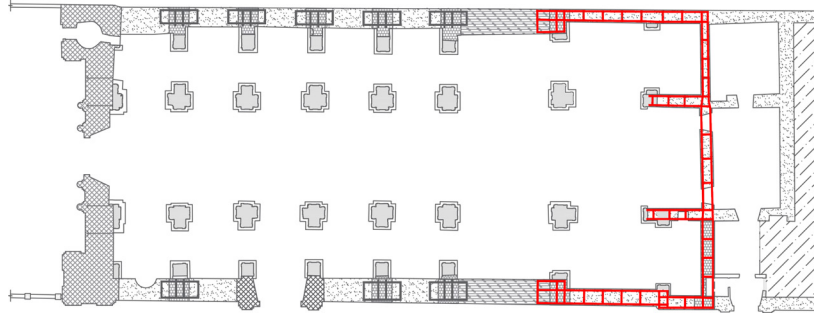


(b)

structure. Each anchoring system is composed of the following: steel ties passing throughout the thickness of the brick front facade; a square steel plate with stiffening elements; and steel profiles with bolts and plates to ensure connection to the internal timber structure (figs. 4.39a, 4.39b).

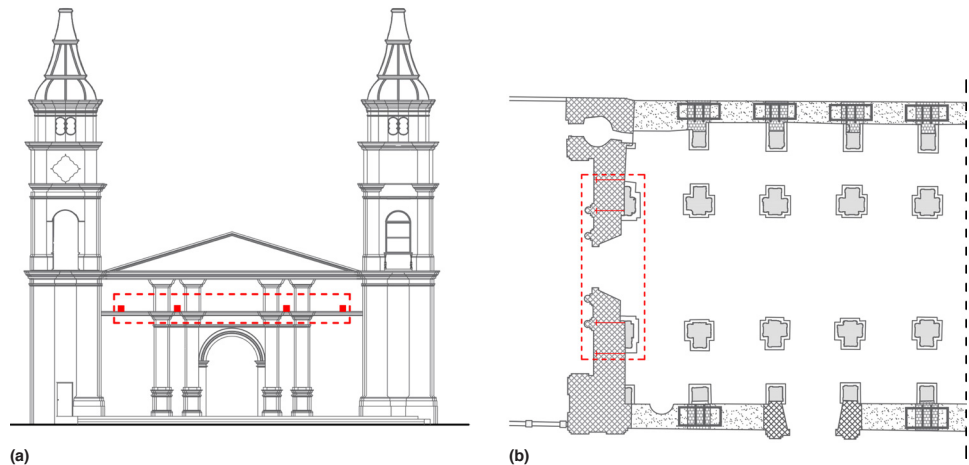
FIGURE 4.38.

Floor plan of the Ica Cathedral, showing location of the proposed timber collar beam (in red) at the back of the cathedral.



FIGURES 4.39A, 4.39B.

(a) Elevation and (b) floor plan of the Ica Cathedral, showing the proposed steel anchoring systems for the front facade.



### Characteristics of the Numerical Model

The FE model of the strengthened structure followed the approach used for the previous model (fig. 4.40). Regarding the strengthening, beam elements embedded in the masonry are used to model the timber anchoring systems as well as the timber members of the collar beam (fig. 4.41). It is important to note that a perfect bond is assumed between these beam elements and the solid linear elements, as the strains of the former are computed from the displacement field of the latter. The steel plates on the front facade are modeled using shell elements with an isotropic homogeneous and linear behavior. Truss elements, as well as beam elements, are used to model the connection of the embedded timber components within the internal structure (fig. 4.42). In particular, the von Mises model criterion is applied to these connecting elements.

### Numerical Analysis

Because a stronger connection is provided between the timber structure and the masonry envelope by means of the strengthening, a sensitivity analysis was carried out regarding the modeling of the connecting elements. In this study, the model of the structure, not including the strengthening, was compared to a model that differed only in the use of enhanced truss elements for these connecting components. Although no significant difference was observed in terms of failure mechanisms, the capacity values obtained for this model were lower than those presented in the section “Unstrengthened Structure of the Ica Cathedral” above. Therefore, the updated version of the model using enhanced truss

**FIGURE 4.40.**  
FE models of the strengthened structure of the Ica Cathedral, which followed the approach used for the previous model.

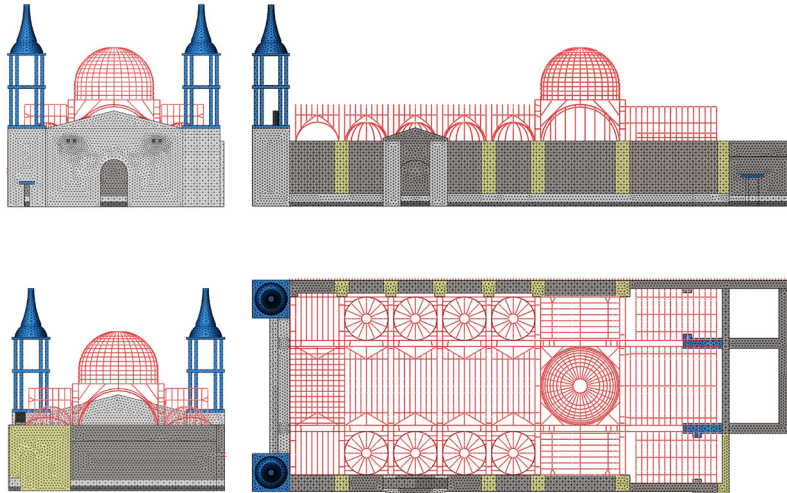


**FIGURE 4.41.**  
Plot showing embedded beam components in the numerical model of the Ica Cathedral.

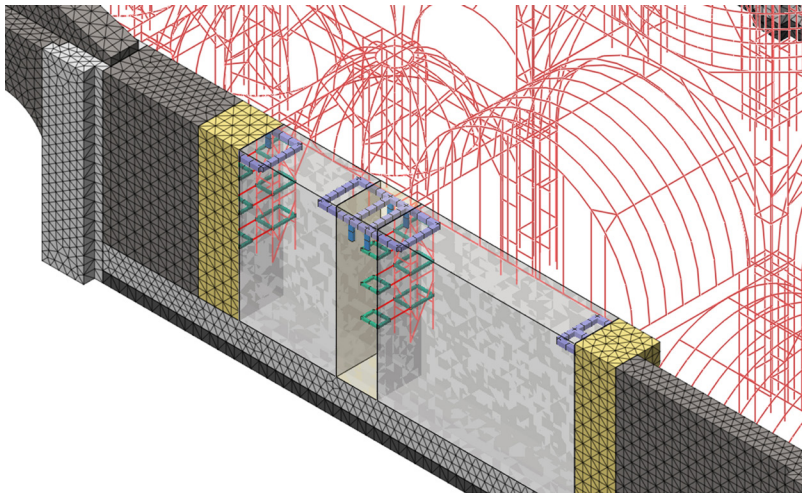
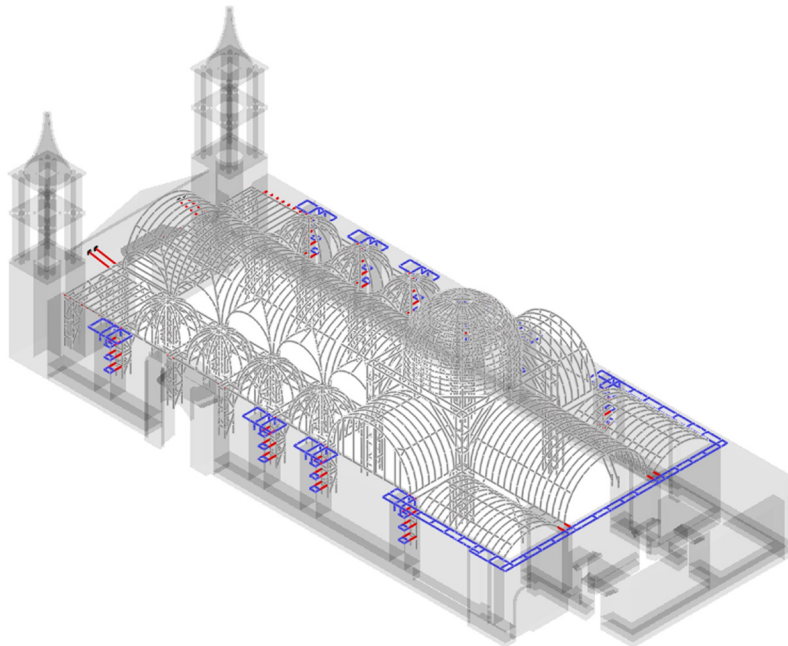


**FIGURE 4.42.**  
Plot showing enhanced truss elements (in red) and embedded beam components (in blue) of the Ica Cathedral.



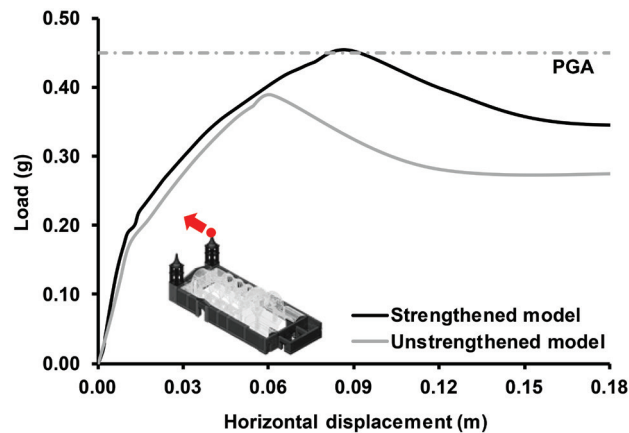
elements was assumed to provide a more conservative scenario and is hereby adopted as the unstrengthened model.

The behavior of the unstrengthened and strengthened models, in terms of load-displacement diagrams, under lateral loading in the X negative direction is summarized in figure 4.43. While the maximum lateral load that can be applied to the unstrengthened model is 0.39 g, a maximum capacity of 0.45 g is calculated for the strengthened model. It is interesting to note that this higher value of lateral load-carrying capacity is obtained for larger displacements, and the ductility of the structure is not compromised by the strengthening.

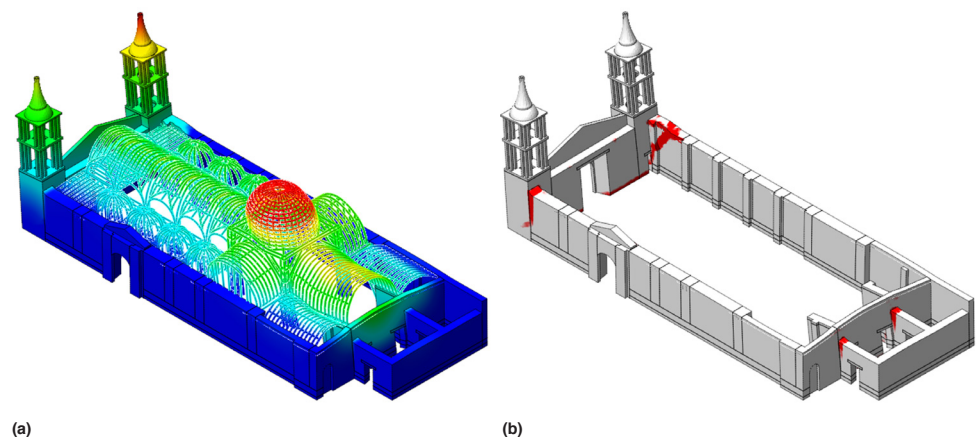
At maximum load, a larger deformation is observed for the southern bell tower compared to the northern bell tower in the strengthened model (fig. 4.44a); similar displacements are observed for the bell towers in the unstrengthened model (see fig. 4.33). Large deformations also occur in the front facade, the northern bell towers, and the walls surrounding the altar and the main dome.

A crack pattern similar to that of the unstrengthened model is observed for the strengthened model when it reaches maximum load capacity (fig. 4.44b). Vertical separation cracks occur in the connection between the bell towers and the lateral longitudinal walls. Moreover, diagonal cracking propagates throughout the adobe wall adjoining the southern bell tower. Additionally, flexural cracks are present at the base of the bell towers and the front facade. Higher tensile damage is also observed in the regions where the transversal walls of the altar are connected to the adjoining walls at the back of the cathedral. Regarding the

**FIGURE 4.43.** Load-displacement diagram for the strengthened and unstrengthened models loaded in X negative direction for the Ica Cathedral.



**FIGURES 4.44A, 4.44B.** Pushover analysis in X negative direction at ultimate load for the Ica Cathedral (strengthened): (a) deformed mesh of the numerical model, indicating maximum displacement (in red) and minimum displacement (in blue); (b) crack patterns (in red) in the masonry envelope.



strengthening elements, maximum values of axial forces and shear forces are lower than their capacities. The most critical part of the timber strengthening is represented by the collar beam with high values of axial forces and biaxial shear forces.

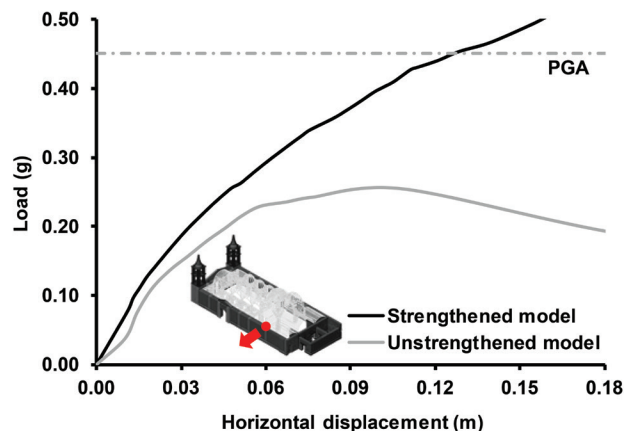
As the structure enters the post-peak part of the capacity curve, tensile damage progresses mainly in the connection between the southern bell tower and the lateral longitudinal wall. Furthermore, the failure mechanism of the strengthened model is identified as the out-of-plane mechanism of the southern bell tower only. A strong increase in tensile axial force is observed for the steel tie close to the southern bell tower at ultimate stage. Still, the maximum internal forces calculated for the strengthening steel elements are lower than the corresponding capacities.

The behavior of the unstrengthened and strengthened models, in terms of load-displacement diagrams, under lateral loading in the Y negative direction is summarized in figure 4.45. Compared to the unstrengthened model—for which a maximum lateral load is calculated as a value of 0.25 g—the strengthened model shows an increase in the capacity and the ability to retain stiffness for much larger loads.

The deformed shape observed for the strengthened model under a lateral load equal to the PGA recommended by the Peruvian code is shown in figure 4.46a. High values of displacements can occur in the northern bell tower, lateral walls, and main dome. It is interesting to note that both longitudinal walls show significant deformation, which is not observed in the unstrengthened model. Under this load, cracking in the masonry envelope is noted over a larger region compared to the more local concentration at the same location in the unstrengthened model (see fig. 4.35), thus exhibiting larger structural integrity (fig. 4.46b). Moreover, diagonal cracking occurs in both longitudinal walls, which are involved in the resisting mechanism of the strengthened model under this load. Cracks are also observed between the northern bell tower and the front facade, progressing from the top to the base of the former. Further damage can be seen in the connection of the transversal wall of the altar with other adjoining walls and throughout the length of the base of the lateral longitudinal walls (see fig. 4.46b).

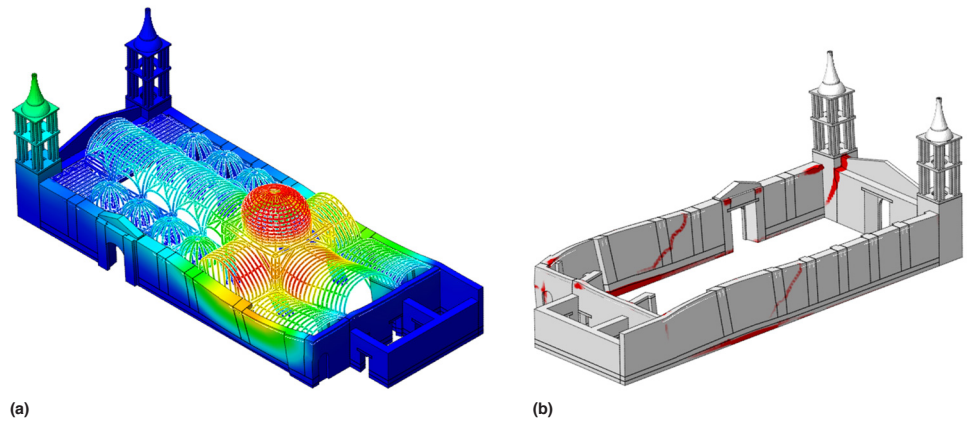
The highest values of internal forces in the strengthening occurs in the collar beam. The elements on the southern side of the collar beam are mainly subjected to high compressive axial forces, while significant tensile axial forces occur in most of the elements on the other side. Significant biaxial shear is present in the connection of the collar beam with the transversal wall dividing the altar and the northern chapel. However, when a lateral load

FIGURE 4.45.  
Load-displacement diagram for the strengthened and unstrengthened models in Y negative direction for the Ica Cathedral.



FIGURES 4.46A, 4.46B.

Pushover analysis in the Y negative direction under a lateral load equal to the recommended PGA for the Ica Cathedral (strengthened): (a) deformed mesh of the numerical model, indicating maximum displacement (in red) and minimum displacement (in blue); (b) crack patterns (in red) in the masonry envelope.



equal to the demand recommended by the Peruvian code is applied to the model, the maximum tensile axial force and shear that occur in the collar beam are lower than the timber ultimate capacity.

### Conclusions

The safety assessment carried out for the Ica Cathedral in its current conditions determined the following: (1) the connections between the two structures are a significant factor influencing the structural behavior; (2) the out-of-plane mechanism of both the front facade and the bell towers occurs for lateral loading in the X negative direction; and (3) the out-of-plane mechanism of both the northwestern corner and the northern bell tower is observed for lateral loading in the Y negative direction. Therefore, adequate strengthening measures were defined to address the main vulnerabilities of the structure.

Regarding pushover analysis, comparison between the results obtained from the strengthened and unstrengthened models showed a significant reduction in displacements and more distributed damage in the strengthened model. The structural performance of the strengthened model was investigated for a lateral load of 0.45 g, which corresponds to the PGA recommended by the Peruvian code for the region (fig. 4.47). The strengthened model showed a seismic capacity higher than this value of lateral load in both analyzed directions. In the X negative direction, the out-of-plane mechanism of the front facade observed in the strengthened model involves mainly the southern bell tower. In the Y negative direction, the out-of-plane mechanism observed for the northwestern corner in the unstrengthened model was substituted by a flexural mechanism involving both lateral longitudinal walls.

FIGURE 4.47.

Maximum lateral capacity (g) in each direction, for models with and without strengthening, for the Ica Cathedral.



In conclusion, when compared to the unstrengthened model, the results obtained from the pushover analyses on the strengthened model showed an improved global seismic behavior of the structure where higher capacities and ductility were observed.

# Unstrengthened Case Studies: Casa Arones and Hotel El Comercio

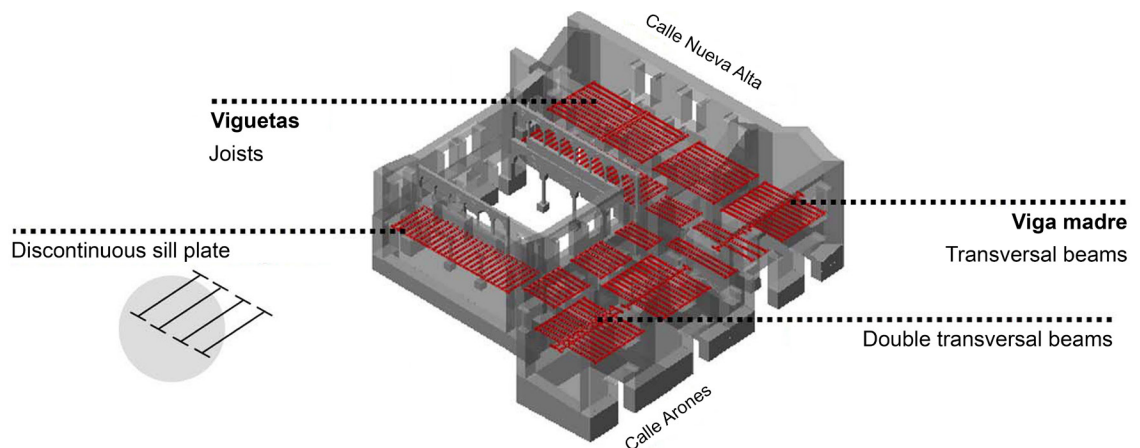
## Characteristics of the Numerical Model of Casa Arones

The numerical model of Casa Arones is characterized by a simplified 3D geometry of the building. Due to the weak connection and ductility of the quincha partitions, they are assumed not to contribute to the global behavior of the structure and thus are not included in the numerical model. The timber beams of the floors have been represented in the geometry of the model, whereas the weight of the layers resting on the beams was considered as an increase in density of the beams.

The floors of Casa Arones are made of a system of parallel timber joists embedded in the masonry wall. It is assumed that some connection between the joists and walls exists, which was represented in the model as a discontinuous sill plate connected to each beam and embedded in the wall (fig. 5.1). This approach was taken after evaluating the effect of different types of connections between timber joists and adobe masonry (see the section “Contribution of the Horizontal Diaphragms” below). On the side of the building facing Calle Arones, the two main longitudinal walls support the floors. Due to the important span and/or the sagging of the floors during the lifetime of the structure, a main timber beam spans the transversal direction. On the contrary, the floors of the building on the side facing Calle Nueva Alta lay on the transversal walls. The floors of the arcades of the patio and of the interior rooms on Calle Arones are composed of a system of timber joists always perpendicular to the patio.

With the exception of the timber ties, the roof was not included in the numerical model. The ties were considered anchored outside with vertical keys. As observed during the survey (Cancino and Lardinois 2012), anchor keys were located on the external surface of the walls with vertical arrangement. The action of the roof structure was represented in the numerical model as a load (vertical and horizontal pressures on the top surface of the wall).

**FIGURE 5.1.**  
Structure of the timber floor of Casa Arones, showing wall-embedded joists and connection between joists and walls by a discontinuous sill plate.



The roof structure of the corridors is very light and negligible in terms of global behavior of the building, so it is also not considered in the model.

The results of the damage identification provided by the previous phase of the project (Cancino and Lardinois 2012) were used to verify the results obtained with the numerical model. Finally, a sensitivity analysis was performed on the structure in order to understand the influence of selected parameters in the global behavior.

### Contribution of the Horizontal Diaphragms

The uncertainties related to the embedment of the timber joists in the adobe masonry is first addressed here. Different possible configurations were tested by representative models with dimensions and material properties similar to those of Casa Arones. Starting from a reference model, five other models were created in which different embedments of the wall-to-floor and wall-to-roof (tie beams) connections were assumed (fig. 5.2). Nonlinear static analyses were performed on the models in the direction in which the horizontal diaphragms can offer their contribution.

The model consists in a two-story building that is 9 m tall and has a rubble stone masonry foundation that is 1 m in height. The adobe walls, whose thickness corresponds to 1 m for the longitudinal walls and 0.7 m for the transversal walls, define an in-plane space of  $5 \times 7$  m. The masonry is modeled using four node linear tetrahedron elements with a mesh size of 0.3 m. The roof is assumed to transfer loads to the longitudinal walls and is defined in the form of a vertical pressure assumed equal to  $5.6 \text{ kN/m}^2$  and a horizontal thrust of  $3 \text{ kN/m}^2$ . The base of the model was fixed and nonlinear properties are specified for the masonry (see the section “Masonry” in chapter 3).

Analysis of Model 1 was approached with limit equilibrium analysis with macro-blocks (see Lourenço, Torrealva, and Pereira, forthcoming) following the kinematic approach to provide a range of values of the structural response. If the material is continuous along the entire height, failure should appear at the base, and the position of the hinge is ruled by the compressive capacity of the material. In this case, the foundation and the wall are made of different material, meaning that both possible locations should be checked. Due to the lower compressive capacity of the adobe masonry, the hinge shifts inward, resulting in a more unfavorable configuration for this material. Based on these findings, four subcases were considered for Model 1 (fig. 5.3): the first two consider a poor connection with the

**FIGURE 5.2.** Representative models considered in the study (geometry and mesh) for Casa Arones, based on a reference model.

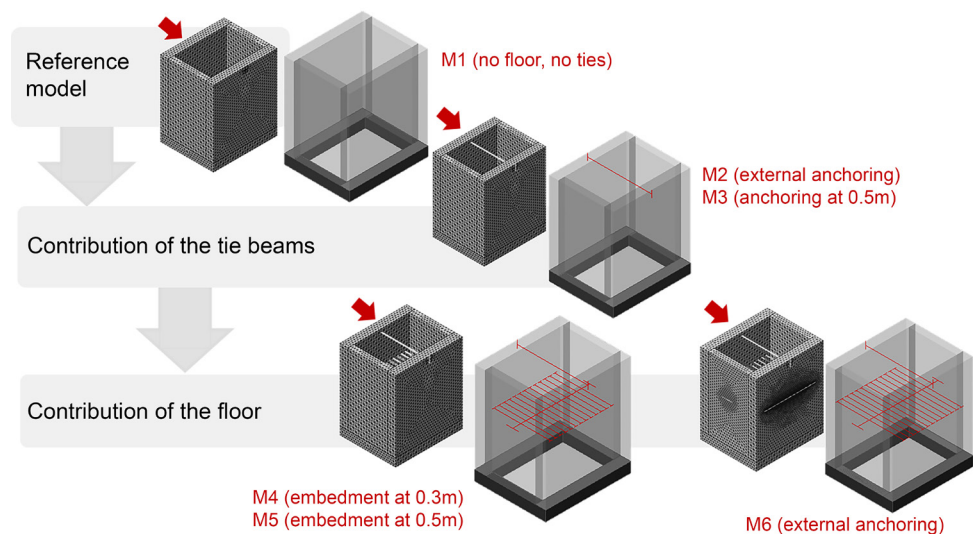
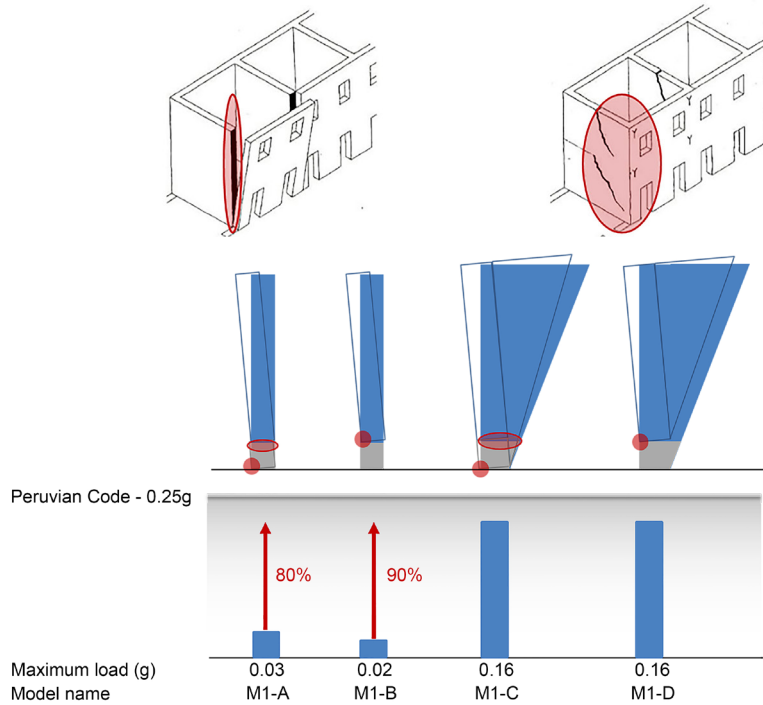


FIGURE 5.3.

Two-story building models for Casa Arones, considered in four subcases. Capacities of the four mechanisms for Model 1 for a wall with a thickness of 1 m and a total height of 10 m were compared.



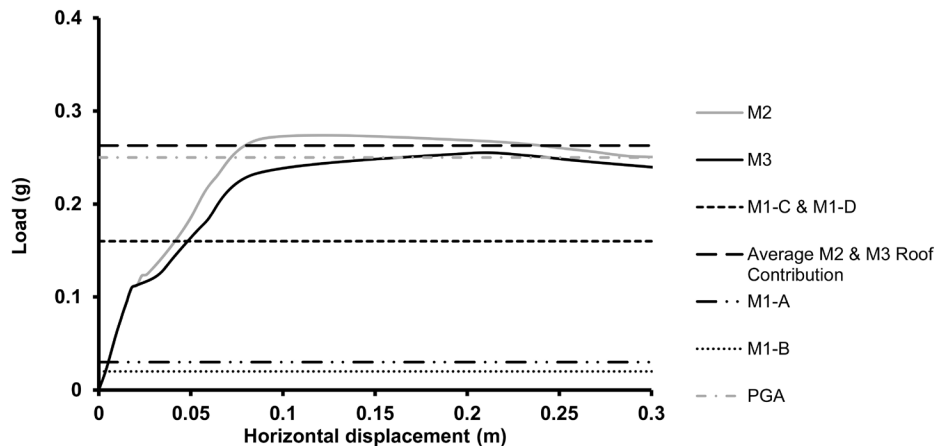
transversal walls, with the hinge formation at the base or at the lowest adobe section; the remaining two consider the contribution of the transversal wall, again with the hinge forming at the base and at the lowest adobe section. When a good connection is ensured, the capacity of the wall increases enormously, with a maximum lateral load of 0.16 g (see fig. 5.3). To ensure this failure mechanism in adobe construction, timber keys would need to be inserted in the corner of the walls.

Model 2 and Model 3 (see fig. 5.2) are based on Model 1, with the addition of a timber tie beam at the roof level, anchored either externally or in the middle thickness of the wall. The beam has a diameter of 0.1 m and is anchored to the walls with a timber key (diameter of 0.06 m) 0.8 m in length. Model 2 considers the tie beam anchored outside, whereas in Model 3 the anchoring is at 0.5 m, which corresponds to the middle of the span of the wall.

The maximum lateral load that can be applied to Model 2 in the X direction corresponds to 0.27 g (fig. 5.4), demonstrating a significant increase in the capacity of the structure due

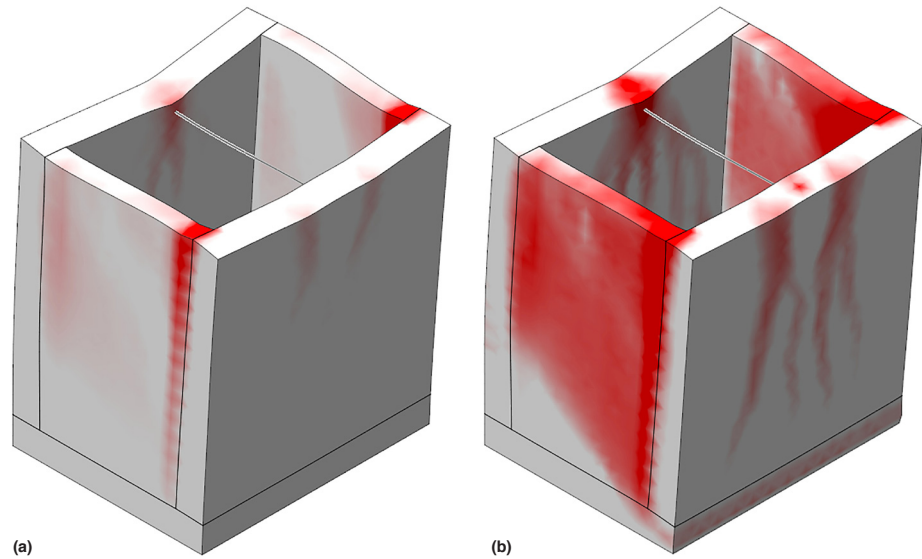
FIGURE 5.4.

Load-displacement diagram for Models 2 and 3 for Casa Arones two-story building models, compared with the results obtained from Model 1 and the limit imposed by the Peruvian code (E.030 2016).



FIGURES 5.5A, 5.5B.

Crack patterns (in red) for Casa Arones two-story building models with the addition of roof ties: (a) peak; (b) ultimate. Only Model 3 is shown.

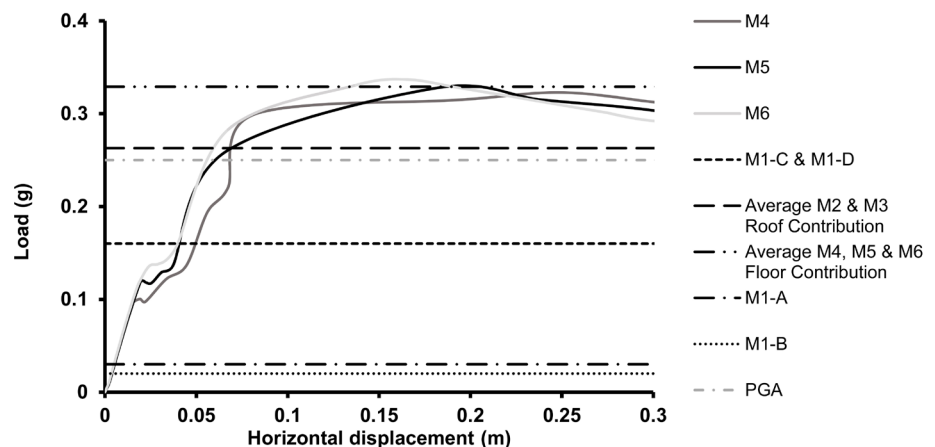


to the tie beam at roof level. As expected, the capacity of Model 3 is slightly lower, corresponding to 0.25 g. Thus, the presence of a well-connected tie beam increases the capacity of the model by 40% with respect to the original model. The presence of the timber tie beam changes the failure mechanism transferring part of the weight of the front longitudinal wall to the back longitudinal wall (figs. 5.5a, 5.5b). This is then resisted by shear of the transversal walls. The weak connection of the adobe masonry between transversal walls leads to a crack at the corners at peak level. It is possible that at this stage, the tie beams are not yet activated but subsequently will be. Finally, even vertical bending cracks appear at the mid-span of the longitudinal wall around the tie, and cracking emerges in the transversal walls.

Models 4, 5, and 6 (see fig. 5.2) have in addition the flooring system with anchoring at 0.3 m inside the wall, middle of the wall or externally, respectively. The floor is represented by a series of joists (diameter of 0.15 m) spaced 0.5 m apart, partly or fully embedded in the masonry. These are fully connected with a transversal beam spanning in a perpendicular direction and embedded in the transversal walls (diameter of 0.2 m). A discontinuous sill plate was considered at the ends of the joists. The weight of the floor was introduced as an increase in the density of the timber joists.

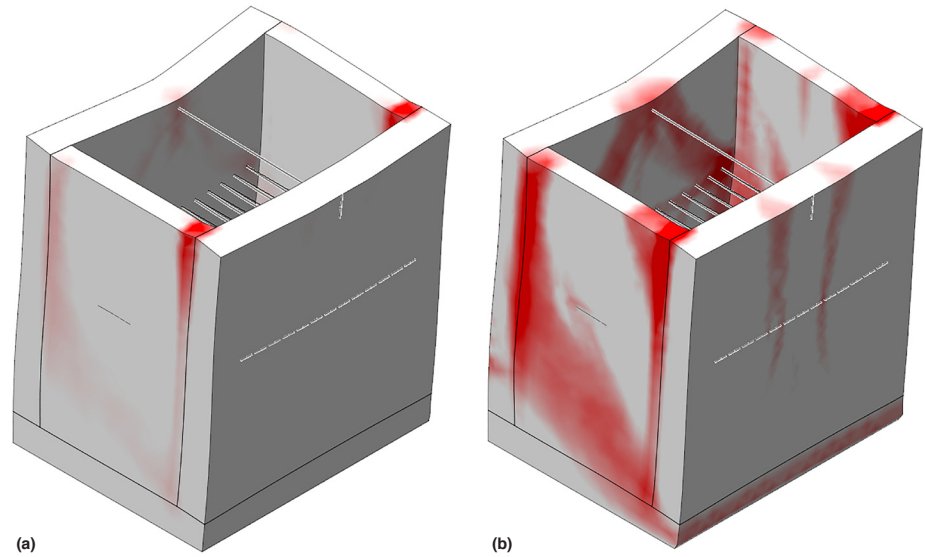
FIGURE 5.6.

Load-displacement diagram for Models 4, 5, and 6 for Casa Arones two-story building models, compared with the results obtained from Model 1 and the limit imposed by the Peruvian code (E.030 2016).



FIGURES 5.7A, 5.7B.

Crack patterns (in red) for Casa Arones two-story building models, with the addition of floor and roof ties: (a) peak; (b) ultimate. Only Model 6 is shown.



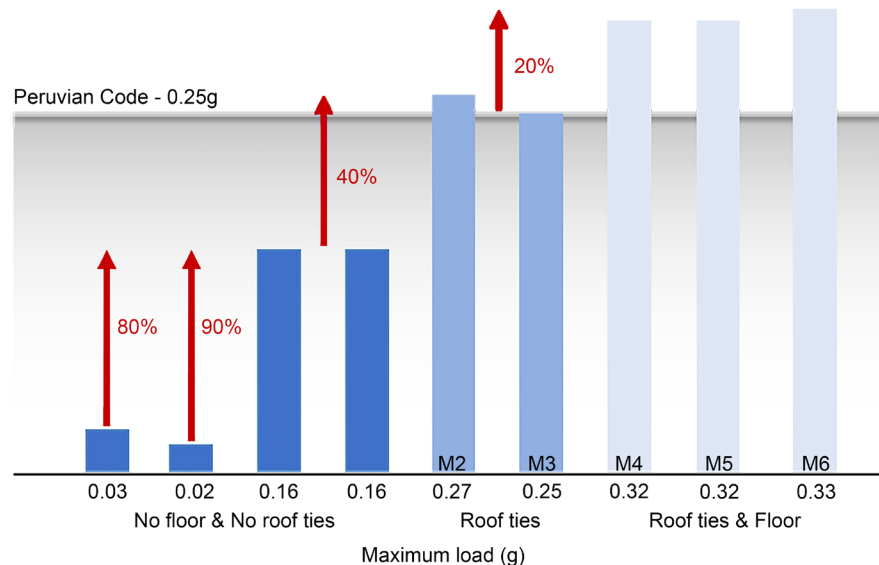
The different connections influenced only marginally the capacity of the models (fig. 5.6). Maximum capacity of the three models increases compared to the previous models. Although the capacity of the models is not as sensitive to the type of wall-to-floor connection, the increase in nonlinear stiffness of the structure provided by the different connections influences the failure mechanism in the post-peak phase. Figures 5.7a and 5.7b show typical results in terms of crack width.

In the case of the tie beams at roof level, the presence of the floor changes load transfer for seismic loading. This creates a second level of connection between the longitudinal walls, which will compress the rear longitudinal wall, provoking shear failure of the transversal walls. The models exhibit a shear increase in the transversal walls, approaching a global rocking mechanism of the structure at failure. The combined movement of the two longitudinal walls is also demonstrated by the large tensile forces that develop in the ties in the nonlinear range.

Results obtained from pushover analysis of the models are presented in figure 5.8. The tie beams in the roof are mostly responsible for the increase in capacity of the structure,

FIGURE 5.8.

Chart showing comparison between maximum capacities for Casa Arones two-story building models.



around 40%, when compared to the original model with well-connected transversal walls. The addition of a connected timber floor contributes less, with an increase in capacity of about 20%. The floor seems to ensure the full combined movement of the two longitudinal walls, particularly in the models that have deeper and external anchoring. This behavior seems to be too optimistic for adequate representation of the performance of historic structures, taking into account the assumptions made in the modeling. Therefore, anchoring of the floor over a depth of 0.3 m was adopted as representative for the modeling of the horizontal diaphragms of Casa Arones, which is a typical value for new timber floors for this type of building in Peru.

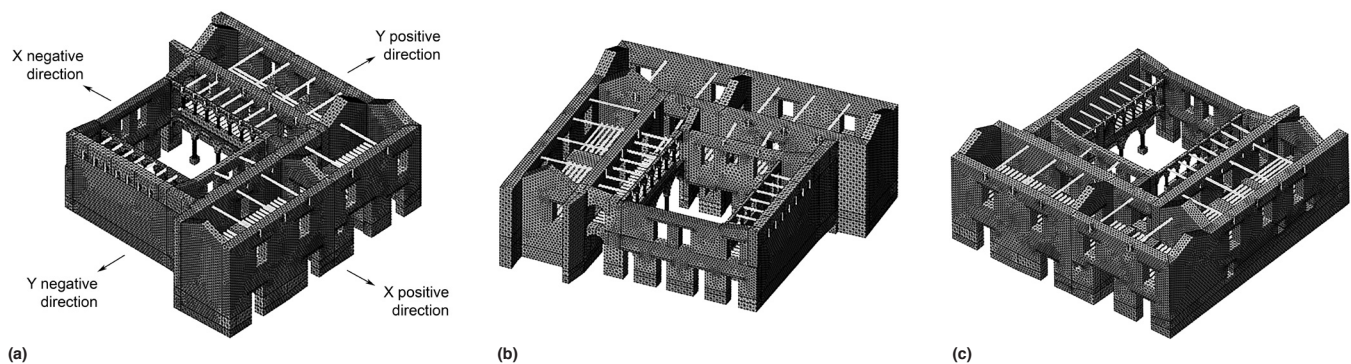
### Numerical Analysis

Figures 5.9a–c present the geometry considered in the numerical model. The model includes the main L-shape volume of the building, the two arcades and the longitudinal wall next to the collapsed area, the timber system of beams in the floor, and the timber anchor ties in the roof. The roof load was applied to the nodes on top of the masonry walls. Total number of nodes was 112,451.

The presence of the neighboring university building and, consequently, its stiffening effect on the south wall was not taken into account. The confining action of the adjacent building depends on its morphological characteristics, which were not available. In general, the block effect due to adjacent buildings yields a beneficial effect (Ramos and Lourenço 2004).

The capacity of Casa Arones was studied with pushover analysis and compared to the capacity requested by the code for the area of Cusco, equal to 0.25 g (E.030 2016). The analyses were performed in the X direction of the numerical model in both positive and negative directions (see fig. 5.9a). Pushover analyses are performed only in the positive direction of the Y axis, due to the presence of the adjacent university building in the negative direction.

FIGURES 5.9A–C.  
Views of the FE model of Casa Arones: (a) east view; (b) south view; (c) north view.



The capacity of the structure under horizontal loading in the X positive direction of the model is presented in figure 5.10 in terms of the load-displacement diagram. Maximum load capacity is equal to 0.33 g, which is higher than the limit fixed by the Peruvian code (E.030 2016). The results, expressed in terms of total displacement and principal crack width at ultimate stage, are presented in figure 5.11. The failure mechanism consists of the out-of-plane movement of the longitudinal external wall facing Calle Arones. With the increase in the horizontal load, the deformation of this wall triggers the parallel longitudinal

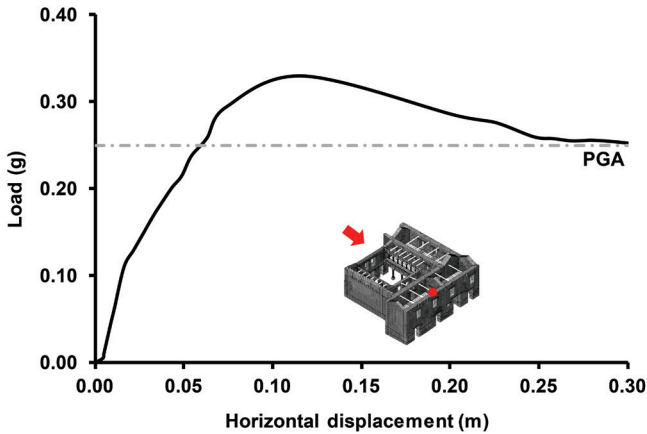
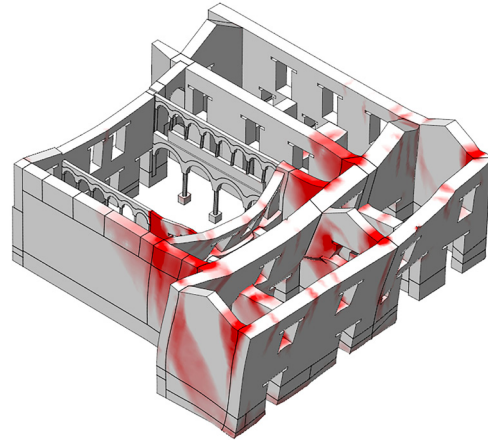


FIGURE 5.10. (LEFT)  
Load-displacement diagram in X positive direction for the FE model of Casa Arones.

FIGURE 5.11. (RIGHT)  
Crack patterns (in red) at ultimate stage for loading in X positive direction for Casa Arones.

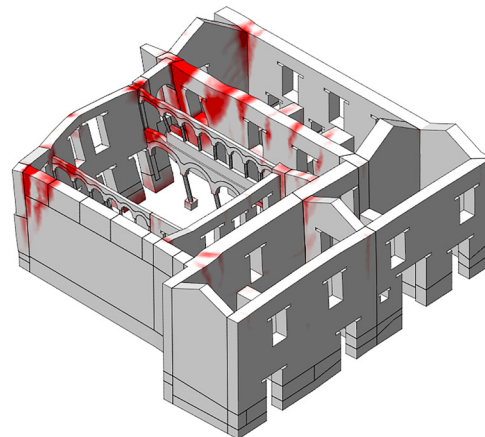
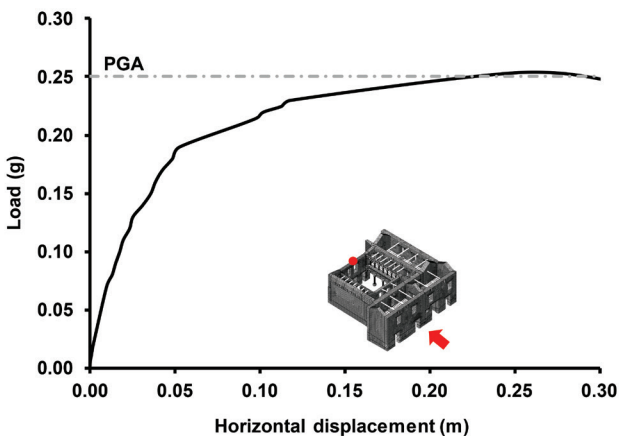


wall due to the presence of the ties. This, in turn, transfers part of the horizontal load to the other (internal) parallel wall. Compression of the rear longitudinal walls generates shear failure at post-peak of the transversal walls. Vertical cracks develop along the height of these longitudinal walls at the connections with the transversal walls. The most relevant cracks appear at the connection between the external longitudinal wall on Calle Arones and the transversal walls, as detected during the survey of the building (Cancino and Lardinois 2012). In the south arcade, the adobe masonry wall section and the stone masonry arcade have separated due to the high difference in stiffness between the two materials.

FIGURE 5.12. (LEFT)  
Load-displacement diagram in X negative direction for Casa Arones.

FIGURE 5.13. (RIGHT)  
Crack patterns (in red) at ultimate stage for loading in X negative direction for Casa Arones.

Next, the capacity of the structure under horizontal loading in the X negative direction of the model is summarized in figure 5.12 in terms of the load-displacement diagram. Maximum load applied is 0.25 g, which corresponds to the value defined in the Peruvian code. The numerical model enters post-peak behavior after this load is applied, with a large value of displacement recorded on the free wall on the west side adjacent to the collapsed area (fig. 5.13). Due to the out-of-plane movement of this wall, vertical cracks develop along the height of the wall at the connections with the arcades and at the edges. In particular, damage in the arcades seems to be concentrated in the first arch on the north side. When maximum load is applied, the most relevant crack appears at the connection between the free rear wall and the south wall.



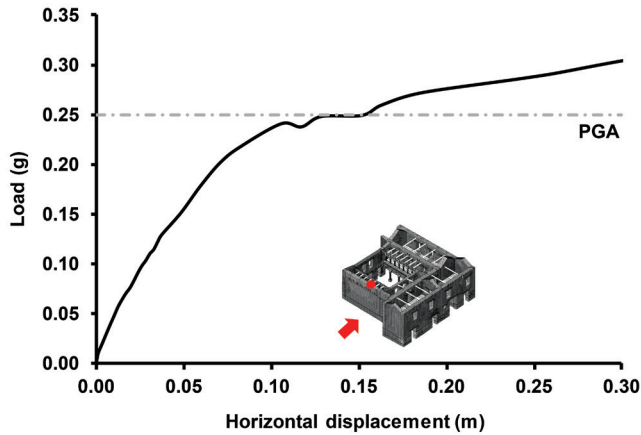


FIGURE 5.14. (LEFT)  
Load-displacement diagram in Y positive direction for Casa Arones.

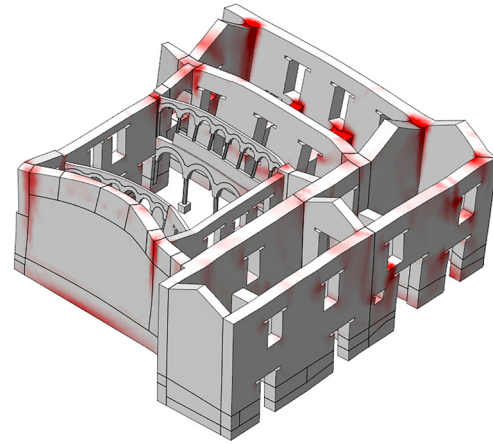


FIGURE 5.15 (RIGHT)  
Crack patterns (in red) at ultimate stage for loading in Y positive direction for Casa Arones.

The capacity of the structure under horizontal loading in the Y positive direction of the model is summarized in figure 5.14 in terms of the load-displacement diagram. The maximum load applied is 0.37 g. The numerical model enters post-peak behavior after this load is applied, with very large value of displacement recorded on the south wall adjacent to the university building (fig. 5.15). The failure mode consists of the out-of-plane movement of the south wall. It is noted that significant out-of-plane displacements also occur in the northern arcade and in the external wall facing Calle Nueva Alta. Vertical cracks appear on the south wall at the connection with the transversal walls, as detected during the survey. However, a relevant crack pattern is detected on the north part of the building on the Calle Nueva Alta side: the out-of-plane movement of the longitudinal walls connected by tie beams generates shear failure of the transversal walls. This is more intense in the longitudinal wall facing Calle Arones and in the last transversal wall adjacent to the collapsed area. It is also noted that the brick arches connecting the free rear wall to the longitudinal wall on Calle Nueva Alta experience relevant in-plane deformation.

### Sensitivity Analysis

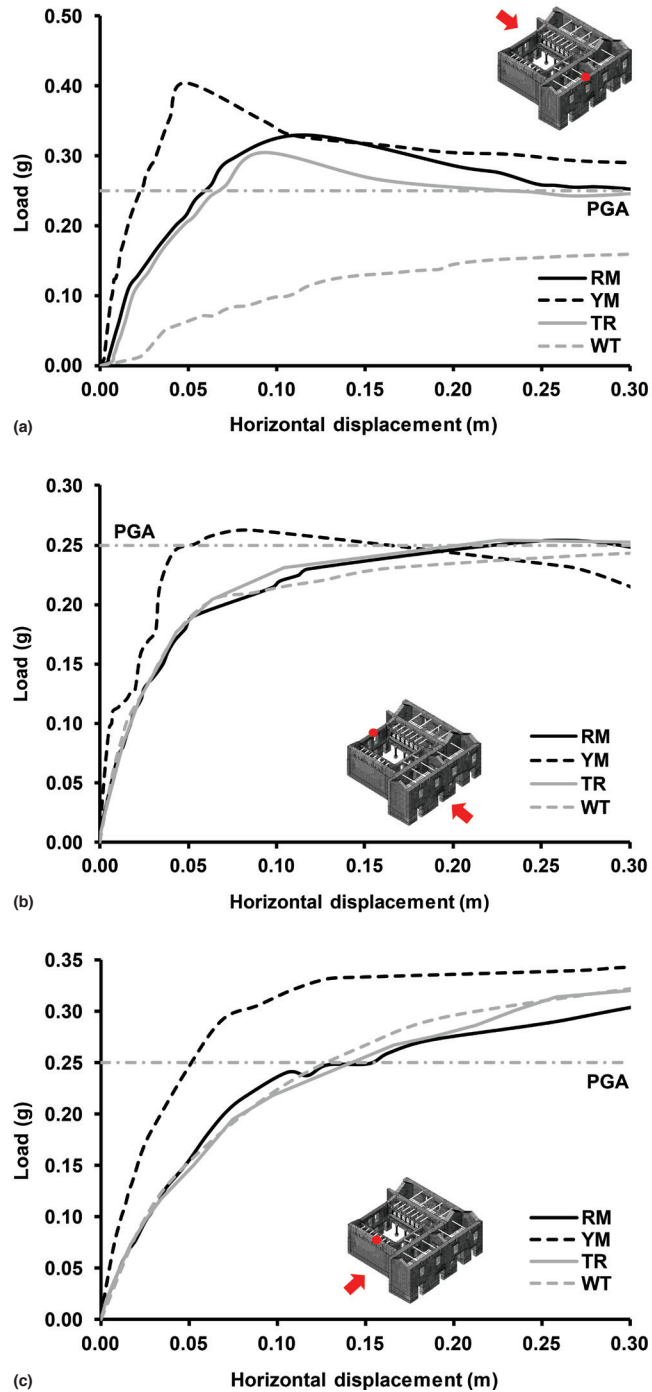
One of the challenging aspects in the study of this building is the uncertainty regarding morphology, geometry, and material properties, owing to the fact that the structure experienced numerous changes over the years. Due to this reason, a sensitivity analysis (as explained in chapter 3) was performed on the structure.

The load-displacement diagrams for this case study show very large values of displacements, with extreme values for the results of the pushover analysis in the Y positive direction. In fact, the structure already shows significant displacement in the elastic range. Therefore, a higher value of Young's modulus of the adobe (245 MPa) was adopted. The new model will be referred to as YM (Young's modulus), while the previous model, or reference model, will be referred to as RM.

To better understand the effect of the roofing system on the structure of Casa Arones, two parameters were considered. First, the effect of the thrust of the roof on the structure of Casa Arones is considered. The model TR (thrust roof) considers the double value of the horizontal thrust in comparison with the RM, which indicates fully stiff supports. Second, the effect of the presence of the tie beams of the roof was studied. In this context, a model was considered without the presence of the roof ties (WT, or without ties), simulating the conditions under which there are no beams or their connection is absent.

FIGURES 5.16A–C.

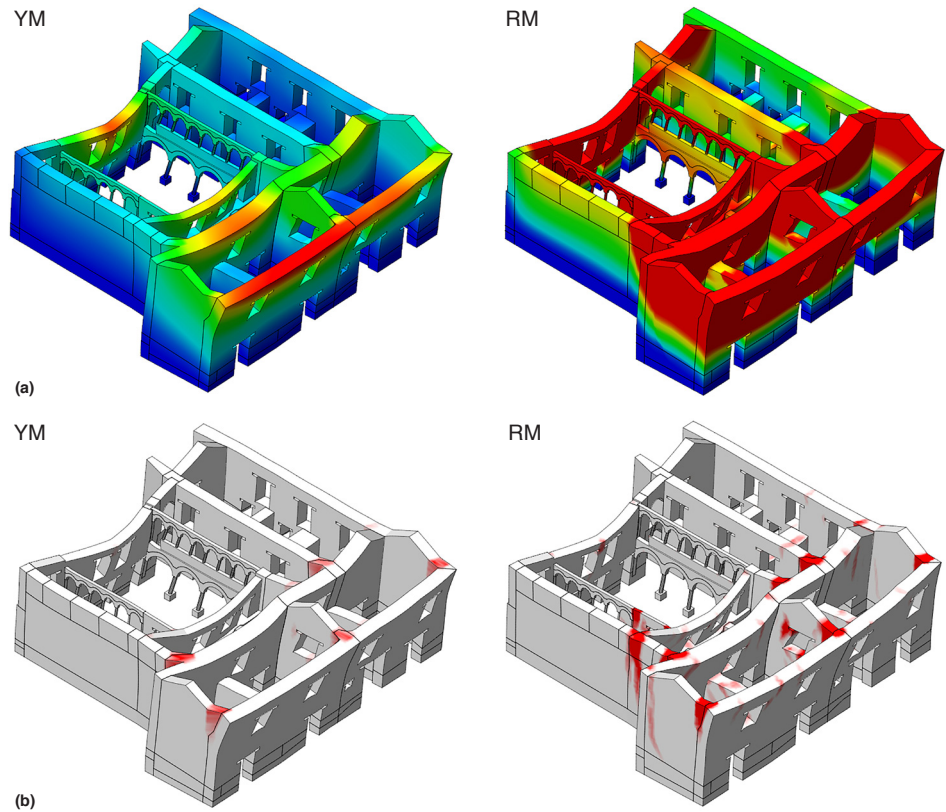
Results of the sensitivity analysis on Casa Arones compared with the results obtained with the RM: (a) X positive direction; (b) X negative direction; (c) Y positive direction.



The results of the pushover analysis in the X positive and negative directions and in the Y positive direction are presented in figures 5.16a–c in terms of load-displacement diagrams compared to the results of the RM. The stiffness of the structure is rather sensitive to the material properties of the adobe (YM) with a reduction of the amplitude of the displacement of one order of magnitude. The only change in maximum capacity is obtained when the structure is loaded in the X positive direction. In particular, the structure has a maximum capacity of 0.4 g compared to the 0.33 g of the RM. The failure mechanism was

FIGURES 5.17A, 5.17B.

Comparison between the response of YM (left) and RM (right) in X positive direction: (a) deformed mesh at peak, indicating maximum displacement (in red) and minimum displacement (in blue); (b) crack patterns (in red) on the deformed mesh at peak.

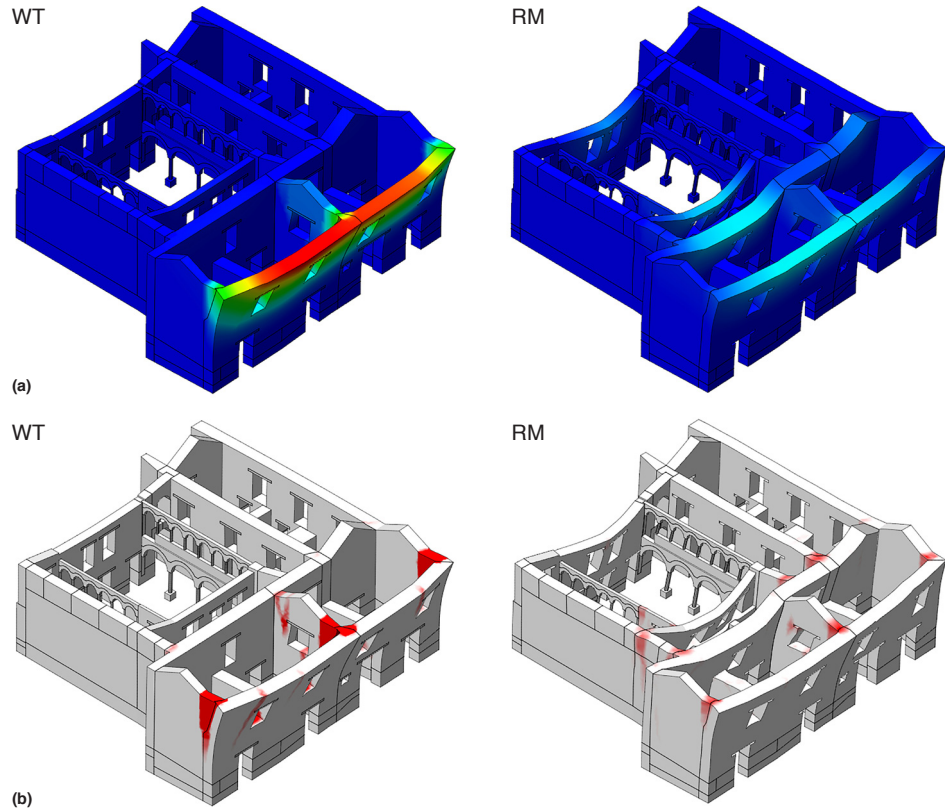


insensitive to the change in the material properties of the adobe (YM). Although the principal crack width presented cannot be visually compared due to the different displacements, it is clear that the RM experiences higher distribution of damage due to the lower stiffness of the structure (figs. 5.17a and 5.17b).

The capacity of the structure is only slightly sensitive to the horizontal thrust of the roof. In particular, see the comparison between the RM and the TR model, where the only difference is in the maximum capacity achieved, which is equal to 0.3 g for the TR model and 0.33 g for the RM (see figs 5.16a–c). After that, the curves converge to the same post-peak behavior. The failure mechanism is not sensitive to this parameter. Due to increased thrust, larger cracks will open at the connection between the longitudinal wall on Calle Arones and the transversal walls. The capacity of the structure is very sensitive to the presence of the roof ties when the structure is loaded in the X positive direction. When the structure WT is considered, the model presents a significantly lower stiffness at early loading stages due to lack of constraint provided by the ties. Maximum lateral load applied is 0.16 g; for the reference model, it is 0.32 g. The numerical model enters post-peak behavior after these loads are applied with a high value of displacements recorded in the longitudinal wall on Calle Arones. The deformed shape of the numerical model is presented in figures 5.18a and 5.18b. The failure mechanism still consists of the out-of-plane failure of the external longitudinal wall on Calle Arones; however, compared to the failure of the RM, the movement of the longitudinal walls is more uniform along the span due to the absence of constraint by the ties. Due to the characteristics of the failure mechanisms, the capacity of the structure under horizontal loading in the X negative and Y positive directions of the model WT remains unchanged.

FIGURES 5.18A, 5.18B.

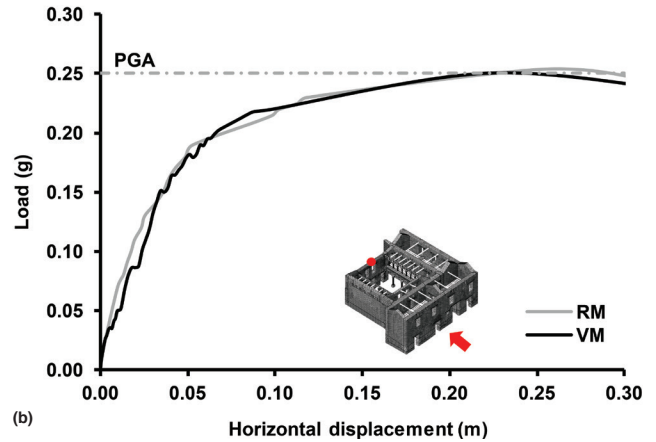
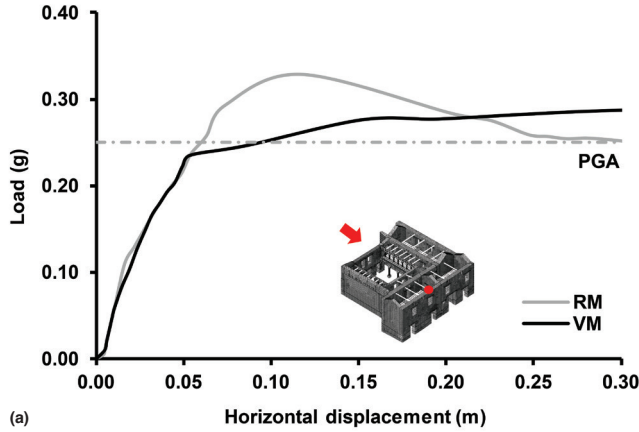
Comparison between the response of WT (left) and RM (right) in X positive direction: (a) deformed mesh at peak, indicating maximum displacement (in red) and minimum displacement (in blue); (b) crack patterns (in red) on the deformed mesh at peak.



The results presented were obtained considering timber as a linear elastic material. This seems adequate for the material assigned to the lintels and flooring, but an evaluation of the capacity of the ties should be conducted, given their relevance on the global behavior of the structure. Following a general approach normally taken for design of the anchor ties (Vinci 2014), the capacity of the ties is evaluated in terms of three contributions: the tensile capacity of the tie beam itself, the capacity of the masonry (bending and shear), and the capacity of the key (bending and shear). The tensile force that would cause the failure of the anchor was calculated as 30 kN. The maximum capacity obtained was assigned to the model, adopting the von Mises failure criterion for the ties.

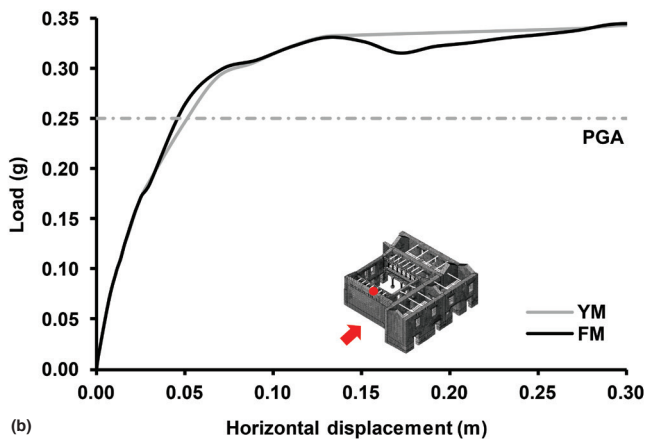
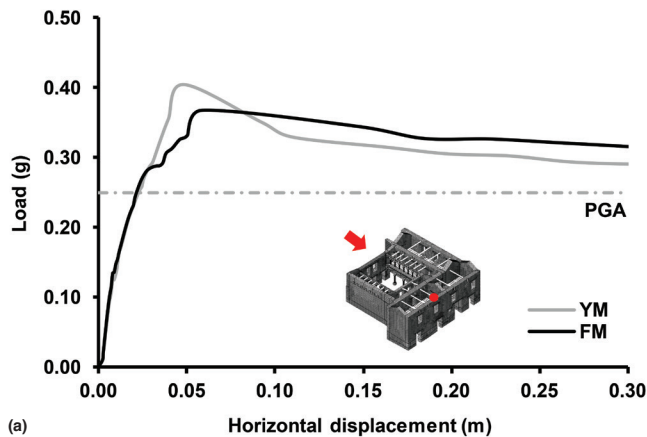
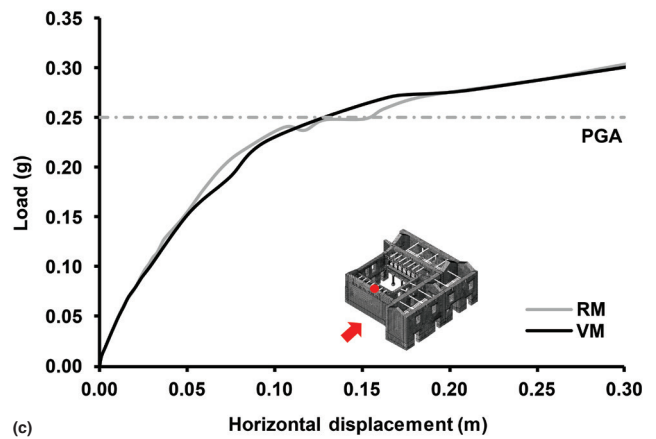
Results are presented in figures 5.19a–c in terms of load-displacement diagrams. The introduction of a limit in the tensile capacity of the timber ties does not change the failure mechanisms of the structure. Pushover analyses in X negative and Y positive directions do not present differences in terms of maximum horizontal capacity when compared to the RM. For post-peak behavior, the softening phase seems to be more pronounced due to the plasticity imposed on the timber ties. In the X positive direction, the model is more sensitive to the presence of the roof ties, and the maximum horizontal capacity of the von Mises model decreases 22% to a value of 0.28 g, indicating a more ductile behavior.

Based on the different results obtained, a final model (FM) was chosen. This model is considered to be the most representative and the best estimate of the behavior of the structure, assuming an increased Young's modulus of 245 MPa and considering a limit in the tensile capacity of the timber roof ties per the von Mises model. As shown in figures 5.20a and 5.20b, the response of the FM in the X positive direction shows a lower capacity equal to 0.36 g, while the response in the Y positive direction matches the results obtained with the YM models.



FIGURES 5.19A–C.

Comparison between the response of the von Mises model and RM in pushover analyses in terms of load-displacement diagrams: (a) X positive direction; (b) X negative direction; (c) Y positive direction.



FIGURES 5.20A, 5.20B.

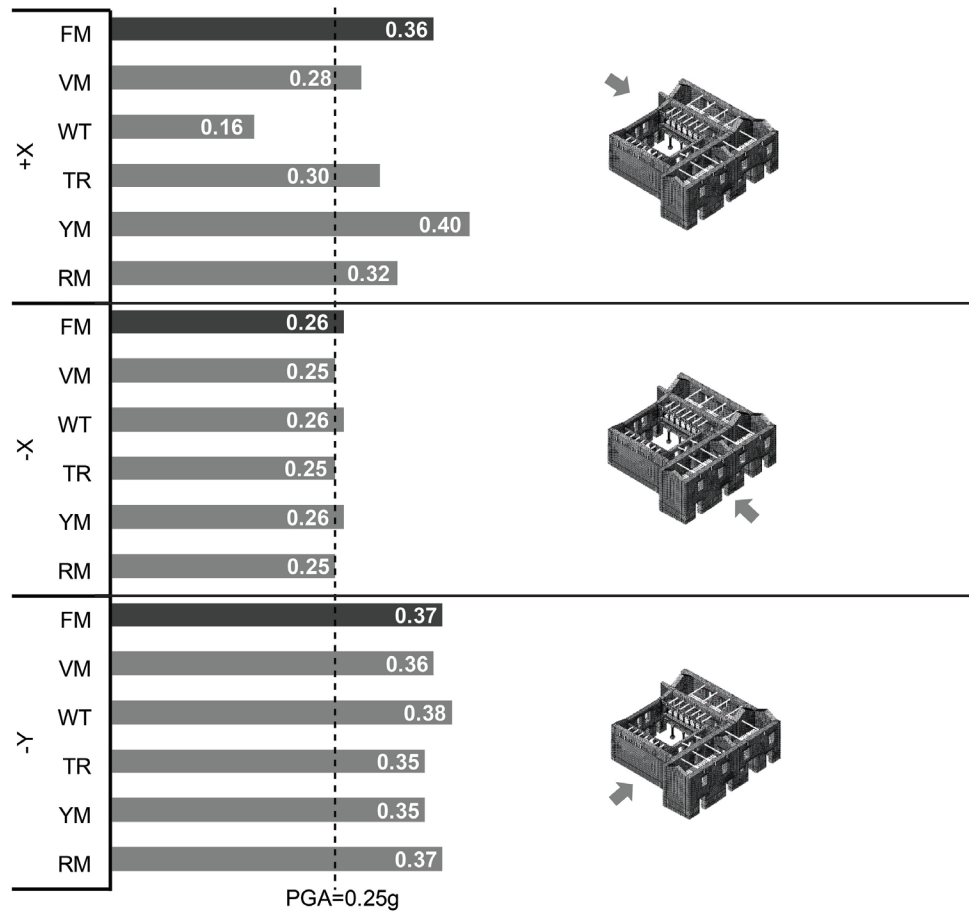
Comparison between the response of FM and YM in pushover analyses in terms of load-displacement diagrams: (a) X positive direction; (b) Y positive direction.

## Conclusions

Pushover analyses were carried out on Casa Arones in order to study the seismic behavior of the building. Different types of connections were discussed to understand the influence of the horizontal diaphragms on the earthen construction. The results show how well connected timber diaphragms can significantly improve the capacity of the structure against

FIGURE 5.21.

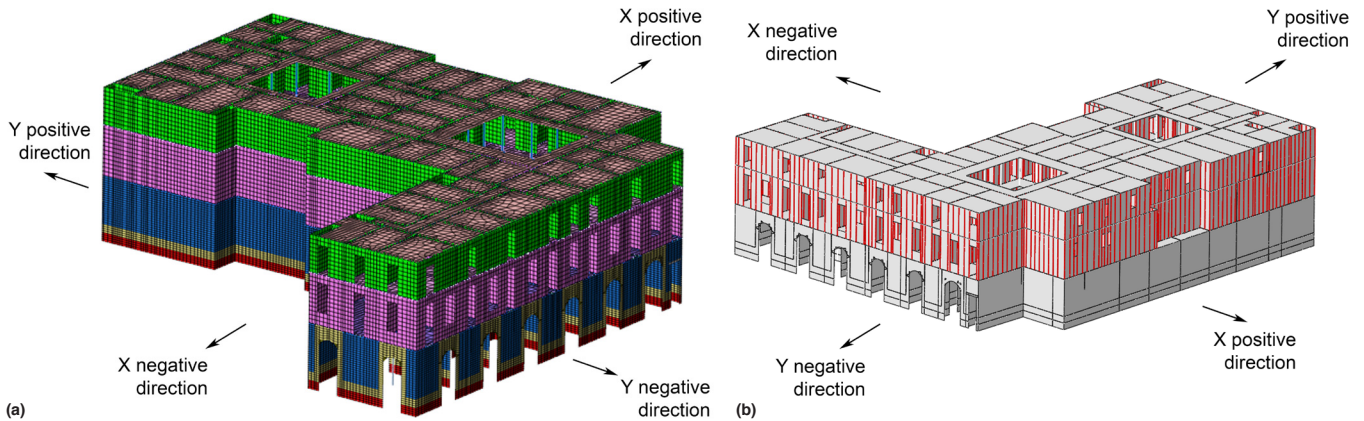
Capacity of the models of Casa Arones. FM = final model, a combination of von Mises yield criterion for tie beams and increased Young's modulus; VM = von Mises yield criterion for ties; WT = no tie beams considered; TR = thrust roof increased; YM = increased Young's modulus; RM = reference model.



out-of-plane failure mechanisms. Due to the displacement profile associated with this failure mechanism, the tying effect is more effective at roof level. It was also noted that the structure studied was not very sensitive to the embedment length of the connection of the timber floor within the adobe wall.

Lack of maintenance is considered the main cause of the current damage condition of Casa Arones. A sensitivity analysis was performed to assess the influence of selected parameters on the global behavior. In particular, a different Young's modulus for the adobe masonry was considered, the full thrust of the roof was applied, and the effect of the absence of the timber ties in addition to their capacity was discussed. Ultimately, a final model was defined. The results in terms of capacity of the pushover analyses are higher than the values given by the Peruvian code, with the exception of the model in which the action of the roof ties was not considered in the X positive direction (fig. 5.21).

The main vulnerabilities of Casa Arones are characterized by the out-of-plane movement of several vertical elements with long span and lack of transversal constraints. In general, the analysis results in the X negative and Y positive directions showed capacity to be almost insensitive to the modeling assumptions. Instead, maximum horizontal capacity of the building in the X positive direction seems to be sensitive to the parameters considered. In particular, the constraint effect of the tie beams plays an important role in maximum capacity of the structure, which has a reduction of about 65% if the ties are removed. This important decrease in capacity is also due to lack of transversal walls in the two rooms facing Calle Arones.



**FIGURES 5.22A, 5.22B.**  
Views of the FE model for Hotel El Comercio: (a) Modal Data model; (b) Test Data model, showing vertical posts (in red).

### Characteristics of the Numerical Model of Hotel El Comercio

Definition of the material properties and representation of the behavior of the quincha panels are the main challenges of this final case study. Based on testing and a review of the literature, two different sets of material properties and two different FE models are presented here. The first numerical model (fig. 5.22a) considers the material properties found in the calibration of a partial model (Modal Data model) of Hotel El Comercio performed by Aguilar et al. (2012), which provides a much higher Young's modulus. The second model (fig. 5.22b) takes into account the results of the testing campaigns (Test Data model) conducted by the Pontificia Universidad Católica del Perú (PUCP), the University of Bath, and the University College London (see the section "Quincha Walls" in chapter 3). Given the considerable difference in elastic properties, it was decided that both approaches would be used to carry out the safety assessment of the building. The quincha panels were modeled using 2D shell elements. In the Test Data model, the vertical posts are included (see fig. 5.22b), using beam elements to ensure an adequate out-of-plane behavior, since the constitutive equation proposed fits only the behavior under in-plane horizontal load.

The foundations of Hotel El Comercio are composed of rubble stone masonry set in a lime mortar. The depth of these elements below the actual floor level varies (Cancino and Lardinois 2012), but a constant average depth was assumed here, as information is limited. Inspection of the collapsed part of the building revealed a different configuration that included alternating courses of rubble stone and fired-brick masonry, even above the foundation. As stated in chapter 2, the base course rises above the foundation to a height of 0.7 to 1.0 m from the finished floor level and is made of fired-brick masonry. In the models, the base course rises to a constant height of 0.8 m, close to the lowest value in the range, to avoid overestimating the favorable impact of this element on structural behavior. Also upon inspection, a proper interlock was observed between fired brick and adobe; therefore, in the models the elements are fully connected. The properties of the elements around the arch door are the same as those of the fired-brick masonry, with a width of 0.5 m.

The walls of the first story are made of adobe masonry and rise to a height of 5.3 m from the finished floor level, with a constant thickness of 0.8 m. Foundation, base course, and lintels above the opening have the same thickness. The second story is characterized by quincha walls with a height of 4.8 m. In the Test Data model, the  $0.12 \times 0.12$  m vertical posts of the frame are included, spaced between 0.5 and 0.9 m. Quincha walls of the third

story rise to a height of 3.5 m with smaller height and thinner elements;  $0.07 \times 0.07$  m vertical posts are included in the same model.

Due to lack of alignment of walls and columns, the representation of the floors in the numerical models must allow carrying the vertical loads to the foundation. The earth layers in the floor slabs increase the load; however, if all floor systems contributed structurally, they also would increase the in-plane stiffness. Because it was not possible to predict, a priori, whether the vertical load has a positive effect, the analysis initially considered only a  $1 \text{ kN/m}^2$  permanent load, neglecting the earth and lime mortar between the sleepers. A sensitivity analysis was then carried out under a higher vertical load.

The floors and roof were determined to have a linear elastic behavior, using the elastic modulus of the timber species. The columns in the patios adhere to the original design of the building and exhibit a lack of vertical alignment and different materials. The wooden and metal columns are more recent, substituted for the walls in the first story. In the models, all the columns are introduced; the shoring elements are neglected except in the rooms between the two patios, where the extreme span prevents proper structural behavior. As it is not possible to foresee the future conformation of this area, the research team decided to leave the actual temporary shoring elements in the models.

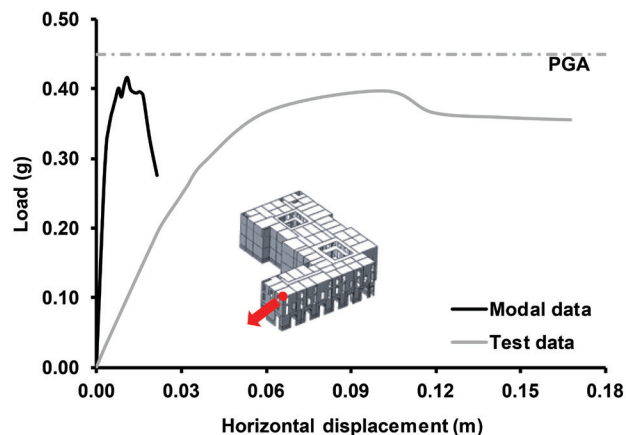
The characterization of the connection between the elements is essential to represent properly the structural behavior. Particularly, the connection between quincha and adobe seems quite weak and is guaranteed mainly by friction.

### Numerical Analysis

The nonlinear analyses performed allow assessment of the structural safety as well as a better understanding of the influence on the global behavior of parameters, such as the connections between the first- and second-story walls, the in-plane floor stiffness, the floor isotropy, and the amount of vertical loading.

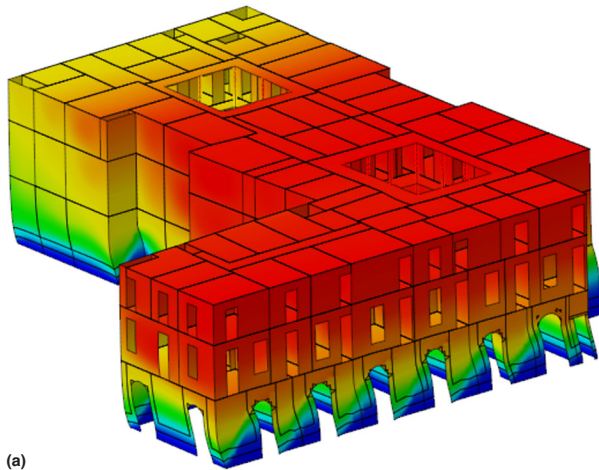
Such sensitivity analysis, reported below, allow definition of two reference models (Modal Data model and Test Data model), which provide the results shown in figure 5.23 in terms of load-displacement curve in the X negative direction. The model with the lowest stiffness presents a much larger displacement. The capacity is about  $0.4 \text{ g}$  and a shear failure at the base is evident, both from the displacements and from the crack patterns (figs. 5.24a, 5.24b).

FIGURE 5.23.  
Load-displacement diagram in X negative direction for Hotel El Comercio, showing Modal Data model and Test Data model.

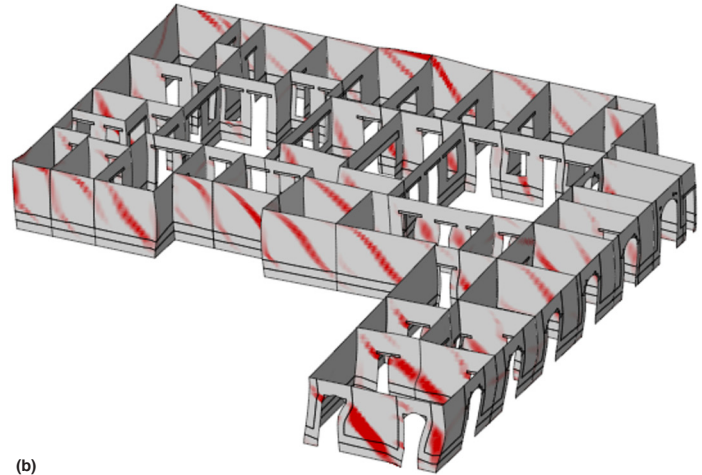


FIGURES 5.24A, 5.24B.

Pushover analysis in X negative direction at ultimate stage for Hotel El Comercio: (a) deformed mesh, indicating maximum displacement (in red) and minimum displacement (in blue); (b) crack patterns (in red) in adobe walls. Only the Modal Data model is shown.



(a)

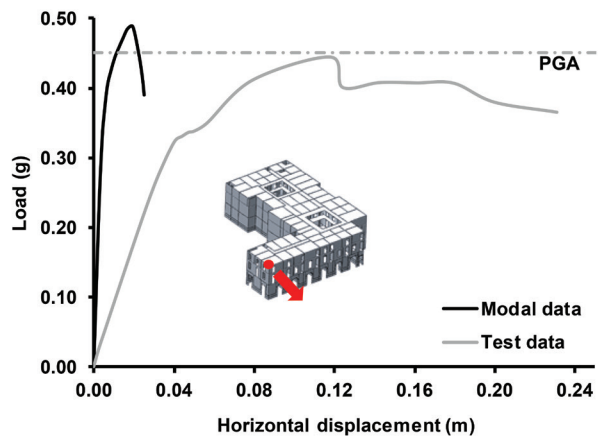


(b)

In the Y direction (positive and negative), the two models present a slightly different capacity, equal to 0.45 g for the Test Data model and 0.5 g for the Modal Data model. Figure 5.25 shows the comparison in terms of load-displacement curve only in the negative direction, as the results are similar. It can be observed that high values of displacement were recorded at the top of the building but are now much more concentrated in the far end of the left wing (fig. 5.26a). Still, from the crack patterns, a shear failure is evident at the base (fig. 5.26b).

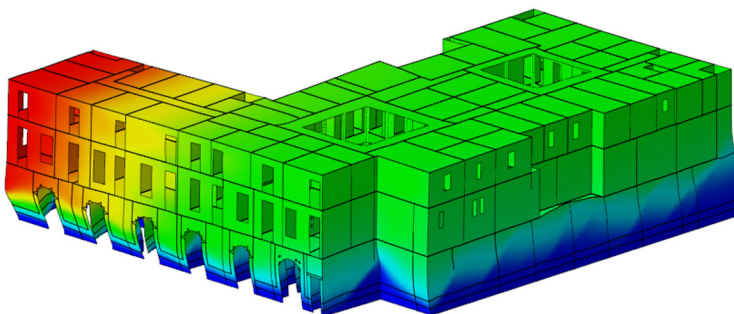
FIGURE 5.25.

Load-displacement diagram in Y negative direction for Hotel El Comercio, showing Modal Data model and Test Data model.

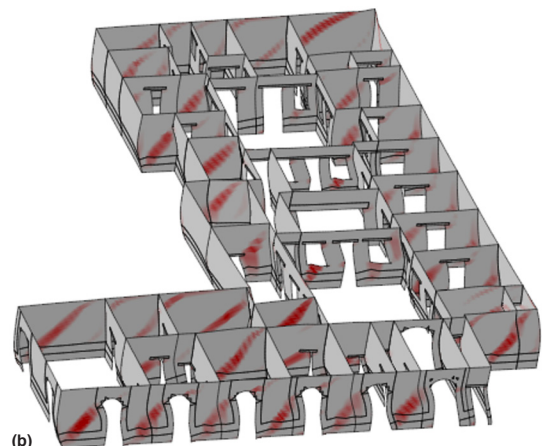


FIGURES 5.26A, 5.26B.

Pushover analysis in Y negative direction at ultimate stage for Hotel El Comercio: (a) deformed mesh, indicating maximum displacement (in red) and minimum displacement (in blue); (b) crack patterns (in red) in adobe walls. Only the Modal Data model is shown.



(a)



(b)

### Sensitivity Analysis

A sensitivity analysis investigated the influence of the following parameters on structural behavior: (a) connection between first-story walls (adobe) and second-story walls (quincha); (b) in-plane floor stiffness; (c) floor isotropy; and (d) amount of vertical loading. The most important load direction to be tested was along the out-of-plane of the main facade; namely, the Y negative direction. Thus, the results are shown mostly in this direction. The out-of-plane of the other facade, the X negative direction, is important as well, though it neglects interaction with the surrounding buildings.

In order to investigate the influence of the connection between the first and second floors of the structure, three configurations were analyzed: fixed, hinged, and interface connection.

Given the uncertainty regarding the interface properties, three different sets were specified, with the intention of representing either a typical or a very weak masonry connection. Here,  $k_n$  is the normal stiffness and  $k_t$  the shear stiffness (table 5.1). As shown in figures 5.27a and 5.27b, the values adopted do not strongly affect structural behavior, even though, upon reducing the stiffness, the displacement at peak increases up to 50% in the Test Data model. The adobe walls govern the global behavior (fig. 5.28), and the collapse mechanism does not change.

Likewise, when comparing a continuous, hinged, or interface connection, almost no difference is found. When rotation around the element's mid-plane is allowed, a very small increase in the displacement is observed. With a deformable interface between the materials, again, a very small increase of the displacement occurs. Figure 5.29 presents a comparison of the results of the analysis in the Y negative direction. This load-displacement diagram shows almost equal results in terms of maximum load factor, and therefore the structure seems to be weakly sensitive to the connection between first floor and second floor.

FIGURES 5.27A, 5.27B.

Influence of the interface connection stiffness between the first and second floors on the load-displacement diagrams for Hotel El Comercio, with load in the Y negative direction: (a) Modal Data model; (b) Test Data model.

TABLE 5.1.

Interface properties for Hotel El Comercio, specifying three different sets: stiff interface, normal interface, and soft interface.

|       | Stiff interface       | Normal interface       | Soft interface         |
|-------|-----------------------|------------------------|------------------------|
| $k_n$ | 5 N/mm <sup>3</sup>   | 5 N/mm <sup>3</sup>    | 0.5 N/mm <sup>3</sup>  |
| $k_t$ | 0.5 N/mm <sup>3</sup> | 0.05 N/mm <sup>3</sup> | 0.05 N/mm <sup>3</sup> |

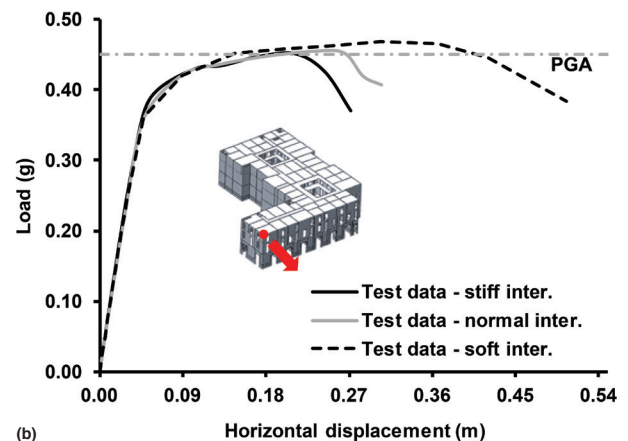
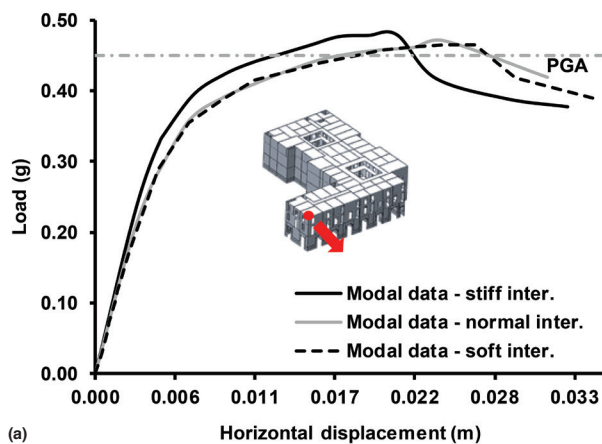
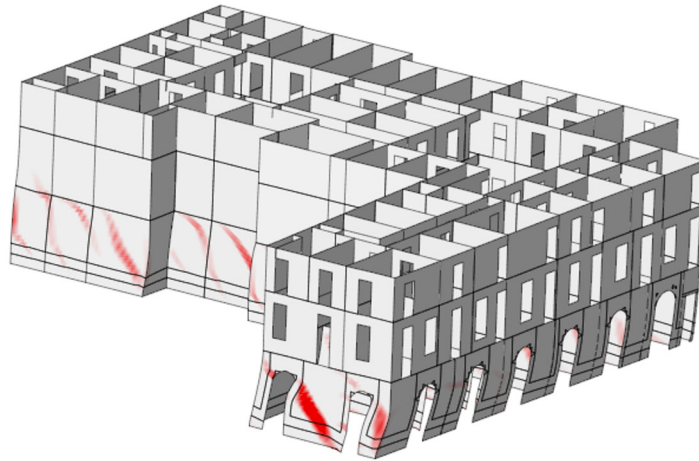


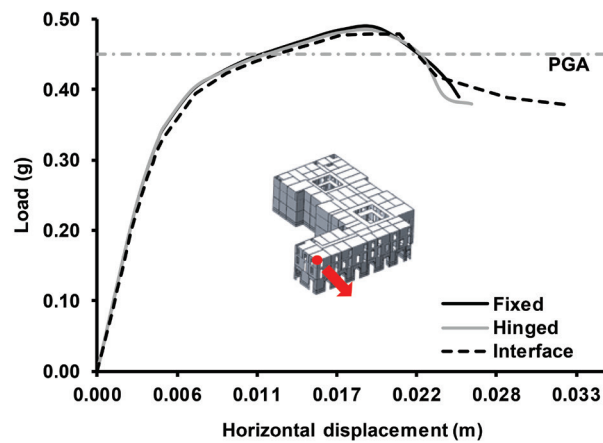
FIGURE 5.28.

Pushover analysis in Y negative direction at ultimate stage for Hotel El Comercio, showing typical crack patterns (in red). Only the Modal Data model is shown.



FIGURES 5.29.

Load-displacement diagram in Y negative direction for Hotel El Comercio, showing influence of the connection between first and second stories (fixed, hinged, or interface). Only the Modal Data model is shown.



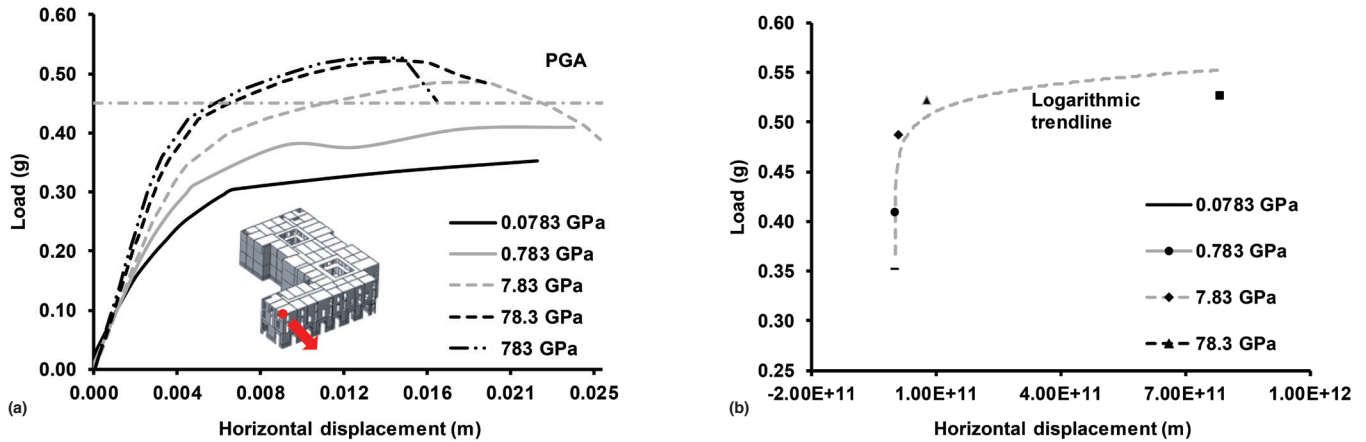
The influence of the in-plane stiffness of the flexible floors on the load capacity of masonry buildings, under lateral loads, is acknowledged in several studies. Strategies to assess the properties of wooden diaphragms are available (see ASCE 2007; NZSEE 2011). Since many uncertainties affect the diaphragm stiffness, two approaches were used. First, isotropic behavior of the diaphragm is assumed, whereas the stiffness varies due to the reduction or increase of Young's modulus (table 5.2). Here, the originally estimated Young's modulus is divided and multiplied by 10 and 100. It is noted that the largest affecting factor effectively eliminates the floor's presence (dividing by 100) or assumes a rigid diaphragm (multiplying by 100).

TABLE 5.2.

Values of Young's modulus of each diaphragm in the five cases analyzed.

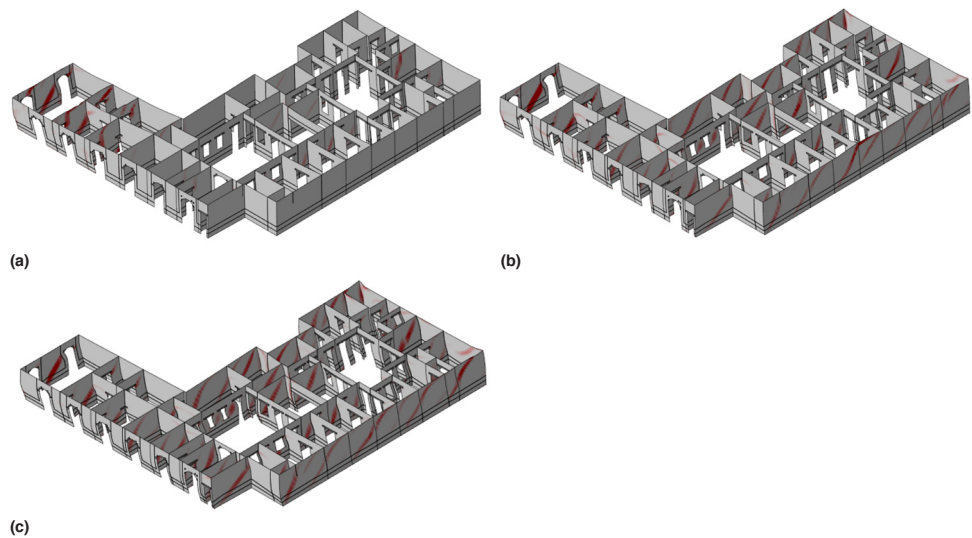
|                 | Case 1     | Case 2    | Case 3   | Case 4   | Case 5  |
|-----------------|------------|-----------|----------|----------|---------|
| Young's modulus | 0.0783 GPa | 0.783 GPa | 7.83 GPa | 78.3 GPa | 783 GPa |

As expected, the load capacity depends significantly on the Young's modulus of the floor (figs. 5.30a, 5.30b). Reducing the in-plane floor stiffness results in a less efficient box behavior and increases the torsion of the building, leading to a concentration of damage in the left wing (as described in chapter 2) (figs. 5.31a–c), where El Cordano bar is located. The relation between the Young's modulus and the load capacity within the adopted range



FIGURES 5.30A, 5.30B.

Pushover analysis in Y negative direction for Hotel El Comercio, showing influence of floor stiffness: (a) load-displacement diagram, Modal Data model; (b) load capacity as a function of the floor Young's modulus. Only the Modal Data model is shown.



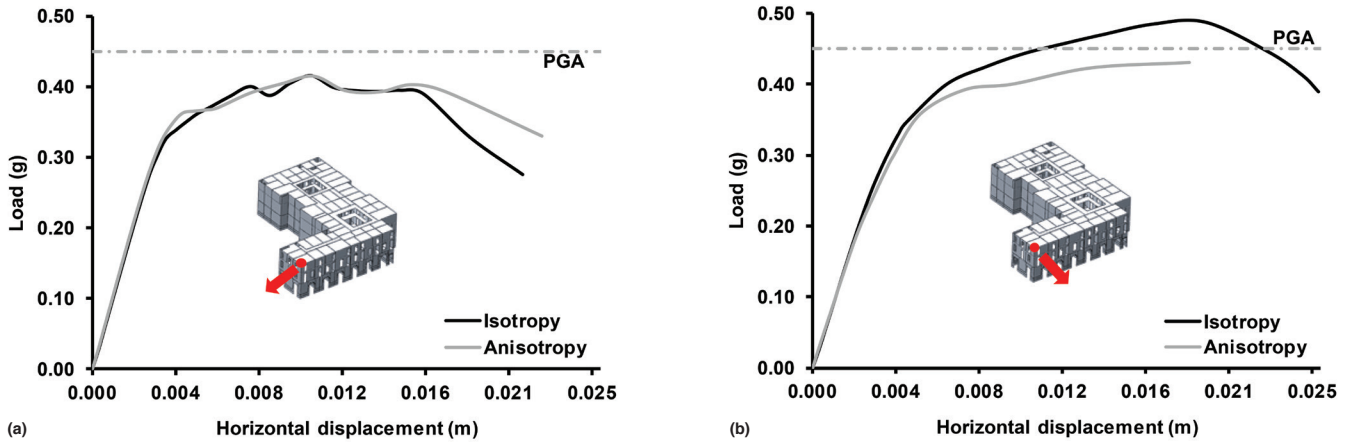
FIGURES 5.31A-C.

Pushover analysis in Y negative direction at ultimate stage for Hotel El Comercio, showing crack patterns (in red) in adobe walls, with influence of the floor Young's modulus: (a) softest floor; (b) RM; (c) stiffest floor. Only the Modal Data model is shown.

turns out to be logarithmic, indicating that the original estimation of the in-plane stiffness is enough to ensure box behavior, that is, the almost constant part of the curve (see fig. 5.30b). Values lower than this threshold can reduce the capacity significantly.

To analyze sensitivity to an orthotropic in-plane floor behavior, in each room the smaller span was chosen as the stiff direction and an insignificant stiffness is assumed orthogonally. The Young's modulus of the stiff direction and less stiff direction are assumed equal to 7.83 GPa and 0.0783 GPa, respectively. Models with isotropy and anisotropy of the slabs are compared, running analyses in X and Y negative directions, as the direction of the shortest span varies and some directional effect could be introduced. In the X negative direction, both load capacity and maximum displacement are only marginally affected by the difference in stiffness (fig. 5.32a), therefore the behavior in the two models seems to be insensitive to this parameter. In the Y negative direction, load capacity and maximum displacement decrease (fig. 5.32b). When anisotropic diaphragms are assumed in this case, much higher torsion of the building occurs and damage tends to concentrate in the left wing, reducing capacity.

The final change in parameters considers an increase in the vertical load. All components of the load are considered in the evaluation of the seismic mass for the pushover analysis; as such, the additional loads due to building usage are introduced as an updated



FIGURES 5.32A, 5.32B. Influence of the floor anisotropy for Hotel El Comercio: (a) load-displacement in X negative direction; (b) load-displacement in Y negative direction. Only the Modal Data model is shown.

density of the elements. In particular, upon adopting the quasi-permanent load provided by European codes (EC0 2005), the new load imposed is equal to  $4.9 \text{ kN/m}^2$ . The third story's floor does not have any earthen filling, so the load is different ( $3.4 \text{ kN/m}^2$ ). The behavior of the building is moderately sensitive to the new, higher, vertical load, with a slight reduction of the load capacity to  $0.44 \text{ g}$  (fig. 5.33).

### Conclusions

Two different models of Hotel El Comercio have been presented, as two different approaches in the characterization of the material properties have been followed. The Test Data model considered the mechanical properties found in the laboratory testing. The Modal Data model considered the material properties from calibration of a partial numerical model of the building with the results of the dynamic identification test. The model with the experimental data is much more flexible, giving an upper bound of the displacements under lateral loading. If the stiffer model is used, the load capacity and collapse mechanisms remain unaltered. The stiffer model allows further reduction in computational costs, as convergence was determined to be much easier.

The numerical models represent the structure in the current condition without strengthening, except for the indispensable repair of the damaged structural elements and reconstruction of a collapsed area. Adobe walls govern the global behavior of the building, and their failure affects its capacity. The collapse mechanism does not change if the constraints adopted for the walls are modified. Quincha panels appear able to take more load than the

FIGURE 5.33. Load-displacement diagram in Y negative direction for Hotel El Comercio, assuming self-weight and combination of vertical loads according to the Ultimate Limit State verification. Only the Modal Data model is shown.

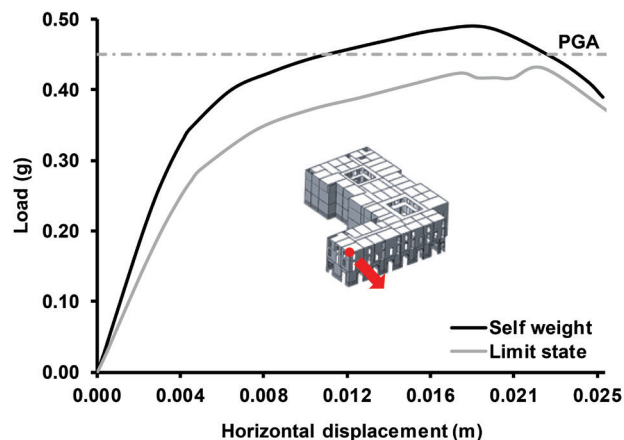
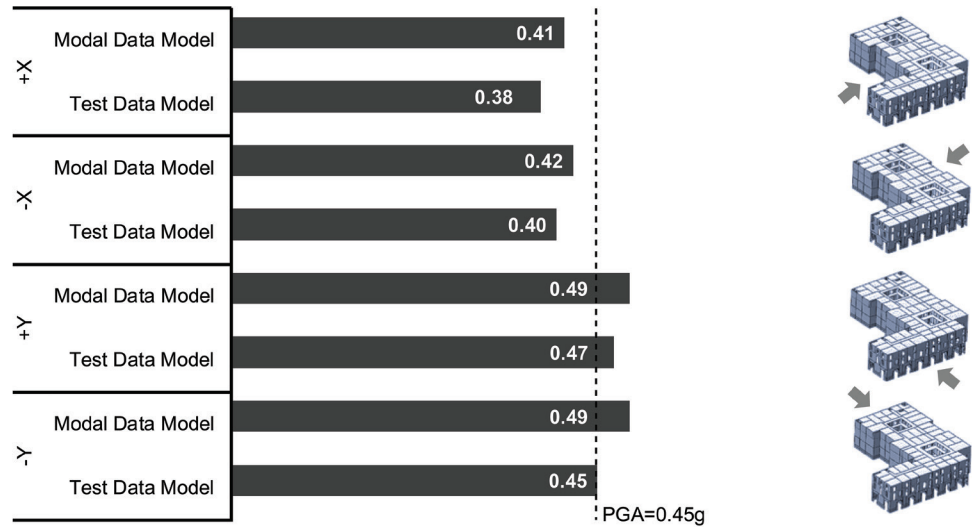


**FIGURE 5.34.**  
Maximum lateral capacity (g)  
in each direction for Hotel El  
Comercio, for both Modal Data  
model and Test Data model.



lower story for both the stiffer model and the more flexible model, without causing severe damage. Still, reducing the global stiffness of the model increases torsion, with concentration of damage in the left wing of the building. This part of the building seems the most sensitive to horizontal action and suffered some modifications of the structural system in the last century, especially in the beam scheme. Thus, local analyses should be performed before undertaking a full intervention in the building.

The slab stiffness in terms of Young's modulus is difficult to estimate and affects the load capacity.

The estimated floor stiffness is sufficient to provide a box-type behavior, but reducing the stiffness leads to a loss in the load capacity up to a maximum of 25% (when dividing the original stiffness by a factor of 100).

If the orthotropic behavior is considered for the slabs (according to orientation of the main joists), the behavior seems more sensitive to load in Y direction than in X direction. However, it does not change significantly.

The load capacity depends only moderately on vertical loading. Still, the usage of the building for excessive vertical loading (such as storerooms or assembly areas) is likely to require global strengthening measures.

As indicated in figure 5.34, the RM (i.e., full connections between walls and mechanical properties from dynamic identification) shows a maximum load factor in Y direction, slightly above the Peruvian code requirement in terms of peak ground acceleration. Maximum load factor in X direction is slightly below the code value, but "block effect," provided by adjacent buildings, is neglected. Depending on the different assumptions considered, the capacity obtained is about 0.4 to 0.5 g, which is in the range of the current code in Peru (E.030 2016).



## Conclusions

This report is part of a series of publications for the Seismic Retrofitting Project, administered under the auspices of the Getty Conservation Institute (GCI). This publication describes the seismic safety assessment of four historic earthen prototype buildings in Peru: the church of Santiago Apóstol de Kuñotambo (the church of Kuñotambo), the Ica Cathedral, Casa Arones, and Hotel El Comercio. The buildings have been studied in their current condition using the information available on geometry, damage identification, and material testing from previous phases of the project (Cancino and Lardinois 2012; Torrealva, Vicente, and Michiels 2018). Subsequent to the assessment of the seismic capacity of the structures in their current condition, a seismic retrofitting design has been evaluated for the church of Kuñotambo and the Ica Cathedral.

A description of the approach followed for the numerical modeling of the prototype buildings has been provided in this report. Specific attention is paid to the characterization of the main structural materials and to the definition of the safety level for these historic buildings. The buildings were studied using nonlinear pushover analysis, and the results reveal the vulnerabilities of the structures, their failure mechanisms, and their seismic performance based on the PGA requirements of the Peruvian national code (E.030 2016). In order to further validate the assumptions considered, sensitivity analyses were also performed.

Behavior of the main structural elements during an earthquake is highlighted and explained through the results of the nonlinear pushover analysis. Historic adobe structures are characterized as very vulnerable to out-of-plane movements if not properly constrained at floor and roof levels. Proper connection between adobe masonry and timber should be provided. If not properly distributed into the masonry, a very fragile local connection can result, relying only on the material properties of the adobe. The presence of well-anchored ties is a key factor, and these ties can be used as part of a retrofitting technique when insufficient transversal walls are present. Otherwise, corner keys and properly connected buttresses are likely to be more efficient solutions.

Guidelines on usage of advanced computations for structural engineers are available (Lourenço and Pereira 2018), as well as guidelines on usage of simplified approaches for safety assessment and strengthening design (Lourenço et al. 2018) for structural engineers, technical architects, and other practitioners.



# References

- Aguilar, R., D. Torrealva, L. F. Ramos, and P. B. Lourenço. 2012. "Operational Modal Analysis Tests on Peruvian Historical Buildings: The Case Study of the 19th Century Hotel Comercio." In *Proceedings of the 15th World Conference in Earthquake Engineering, Lisbon, Portugal, September 24–28*, edited by Sociedade Portuguesa de Engenharia Sismica (SPES). Red Hook, NY: Curran Associates.
- AIC (American Institute for Conservation of Historic and Artistic Works). 1994. *Code of Ethics and Guidelines for Practice*. American Institute for Conservation of Historic and Artistic Works, Washington, DC.
- Angelillo, M., P. B. Lourenço, and G. Milani. 2014. "Masonry Behavior and Modeling." In *Mechanics of Masonry Structures*, vol. 551, edited by M. Angelillo, 1–26. Vienna: CISM International Centre for Mechanical Sciences.
- ASCE-SEI 41-06. 2007. *Seismic Rehabilitation of Existing Buildings*. American Society of Civil Engineers, Reston, VA.
- Cancino, C. 2011. *Damage Assessment of Historic Earthen Buildings after the August 15, 2007, Pisco Earthquake: Research Report*. Los Angeles: Getty Conservation Institute.
- Cancino, C., and S. Lardinois. 2012. *Seismic Retrofitting Project: Assessment of Prototype Buildings: Research Report*. In collaboration with D. D'Ayala, C. Fonseca Ferreira, D. Torrealva Dávila, E. Vicente Meléndez, and L. Villacorta Santamato. Los Angeles: Getty Conservation Institute.
- Ciocci, M. P., S. Sharma, and P. B. Lourenço. 2017. "Ica Cathedral, Peru: Safety Assessment and Strengthening." Paper presented at the 13th Canadian Masonry Symposium, Halifax, Canada, June 4–7.
- . 2018. "Engineering Simulations of a Super-Complex Cultural Heritage Building: Ica Cathedral in Peru." *Meccanica* 53 (7): 1931–58.
- Custodio, J. C. C., M. A. Mallque, and M. C. Delgado. 2012. *Estudio anatomico e identificacion de especies forestales. Evaluacion estructural y especificaciones tecnicas de las maderas de la catedral de Ica*. Centro de Produccion Forestal, Universidad Nacional Agraria la Molina.
- De Corso, N. 2013. "Peru Field Notebook: An Update from Kuño Tambo." *The Iris* (blog). Retrieved from <http://blogs.getty.edu/iris/peru-field-notebook-an-update-from-kuno-tambo/>
- DIANA. 2014. *Displacement method ANAlyser User's Manual*, Release 9.4. Retrieved from <https://dianafea.com/DIANA-manuals>
- E.010. 2006. *Reglamento nacional de edificaciones, Título III.2: Estructuras, Norma E.010: Madera*. Instituto de la Construcción y Gerencia, Peru.
- E.030. 2016. *Reglamento nacional de edificaciones, Título III.2: Estructuras, Norma E.030: Diseño Sismorresistente*. Instituto de la Construcción y Gerencia, Peru.
- EC0 (EN 1990). 2005. *Eurocode 0: Basis of Structural Design*. European Committee for Standardization.
- EC6 (EN 1996-1-1). 2005. *Eurocode 6: Design of Masonry Structures*, Part 1-1: General Rules for Reinforced and Unreinforced Masonry Structures. European Committee for Standardization.

- EC8-3 (EN 1998-3). 2005. *Eurocode 8: Design of Structures for Earthquake Resistance, Part 3: Assessment and Retrofitting of Buildings*. European Committee for Standardization.
- FEMA 306. 1998. *Evaluation of Earthquake Damaged Concrete and Masonry Wall Buildings—Basic Procedures Manual*. Applied Technology Council (ATC-43 Project).
- Getty Conservation Institute and Dirección Desconcentrada de Cultura—Cusco. 2017. “Case Study: Kuñotambo.” Seismic Retrofitting Project. Retrieved from [www.getty.edu/conservation/our\\_projects/field\\_projects/seismic/case\\_study\\_kunotambo.html](http://www.getty.edu/conservation/our_projects/field_projects/seismic/case_study_kunotambo.html)
- Hardy M., C. Cancino, and G. Ostergren. 2009. *Proceedings of the Getty Seismic Adobe Project, 2006 Colloquium*. Los Angeles: Getty Conservation Institute.
- ICOMOS (International Council of Monuments and Sites). 2003. *ICOMOS Charter: Principles for the Analysis, Conservation and Structural Restoration of Architectural Heritage*. Ratified by the ICOMOS 14th General Assembly, Victoria Falls, Zimbabwe.
- IS 13827. 1993. *Improving Earthquake Resistance of Earthen Buildings: Guidelines*. Bureau of Indian Standards, New Delhi.
- JCSS. 2006. *Probabilistic Model Code, Part 3.5: Timber*. Joint Committee on Structural Safety (JCSS). Retrieved from [https://www.jcss.byg.dtu.dk/Publications/Probabilistic\\_Model\\_Code](https://www.jcss.byg.dtu.dk/Publications/Probabilistic_Model_Code)
- Karanikoloudis, G., and P. B. Lourenço. 2018. “Structural Assessment and Seismic Vulnerability of Earthen Historic Structures.” *Engineering Structures* 160: 488–509.
- Lourenço, P. B. 1996. “Computational Strategies for Masonry Structures.” PhD thesis, University of Technology, Delft, Netherlands.
- Lourenço, P. B., M. P. Ciocci, F. Greco, G. Karanikoloudis, C. Cancino, D. Torrealva, and K. Wong. 2018. “Traditional Techniques for the Rehabilitation and Protection of Historic Earthen Structures: The Seismic Retrofitting Project.” *International Journal of Architecture Heritage*. DOI: 10.1080/15583058.2018.1497232
- Lourenço, P. B., G. Karanikoloudis, and F. Greco. 2016. “In situ Testing and Modeling of Cultural Heritage Buildings in Peru.” In *Structural Analysis of Historical Constructions: Anamnesis, Diagnosis, Therapy, Controls: Proceedings of the 10th International Conference on Structural Analysis of Historical Constructions (SAHC, Leuven, Belgium, 13–15 September 2016)*, edited by K. Van Belen and E. Verstryngne, 850–57. Leuven: CRC Press.
- Lourenço, P. B., N. Mendes, L. F. Ramos, and D. V. Oliveira. 2011. “Analysis of Masonry Structures without Box Behaviour.” *International Journal of Architectural Heritage* 5 (4–5): 369–82.
- Lourenço, P. B., N. Mendes, L. F. Ramos, and A. Trujillo. 2012. “Seismic Performance of the St. George of the Latins Church: Lessons Learned from Studying Masonry Ruins.” *Engineering Structures* 40: 501–18.
- Lourenço, P. B., and J. M. Pereira. 2018. *Seismic Retrofitting Project: Recommendations for Advanced Modeling of Historic Earthen Sites: Research Report*. In collaboration with G. Karanikoloudis, F. Greco, and C. Cancino. Los Angeles: Getty Conservation Institute. Retrieved from [http://www.getty.edu/conservation/publications\\_resources/pdf\\_publications/recommendations\\_advanced\\_modeling.html](http://www.getty.edu/conservation/publications_resources/pdf_publications/recommendations_advanced_modeling.html)
- Lourenço, P. B., D. Torrealva, and J. M. Pereira. Forthcoming. *Seismic Retrofitting Project: Simple Calculations for Historic Earthen Sites*. In collaboration with F. Greco and C. Cancino. Los Angeles: Getty Conservation Institute.
- Lumantarna, R., D. T. Biggs, and J. M. Ingham. 2014. “Uniaxial Compressive Strength and Stiffness of Field-Extracted and Laboratory-Constructed Masonry Prisms.” *ASCE Journal of Materials* 26 (4): 567–75.
- Moscoso, H. C., M. R. Candia, H. R. Rossell, P. C. Ocampo, D. Torrealva, R. Q. Cardenas, R. Z. Gutierrez, M. S. Alvarez, and P. R. Calla. 2015. *Proyecto: Expediente técnico de recuperación del monumento virreinal Templo Santiago Apóstol Kuño Tambo, CORTE A–A (Plan No. PR-04)*,

- CORTE D–D (Plan No. PR-05)*. Cusco: Ministry of Culture; Los Angeles: J. Paul Getty Trust. In Spanish.
- NTC. 2008. *Norme tecniche per le costruzioni—Il Capo del Dipartimento della Protezione Civile*. With Circolare no. 617 (2009). Il Ministro Delle Infrastrutture, Italy.
- NZSEE (New Zealand Society for Earthquake Engineering). 2011. *Assessment and Improvement of Unreinforced Masonry Buildings for Earthquake Resistance*. New Zealand Society for Earthquake Engineering, Wellington.
- OPCM 3431. 2005. *Primi elementi in materia di criteri generali per la classificazione sismica del territorio nazionale e di normative tecniche per le costruzioni in zona sismica*. Ordinanza del Presidente del Consiglio dei ministri (OPCM), Italy, March 20, 2003, no. 3274, modified in the OPCM, May 3, 2005, no. 3431.
- Paulay, T., and M. J. N. Priestley. 1992. *Seismic Design of Reinforced Concrete and Masonry Buildings*. New York: John Wiley & Sons.
- Percy, K., C. Hanley, M. Santana Quintero, S. Fai, C. Ouimet, C. Cancino, L. Rainer, and L. Villacorta-Santamato. 2013. "Recording Earthen Architecture at the Peruvian Andes: The Case of Kuñotambo Church's Historic Wall Paintings." Paper presented at the Twenty-Fourth International CIPA Symposium, Strasbourg, France, September 2–6.
- Pluijm, R. van der. 1999. "Out-of-Plane Bending of Masonry: Behavior and Strength." PhD thesis, Eindhoven University of Technology.
- Ramos, L. F., and P. B. Lourenço. 2004. "Advanced Numerical Analysis of Historical Centers: A Case Study in Lisbon." *Engineering Structures* 26: 1295–1310.
- Rots, J. G. 1997. *Structural Masonry: An Experimental/Numerical Basis for Practical Design Rules*. CUR Report 171. Abingdon, UK: Taylor & Francis Group.
- Tolles, E. L., E. E. Kimbro, and W. S. Ginell. 2002. *Planning and Engineering Guidelines for the Seismic Retrofitting of Historic Adobe Structures: Research Report*. Los Angeles: Getty Conservation Institute. Also in Spanish.
- Tomažević, M. 1999. *Earthquake-Resistant Design of Masonry Buildings*. Innovation in Structures and Construction, vol. 1. Edited by A. S. Elnashai and P. J. Dowling. London: Imperial College Press.
- Tomažević M., and M. Lutman. 2007. "Heritage Masonry Buildings in Urban Settlements and the Requirements of Eurocodes: Experience of Slovenia." *International Journal of Architectural Heritage* 1 (1): 108–30.
- Torrevalva, D., and E. Vicente. 2016. *Proyecto: Expediente técnico de recuperación del monumento virreinal Templo Santiago Apóstol Kuño Tambo, Consolidación de muros y contrafuertes (Plan No. E-02), Intervención y consolidación de cimentación—Primer nivel—Planta (Plan No. E-01)*. Cusco: Ministry of Culture; Los Angeles: J. Paul Getty Trust.
- Torrevalva, D., E. Vicente, and T. Michiels. 2018. *Seismic Retrofitting Project: Testing of Materials and Building Components of Historic Adobe Buildings in Peru: Research Report*. In collaboration with F. Greco, C. Cancino, and K. Wong. Los Angeles: Getty Conservation Institute. Retrieved from [http://www.getty.edu/conservation/publications\\_resources/pdf\\_publications/pdf/testing\\_materials.pdf](http://www.getty.edu/conservation/publications_resources/pdf_publications/pdf/testing_materials.pdf)
- Vinci, M. 2014. *I tiranti in acciaio nel calcolo delle costruzioni in muratura*. Palermo: Dario Flaccovio Editore.
- Vintzileou, E. 2008. "Effect of Timber Ties on the Behavior of Historic Masonry." *Journal of Structural Engineering* 134 (6): 961–72.
- Zanotti, S. 2015. "Seismic Analysis of the Church of Kuño Tambo (Peru)." SAHC master's thesis, University of Minho, Portugal.





The Getty Conservation Institute